# *Research in*
# AGRICULTURAL ENGINEERING

Czech Academy of Agricultural Sciences

**VOLUME 59**
**Special Issue**
**Prague 2013**
ISSN 1212-9151 (Print)
ISSN 1805-9376 (On-line)

# *Research in* AGRICULTURAL ENGINEERING

**formerly ZEMĚDĚLSKÁ TECHNIKA since 1955 to 1999**

An international peer-reviewed journal published by the Czech Academy of Agricultural Sciences and financed by the Ministry of Agriculture of the Czech Republic

**Aims and scope:** The journal of RAE publishes original research papers devoted to all scientific and applied aspects of Agricultural Engineering including those laying on the border with other scientific disciplines, for example mechatronics, IT, robotics, ecology, energetics, economy, ergonomic, applied physics, biochemistry, biotechnology, bionics and waste management. Special at attention is devoted to new technologies with respect to their environmental aspects and agricultural products quality control. Papers are published in English (British spelling).

**Abstracts** are comprised in:
- Agrindex of AGRIS/FAO database
- CAB Abstracts
- Czech Agricultural and Food Bibliography
- SCOPUS

**Periodicity:** 4 issues per year, volume 60 appearing in 2014.

**Editorial Office**

Research in Agriculture Engineering, Ing. Eva Karská, Executive Editor, Czech Academy of Agricultural Sciences, Slezská 7, 120 00 Prague 2, Czech Republic, phone: + 420 227 010 606, fax: + 420 227 010 116, e-mail: rae@cazv.cz

**Subscription information**

Subscription orders can be entered only by calendar year and should be sent to: Czech Academy of Agricultural Sciences, Slezská 7, 120 00 Prague 2, Czech Republic. Subscription price is 155 USD (subscribers from the Czech Republic can apply for special rates).

**Electronic access**

Full papers from Vol. 48 (2002), instructions to authors and information on all journals edited by the Czech Academy of Agricultural Sciences are available at http://agriculturejournals.cz/web/rae.htm

**Online Manuscript Submission**

All manuscripts must be submitted to the journal website (http://agriculturejournals.cz/web/rae.htm). Authors are requested to submit the text, tables, and artwork in electronic form to this web address. Authors unable to submit an electronic version should contact by e-mail the Editorial Office.
Both the dates of the receipt of the manuscript and of the acceptance by the Managing Editorial Board for publishing will be indicated in the printed contribution.





MK ČR E 6698

Research in **AGRICULTURAL ENGINEERING**

formely ZEMĚDĚLSKÁ TECHNIKA

**Volume 59** **2013**

Research in AGRICULTURAL ENGINEERING

Volume 59, 2013, Special Issue

## CONTENTS



**Go to the website for information about Research in Agricultural Engineering:**
**http://www.agriculturejournals.cz/web/RAE.htm**

# Comparison of thermal and rheologic properties of Slovak mixed flower honey and forest honey

M. Božiková, P. Hlaváč

*Department of Physics, Faculty of Engineering, Slovak University of Agriculture in Nitra, Nitra, Slovak Republic*

**Abstract**

Božiková M., Hlaváč P., 2013. **Comparison of thermal and rheologic properties of Slovak mixed flower honey and forest honey**. Res. Agr. Eng., 59 (Special Issue): S1–S8.

The article deals with the comparison of thermal and rheologic properties of two types of honey – mixed flower honey and forest honey made in Slovak Republic. All honey parameters were measured during temperature manipulation in the temperature interval from 5 to 45°C. Two series of thermal and rheologic parameters measurements were done. Firstly samples of both types of fresh honey were measured at the beginning of storage and then the same samples of honey were measured again after one week of storage. The measuring of thermal parameters i.e. thermal conductivity, thermal diffusivity and specific heat was performed by the instrument Isomet 2104, which uses Hot Wire method, and the principle of measuring being based on the analysis of time-temperature relation. The measurements of dynamic viscosity were done by the viscometer Anton Paar (DV-3P), the principle of measuring being based on the dependence of the sample resistance on the probe rotation. Other rheologic parameters as kinematic viscosity and fluidity, were also determined. For the rheologic parameters measurements exponential relations are typical while for the thermal parameters linear relations were obtained.

**Keywords**: samples of honey; temperature; thermophysical properties; rheological parameters; time of storage

Controlled processes in manufacturing, handling, and holding require precise knowledge of physical quantities of materials. For the quality evaluation of food materials it is important to know their physical properties particularly, mechanical, rheologic and thermophysical (Božiková, Hlaváč 2010).

In this article are presented theoretical parts from thermophysics and rheology, thermophysical and rheologic measurement methods and the results of thermophysical and rheologic parameters measurements for different types of honey. Some rheologic and thermophysical properties of honey are mentioned in literature. Bhandari et al. (1999) examined rheologic properties of Australian honeys. They found out that rheologic properties of honey depend on the composition of individual sugars, and the amounts and types of colloids present in honey. Zaitoun et al. (2000) examined rheologic properties of selected light-coloured Jordanian honeys. They found out that the viscosity of honey decreases with the water content. The water content is the major factor that influences the keeping quality or storability of honey. Chirife and Buera (1997) described a simple model for predicting the viscosity of sugar and oligosaccharide solutions. They found out that disaccharides, composed of two monomeric monosaccharides, give rise to a higher viscosity than monosaccharides when com-

pared in the same mass fraction. JUNZHENG and CHANGYING (1998) were interested in the rheologic model of natural honeys in China. They and many other authors reported that honeys behave as Newtonian fluid. Honey viscosity was Newtonian, even in reduced-calorie varieties, and adhered to the Arrhenius equation, the viscosity exponentially decreasing with the temperature (COHEN, WEIHS 2010). WHITE et al. (1964) examined the effect of storage and processing temperature on the honey quality. In their investigation they found out that dark-coloured types of honey tend to be affected by heat faster than the light-coloured types. It is natural for many types of honey to granulate or crystallise upon storage. Since the retail honey market largely favours liquid honey, some types of processing are necessary to maintain the liquid state. This is most commonly done by straining, heating, or filtration (WHITE 1999). In honey processing, heating is applied for the following reasons: to warm it sufficiently to facilitate straining, handling, and packing; to delay granulation. Other reason for honey heating is to destroy yeasts that may be present; hence, the keeping quality of the honey respective is assured (WHITE 1975).

Generally, physical properties of honey are influenced by various factors such as: the type of flowers, way of processing and most of all area of origin, etc. The research of honey physical properties in Slovak Republic is at the beginning and particular properties are not known. Our research was oriented on measuring the rheological and thermophysical properties of honey.

## MATERIALS AND METHODS

According to Codex Alimentarius of the Slovak Republic (2004) honey is a natural sweet substance, produced by honeybees from the nectar of plants or from secretions of living parts of plants, or excretions of plant-sucking insects on the living parts of plants, which the bees collect, transform by combining with specific substances of their own, deposit, dehydrate, store and leave in honeycombs to ripen and mature.

Honey is the primary product of bees and belongs among natural sweeteners; it is also known for its health promoting effects. The main parts of honey are nectar and honeydew. Nectar is the secretion of the plant organs and it consists of concentrated solution of sugars (glucose, fructose, sucrose, and maltose). Honeydew is plant juice, which passed through the part of the bee digestive tract. Its main ingredients are also sugars, but in more varied composition. Honey is a mixture of sugars, water, and other components. The specific composition of a honey depends mostly on the mixture of flowers visited by bees producing the honey and it is different in relation to locations, terms and particular colony of bees. Honey in general consists of fructose (approximately 38%), glucose (about 31%), sucrose (around 1%), other sugars (about 9%), water (approximately 17%), ash (around 0.17%), and other substances (HLAVÁČ 2010).

Two different types of honey were measured – mixed flower honey and forest honey. The general composition of both samples has been presented above; however there were some differences between the samples. For example, the colour of honey made the greatest difference, but it did not influence the thermophysical and rheological properties. The next difference was in the water content: forest honey had 17.86% and mixed flower honey had 16.33% of water.

All honey samples were analysed in laboratory settings (laboratory temperature 20°C, atmospheric pressure 1,013 hPa and relative air humidity 45%). Rheologic properties were measured in the temperature range (20–45°C), thermophysical properties were measured in the temperature range of (5–45°C). Temperatures higher than 20°C were obtained by heating in the water bath and lower temperatures were obtained by cooling in the refrigerator. The honey samples were without bubbles, lest the precision of the measurements should affected by them. The state of the samples during the measurements was different according to the sample temperature.

For the quality protection in practice, we need many series of measurements in a short time, so the current research prefers non stationary – dynamic methods for thermophysical and rheologic parameters measurements to the stationary methods which usually take a long time. On the basis of the facts presented, dynamic methods of thermophysical and rheologic parameters measurement were chosen and are described in the following text.

**Thermophysical parameters and method of measurement**. For thermophysical parameters measurements a dynamic method Hot Wire method (HW method) was used. HW method is a standard transient dynamic technique which is based on the measurement of the time – temperature relation in a defined distance from the heat source (hot wire) (DAVIS 1984). The heating wire as well

as the temperature sensor (thermocouple) is encapsulated in a probe that electrically insulates the hot wire and the temperature sensor from the test material (WECHSLER 1992). Heat flux is generated for an appropriate time interval through a long thin uniform wire buried in the sample and the temperature response is measured by the change in the wire resistance. The response is analysed in accordance with a model characterised by the particular formula found by the solution of the partial differential equations using boundary and initial conditions corresponding to the experimental set up presented in the literature BOŽIKOVÁ and HLAVÁČ (2010). By HW method, we can obtain the value of thermal conductivity and we can calculate the thermal diffusivity and specific heat.

According to KREMPASKÝ (1969), thermal conductivity λ, thermal diffusivity $a$ and specific heat $c$ belong among thermophysical characteristics.

Thermal conductivity λ is the property of a material which relates its ability to conduct heat. The heat transfer by conduction involves the transfer of energy within a material without any motion of the material as a whole. Conduction takes place when a temperature gradient exists in a solid (or stationary fluid) medium. Conductive heat flow occurs in the direction of decreasing temperature because higher temperature equates to higher molecular energy or more extensive molecular movement. Energy is transferred from the more energetic molecules to the less energetic ones when neighbouring molecules collide. This thermophysical parameter depends on many factors (KREMPASKÝ 1969). Thermal conductivity is defined by Fourier's law, Eq. (1):

$$\vec{q} = -\lambda \operatorname{grad} T \qquad (\mathrm{W/m^2}) \qquad (1)$$

where:

λ – thermal conductivity (W/m.K)

$\vec{q}$ – vector of heat flow density (W/m$^2$)

$T$ – thermodynamic temperature (K)

Thermal diffusivity $a$ characterises the velocity of temperature equalisation in the material during-non stationary processes. In numerical view it, equals the temperature change of unit volume caused by heat, which is transferred in unit time, by unit surface of the coat with unit thickness, in unit temperature difference on its facing side.

During the measurement of thermal diffusivity, it is estimated, how quickly a body can change its temperature; it increases with the ability of the body to conduct heat and it decreases with the amount of heat needed to change the temperature the body.

$$a = \frac{\lambda}{c\rho} \qquad (\mathrm{m^2/s}) \qquad (2)$$

where:

$a$ – thermal diffusivity (m$^2$/s)

$c$ – specific heat (J/kg.K)

ρ – density of material (kg/m)

Specific heat $c$ is defined as the heat which is necessary for a heating material of unit mass per 1 K; and by Eq. (3):

$$c = \frac{C}{m} = \frac{\partial Q}{m\,\partial T} \qquad (\mathrm{J/kg.K}) \qquad (3)$$

where:

$C$ – heat capacity (J/K)

$Q$ – heat (J)

$T$ – thermodynamic temperature (K)

$m$ – mass of material (kg)

This physical parameter is important for different technical and practical applications. The measuring of thermal parameters was performed with a digital instrument Isomet 2104 (Applied Precision SAS, Bratislava, Slovak Republic). Principle of measuring with this instrument is based on recording the time – temperature dependence during the sample heating. Thermal parameters of the measured sample are calculated from the dependence obtained. The measurement is based on the analysis of the temperature response of the analysed material to the heat flow impulses. If we use needle probe for the measurements of thermophysical parameters, the experimental arrangement is modelled by HW method, which is described by LIANG (1995) and ASSAEL et al. (2002).

**Rheologic parameters and method of measurement**. Dynamic viscosity is defined as the resistance of a fluid to flow. Viscosity changes with temperature. The difference between the effects of temperature on the viscosity of fluids and gases is related to the difference between their molecular structures. Viscosity of most of the liquids decreases with increasing temperature. Theories have been proposed regarding the effect of temperature on viscosity of liquids. According to Eyeing's theory, the molecules of liquids continuously move into the vacancies (BIRD et al. 1960).

This process permits flow but requires energy. Activation energy is more readily available at higher temperatures and the fluid flows easily. The tem-

perature effect on viscosity can be described by an Arrhenius type equation:

$$\eta = \eta_0 e^{-\frac{E_A}{RT}} \quad \text{(Pa.s)} \tag{4}$$

where:

$\eta$ – dynamic viscosity (Pa.s)
$\eta_0$ – reference value of dynamic viscosity (Pa.s)
$E_A$ – activation energy (J/mol)
$R$ – gas constant (J/mol.K)
$T$ – absolute temperature (FIGURA, TEIXEIRA 2007) (K)

Liquid molecules are closely spaced with strong cohesive forces between them. The temperature dependence of viscosity can also be explained by cohesive forces between the molecules (MUNSON et al. 1994). As temperature increases, these cohesive forces between the molecules decrease and the flow becomes freer. As a result the viscosities of liquids decrease as the temperature increases. In liquids, the intermolecular (cohesive) forces play an important role. The viscosities of liquids show little dependence on the density, molecular velocity, or mean free path. In most liquids, viscosity is constant up to a pressure of 10,134 MPa, but at higher pressures it increases as the pressure increases (SAHIN, SUMNU 2006).

Kinematic viscosity $\nu$ is defined as a ratio of dynamic viscosity $\eta$ to the density of the fluid $\rho$ at the same temperature:

$$\nu = \frac{\eta}{\rho} \quad \text{(m}^2\text{/s)} \tag{5}$$

Fluidity $\varphi$ is defined as the reciprocal value of dynamic viscosity $\eta$:

$$\varphi = \frac{1}{\eta} \quad \text{(1/Pa.s)} \tag{6}$$

The measuring of dynamic viscosity was performed with a digital viscometer Anton Paar DV-3P (Anton Paar GmbH, Graz, Austria). Digital viscosimeter Anton Paar DV-3P is a rotational viscometer, which measures the torque of a spinning probe embedded into the sample. The spinning cylinder or spindle is interconnected through a spring to the engine shaft, which is rotating at defined velocity. The angle of the angular rotation shaft is measured electronically. From the measured values, on the base of internal calculations are directly displayed the values of dynamic viscosity. This instrument works with several types of spindles and uses a wide area of velocity, which allows the measurement of viscosity in a large extent.

## RESULTS

### Results of thermophysical parameters measurements

Samples of mixed flower honey and forest honey were stored at laboratory temperature and were measured in different days during storage. The measurements were performed in the temperature interval ranking from laboratory temperature (22°C for rheologic measurements) respectively (from 5°C for thermophysical measurements) to 43°C. Dependencies of thermophysical and rheologic parameters on temperature and also on the storage time were examined. The graphical relations show two measurements: the first measurement (at the beginning of storage) and next measurement (after one week of storage). The results obtained with mixed flower honey are showed in Figs 1a–6a. As to the sample of forest honey the results are presented on Figs 1b–6b.

Temperature dependencies of thermal conductivity and specific heat can be described by linear increasing functions (Eqs 7 and 9) and in the case of temperature dependence of thermal diffusivity linear decreasing function (Eq. 8) can be used:

$$\lambda = A + B\left(\frac{t}{t_0}\right) \quad \text{(W/m.K)} \tag{7}$$

$$a = C - D\left(\frac{t}{t_0}\right) \quad \text{(m}^2\text{/s)} \tag{8}$$

$$c = E + F\left(\frac{t}{t_0}\right) \quad \text{(J/kg.K)} \tag{9}$$

where:

$t$ – temperature (°C)
$t_0$ – equals to 1°C
$\lambda$ – thermal conductivity (W/m.K)
$a$ – thermal diffusivity (m$^2$/s)
$c$ – specific heat (J/kg.K)
$A, B, C, D, E, F$ – constants dependent on kind of material, and on ways of processing and storing

In all cases were the coefficients of determination very high (Table 1).

Figs 1–3 demonstrate linear relations between thermophysical parameters and temperature during temperature stabilisation of honey samples. The study of the relationships between thermal conductivity, thermal diffusivity, specific heat and temper-

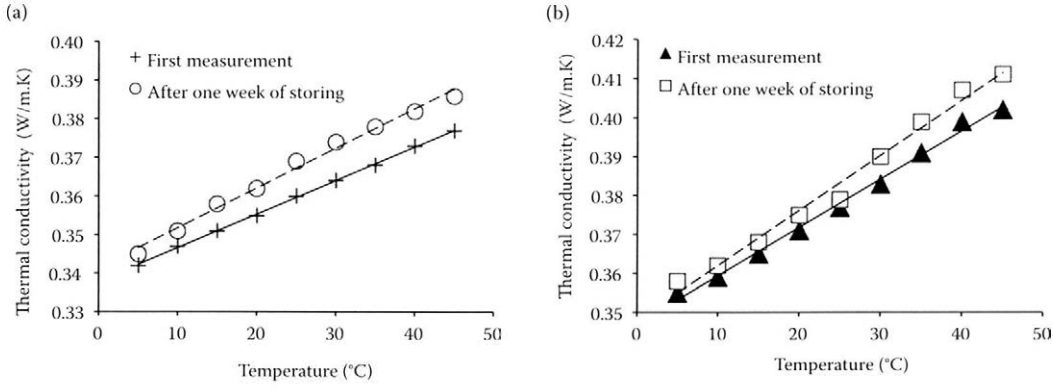


Fig. 1. Effect of temperature changes on thermal conductivity of (a) mixed flower honey and (b) forest honey

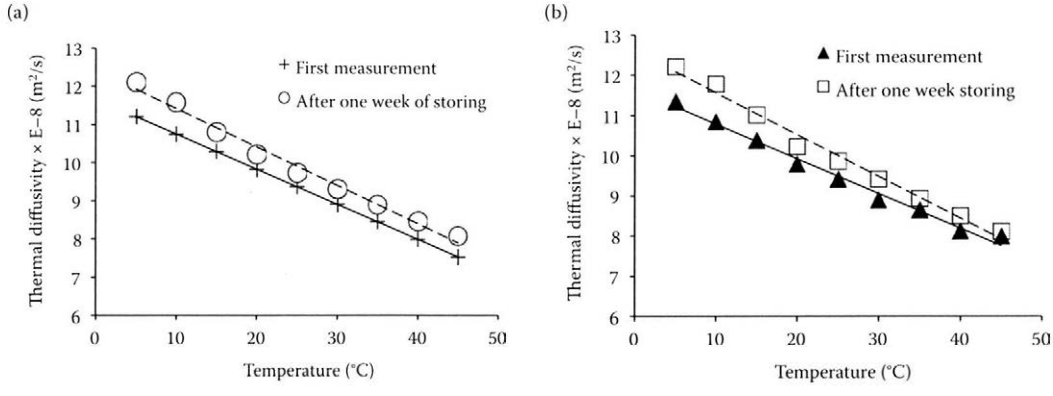


Fig. 2. Effect of temperature changes on thermal diffusivity of (a) mixed flower honey and (b) forest honey

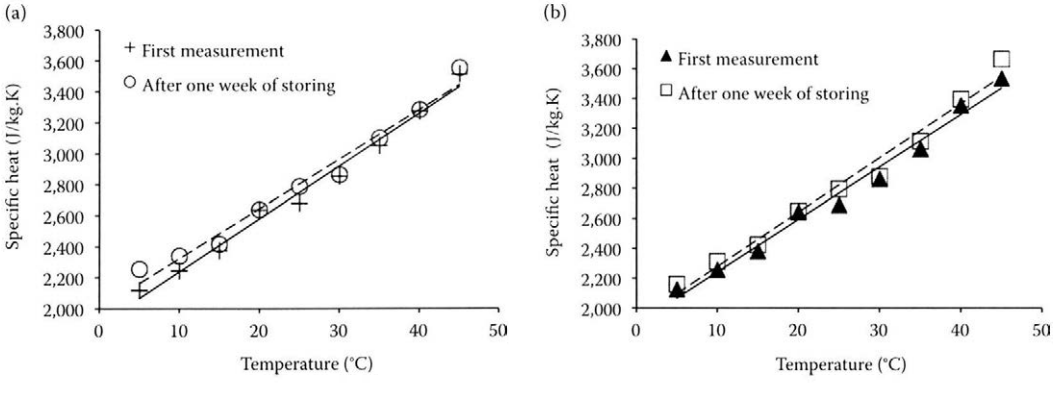


Fig. 3. Effect of temperature changes on specific heat of (a) mixed flower honey and (b) forest honey

ature showed that increasing temperature of the honey had a linear increasing effect on thermal conductivity and specific heat. The second measured thermal parameter – thermal diffusivity revealed linear decreasing progress during the temperature stabilisation process (Fig. 2). All results obtained for thermal conductivity and thermal diffusivity are in a good agreement with the literature Ginzburg (1985) and White (1975). From the presented results for thermophysical measurements it is clear that the thermal conductivity of high viscosity liquids or suspensoid materials can be measured with

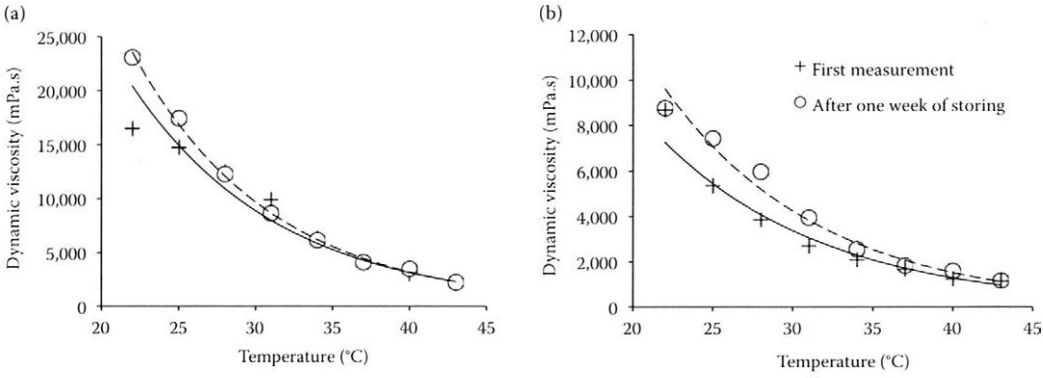


Fig. 4. Effect of temperature changes on dynamic viscosity of (a) mixed flower honey and (b) forest honey

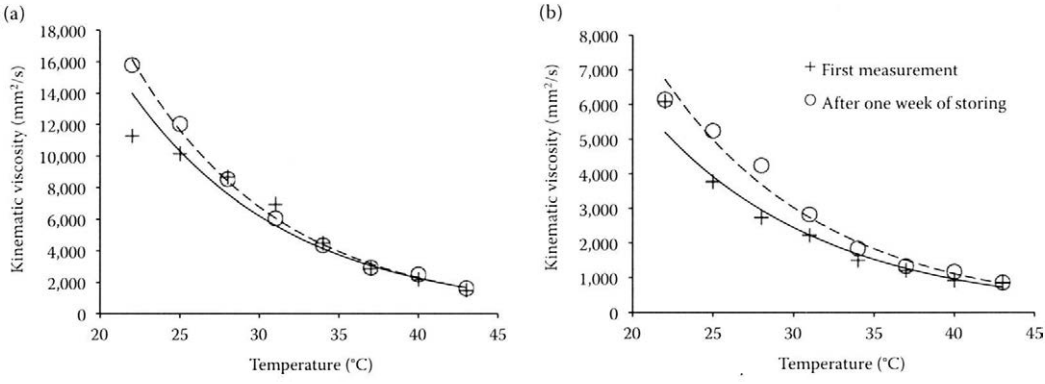


Fig. 5. Effect of temperature changes on kinematic viscosity of (a) mixed flower honey and (b) forest honey

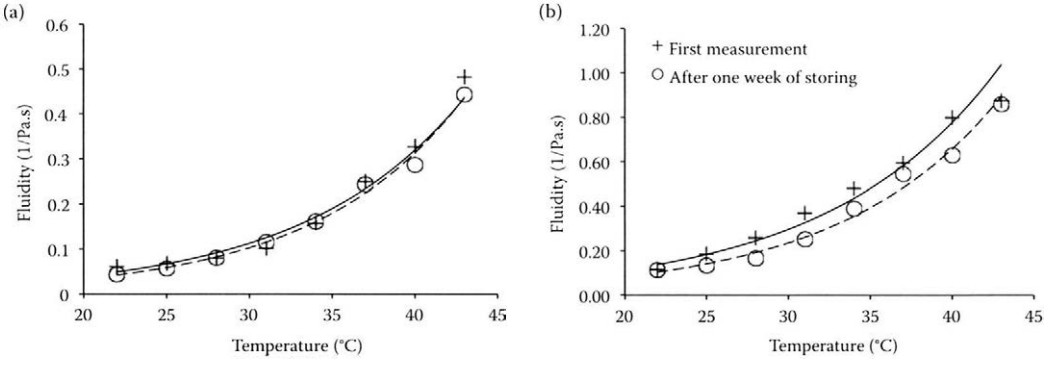


Fig. 6. Effect of temperature changes on fluidity of (a) mixed flower honey and (b) forest honey

HW method. For the data reliability protection, a series of one hundred measurements were done for every point in the presented graphic relations. Each point in the graphics characteristics was obtained as the average of the values measured.

## Results for rheologic parameters measurements

The temperature dependencies of dynamic and kinematic viscosities can be described by decreas-

Table 1. Coefficients *A, B, C, D, E, F* of regression Eqs 7–9 and coefficients of determination ($R^2$)

| | *A* (W/m.K) | *B* (W/m.K) | $R^2$ | *C* (mm²/s) | *D* (mm²/s) | $R^2$ | *E* (J/kg.K) | *F* (J/kg.K) | $R^2$ |
|---|---|---|---|---|---|---|---|---|---|
| **Flower honey measurement** | | | | | | | | | |
| First | 0.337917 | 0.00087 | 0.999428 | 0.1167 | 0.00092 | 1 | 1,895.35 | 34.21 | 0.985916 |
| Next | 0.341472 | 0.00103 | 0.991152 | 0.1242 | 0.00101 | 0.987847 | 2,001.91 | 32.13 | 0.976848 |
| **Forest honey measurement** | | | | | | | | | |
| First | 0.347000 | 0.00124 | 0.994138 | 0.1166 | 0.00087 | 0.988398 | 1,899.44 | 35.04 | 0.983495 |
| Next | 0.347889 | 0.00141 | 0.987057 | 0.1261 | 0.00104 | 0.987225 | 2,015.64 | 36.24 | 0.978808 |

Table 2. Coefficients *G, H, K, L, M, N* of regression Eqs 10–12 and coefficients of determination ($R^2$)

| | *G* (mPa.s) | *H* (l) | $R^2$ | *K* (mm²/s) | *L* (1) | $R^2$ | *M* (1/Pa.s) | *N* (1) | $R^2$ |
|---|---|---|---|---|---|---|---|---|---|
| **Flower honey measurement** | | | | | | | | | |
| First | 202,185 | 0.104 188 | 0.969056 | 130,067 | 0.101353 | 0.967424 | 0.004975 | 0.104037 | 0.968316 |
| Next | 270,597 | 0.110 972 | 0.996520 | 174,024 | 0.108127 | 0.996333 | 0.003646 | 0.111313 | 0.996425 |
| **Forest honey measurement** | | | | | | | | | |
| First | 60,147.9 | 0.096 11 | 0.974692 | 41,287.8 | 0.09412 | 0.978836 | 0.016612 | 0.09614 | 0.974640 |
| Next | 91,376.4 | 0.102 37 | 0.984745 | 60,520.7 | 0.09983 | 0.984745 | 0.010924 | 0.10244 | 0.985470 |

ing exponential functions (Eqs 10 and 11) and in the case of temperature dependencies of fluidity increasing exponential functions (Eq. 12) can be used:

$$\eta = G e^{-H\left(\frac{t}{t_0}\right)} \quad \text{(Pa.s)} \tag{10}$$

$$\nu = K e^{-L\left(\frac{t}{t_0}\right)} \quad \text{(m}^2\text{/s)} \tag{11}$$

$$\varphi = M e^{N\left(\frac{t}{t_0}\right)} \quad \text{(1/Pa.s)} \tag{12}$$

where:

$\eta$ – dynamic viscosity (Pa.s)
$\nu$ – kinematic viscosity (m²/s)
$\varphi$ – fluidity (1/Pa.s)
$t$ – temperature (°C)
$t_0$ – equals to 1°C
*G, H, K, L, M, N* – constants dependent on kind of material, and on the ways of processing and storing

The influence of storage or storage time on rheologic properties of both types of honey was also examined.

The relations between the temperature and rheologic parameters like: dynamic viscosity and kinematic viscosity of the mixed flower honey and forest honey had a decreasing exponential shape which is in accordance with Arrhenius Eq. (4) while and temperature dependencies of fluidity had an increasing exponential shape for all measurements (Figs 4–6). The coefficients of determination were very high in all measurements, approximately in the range (0.97–0.99) (Table 2). Generally, the viscosity values of the mixed flower honey were higher than those of the forest honey sample and, on the contrary the values of fluidity were higher with the forest honey sample. The effect of the storage of the honey samples was also found.

From the presented results it is clear that dynamic and kinematic viscosity values were a little bit higher after storage due to the loosening of water during storage. The values of fluidity were a little bit smaller after storage, which was caused by the loosening of water respectively by crystallisation during the storage. Similar results were obtained by authors Sahin and Sumnu (2006), Figura and Teixeira (2007), and Cohen and Weihs (2010).

## DISCUSSION AND CONCLUSION

Very specific are food materials possessing variable chemical and physical properties depending

on the manipulation, external conditions and other factors which determine their behaviour. This article presents selected physical properties of honey. Out of many parameters of honey, mainly rheologic and thermal properties are very important in view of its mechanical and thermal manipulation. Based on facts presented, thermal and rheologic properties of selected Slovak honeys were examined, i.e. mixed flour honey and forest honey.

Thermophysical properties i.e. thermal conductivity, thermal diffusivity and specific heat and rheologic properties like dynamic viscosity, kinematic viscosity and also the fluidity of flower honey and forest honey were measured, analysed and also effects of temperature and storage time were examined. The results presented is clearly show that physical properties of all types of honey depend mostly on the temperature, time of storage, honey composition, and mixture of flowers visited by bees producing the honey and that they are different according to the locations, terms, and particular colony of bees.

## References


Assael M.J., Dix M., Gialou K., Vozár L., Wakeham W.A., 2002. Application of the transient hot-wire technique to the measurement of the thermal conductivity of solids. International Journal of Thermophysics, *3*: 615–633.

Bhandari B., D'Arcy B., Chow S., 1999. Rheology of selected Australian honeys. Journal of Food Engineering, *41*: 65–68.

Bird R.B., Stewart W.E., Lightfott E.N., 1960. Transport Phenomena. New York, John Wilie & Sons: 780.

Božiková M., Hlaváč P., 2010. Selected Physical Properties of Agricultural and Food Products. Nitra, SUA in Nitra: 178.

Codex Alimentarius of the Slovak Republic, 2004. Decree No. 1188/2004-100 of the Ministry of Agriculture and Ministry of Health of the Slovak Republic. 3rd part. Head IX relating to honey. Vestník Ministerstva pôdohospodárstva Slovenskej republiky, *15*: 43–48.

Chirife J., Buera M.P., 1997. A simple model for predicting the viscosity of sugar and oligosaccharide solutions. Journal of Food Engineering, *33*: 221–226.

Cohen I., Weihs D., 2010. Rheology and microrheology of natural and reduced-calorie Israeli honeys as a model for high-viscosity Newtonian liquids. Journal of Food Engineering, *100*: 366–371.

Davis W.R., 1984. Compendium of Thermophysical Property Measurement Methods. Vol. 1, Survey of Measurement Technique. New York, Plenum Press: 231.

Figura L.O., Teixeira A.A., 2007. Food Physics, Physical Properties – Measurement and Applications. New York, Springer: 550.

Ginzburg A.S., 1985. Termofyzikální vlastnosti potravinářských výrobků. [Thermophysical Properties of Food Materials.] Prague, SNTL: 291.

Hlaváč P., 2010. Rheologic properties of food materials. [Ph.D. Thesis.] Nitra, SUA in Nitra: 1–135.

Junzheng P., Changying J., 1998. General rheological model for natural honeys in China. Journal of Food Engineering, *36*: 165–168.

Krempaský J., 1969. Meranie termofyzikálnych veličín. [Measurements of Thermophysical Parameters]. Bratislava, Veda: 335.

Liang X.G., 1995. The boundary induced error on the measurement of thermal conductivity by transient hot wire method. Measurement Science and Technology, *6*: 467–471.

Munson B.R., Young D.F., Okiishi T.H., 1994. Fundamentals of fluid mechanics. New York, John Wilie & Sons: 843.

Sahin S., Sumnu S.G., 2006. Physical Properties of Foods. New York, Springer: 257.

Wechsler A.E., 1992. The probe method for measurement of thermal conductivity. In: Maglić K.D., Cezairliyan A., Peletsky V.E. (eds.), Compendium of Thermophysical Property Measurement Methods, Vol. 2 – Recommended Measurement Techniques and Practices. New York, London, Plenum Press: 281.

White J.W., 1975. Physical characteristics of honey. In: Crane E. (ed.), Honey, a Comprehensive Survey. London, Heinemann: 207–239.

White J.W., 1999. Honey. In: The Hive and the Honey Bee. Hamilton, Dandant & Sons: 491–530.

White J.W., Kushnir I., Subers M.H., 1964. Effect of storage and processing temperatures on honey quality. Food Technology, *18*: 153–156.

Zaitoun S., Ghzawi A., Al Malah K., Abu Jdayil B., 2000. Rheological properties of selected light colored Jordanian honey. International Journal of Food Properties, *4*: 139–148.


Received for publication July 2, 2012
Accepted after corrections February 6, 2013

*Corresponding author*:

doc. RNDr. Monika Božiková, Ph.D., Slovak University of Agriculture in Nitra, Faculty of Engineering, Department of Physics, Tr. A. Hlinku 2, 949 76 Nitra, Slovak Republic
phone: + 421 376 414 711, fax: + 421 37 741 7003, e-mail: monika.bozikova@uniag.sk

# Ammonia concentration in farrowing pens with permanent limited range of motion for lactating sows

M. Dubeňová[1], R. Gálik[2], Š. Mihina[2], T. Šima[2]

[1]*Department of Production Engineering, Faculty of Engineering, Slovak University of Agriculture in Nitra, Nitra, Slovak Republic*
[2]*Department of Machines and Production Systems, Faculty of Engineering, Slovak University of Agriculture in Nitra, Nitra, Slovak Republic*

**Abstract**

Dubeňová M., Gálik R., Mihina Š., Šima T., 2013. **Ammonia concentration in farrowing pens with permanent limited range of motion for lactating sows**. Res. Agr. Eng., *59* (Special Issue): S9–S14.

Livestock production significantly contributes to emissions of polluting gases emissions like ammonia ($NH_3$) and greenhouse gases. Pig production is globally responsible for about 15% of ammonia emissions. The aims of this paper were the comparison of the ammonia concentrations in the farrowing pens with permanent limited range of motion between the zones of lactating sows and piglets and the impact of the day hour on ammonia concentration in this place. Photoacoustic infrared measuring devices INNOVA were used. The average values of $NH_3$ concentration ranged from 0.787738 ppm (0.547478 mg/m$^3$) to 0.818091 ppm (0.568573 mg/m$^3$). The minimum concentration of $NH_3$ was measured in the second lactating sows zone (0.262535 ppm, 0.182462 mg/m$^3$) and the maximum concentration was measured in the piglets zone (1.61803 ppm, 1.124531 mg/m$^3$). Values measured met the requirements of the Decree No. 230/1998 of the Ministry of Agriculture and Rural Development of the Slovak Republic which allows the maximum concentration of $NH_3$ in the pig building 20 ppm (13.9 mg/m$^3$). There were no differences between the concentrations of the greenhouse gases (GHGes) in the zones of lactating sows and piglets.

**Keywords**: gas; farrowing pen; pig; piglet

Livestock production significantly contributes to the emissions of polluting gases like ammonia ($NH_3$) and greenhouse gases (Philippe et al. 2012). Ammonia is an important pollutant gas that accelerates fine particulate formation in the atmosphere and plays a crucial role in the acidification and eutrophication of ecosystem (Krupa 2003). Ammonia largely originates from agriculture representing about 95% of anthropogenic emissions (Galloway et al. 2004). The livestock sector is responsible for about 65% of global $NH_3$ emissions (Steinfeld et al. 2006), and pig production is globally responsible for about 15% of ammonia emissions (Olivier et al. 1998). By 2050, the global emissions of $NH_3$ are expected to double, principally owing to the demographic growth, changes in food preferences and the agricultural intensification (Clarisse et al. 2009). The main factors influencing $NH_3$ production are the floor type, the manure removal system (Mihina et al. 2011), the climatic conditions inside

Supported by the Scientific Grant Agency VEGA of the Ministry of Education of the Slovak Republic and the Slovak Academy of Sciences, Grant No. 1/0609/12.

the building, diet composition, and feed efficiency of animals (PHILIPPE et al. 2011a). Ammonia emissions are clearly correlated with the behaviour, ambient temperature, animal density (GUINGAND et al. 2010), ventilation system (TOPISIROVIC et al. 2010a, b), and floor system (PHILIPPE et al. 2006, 2010, 2011b; CABARAUX et al. 2009). The ventilation systems are mostly used to reduce and control dust concentration in pig houses (TOPISIROVIC, RADIVOJEVIC 2005; ECIM-DJURIC, TOPISIROVIC 2010). The Decree No. 230/1998 of the Ministry of Agriculture and Rural Development of the Slovak Republic allows maximum concentration of $NH_3$ in the pig building to be 20 ppm.

The aims of this paper are the comparison of the ammonia concentrations in the farrowing pens with a permanent limited range of motion between the zones of lactating sows and piglets, and the impact of the day hour on ammonia concentration in this place.

## MATERIAL AND METHODS

Three farrowing pens with permanent limited range of motion in the same barn were monitored. Samples of air were collected in each pen both in the lactating sows zone and the piglets zone. Monitoring was conducted during 24-h intervals with five repetitions ($n$ = 5).

**Characteristics of animals**. Sows of Large White breed with their piglets were used in the experiment. Basic characteristics of the pigs are shown in Table 1.

**Research place**. Pigs were housed in farrowing pens with permanent limited range of motion of lactating sows. Measurements were done in the Experimental Centre for Livestock of the Department of Animal Husbandry, Faculty of Agrobiology and Food Resources, Slovak University of Agriculture in Nitra, Nitra, Slovak Republic. Pens were 2 m wide and 2.4 m long. Natural ventilation and a fully slatted floor were used. The slurry was removed twice a month, and excreta was manually mechanically removed twice a day. The lactating sows were fed by a valve for feed wetting. The piglets had their own nipple drinkers. The sampling points in the piglets zone were placed in the corner of the bedded system for piglets, at the height of 0.25 m. The sampling points in the lactating sows zone were placed in the middle of the pen, at the height of 0.5 m.

**Measuring devices**. Devices of INNOVA (LumaSense Technolgies, Inc., Ballerup, Denmark) were used for the measurement of the gases concentration. The measuring system consists of three main parts. The first part is INNOVA 1412 – Photoacoustic field gas-monitor. The measurement system is based on the photoacoustic infrared detection method. Gaś selectivity is achieved through

Table 1. Basic characteristic of lactating sows and piglets (DUBEŇOVÁ et al. 2012b)

| Sample point | Sow weight (kg) | Piglets age (days) | Piglets weight (kg) | | Farrowing order | No. of piglets (pcs) |
|---|---|---|---|---|---|---|
| | | | range | average | | |
| 1 | 303 | 8 | 1.26–2.69 | 1.99 | 5 | 14 |
| 2 | 333 | 15 | 2.35–7.50 | 6.03 | 4 | 6 |
| 3 | 304 | 14 | 3.97–5.06 | 4.62 | 3 | 9 |

Table 2. Summary statistics of ammonia concentration in lactating sows zones (LSZ, number) and piglets zones (PZ, number); $n$ (number of measurement repetitions) = 5

| Sample | Count | Average (ppm) | SD (ppm) | Coeff. of variation (%) | Min. (ppm) | Max. (ppm) |
|---|---|---|---|---|---|---|
| LSZ1 | 216 | 0.810339 | 0.309596 | 38.21 | 0.290528 | 1.44897 |
| LSZ2 | 216 | 0.787738 | 0.324091 | 41.14 | 0.262535 | 1.82 |
| LSZ3 | 216 | 0.818066 | 0.326329 | 39.89 | 0.317265 | 1.52001 |
| PZ1 | 216 | 0.801471 | 0.318229 | 39.71 | 0.268961 | 1.61803 |
| PZ2 | 216 | 0.789686 | 0.337314 | 42.72 | 0.271418 | 1.47976 |
| PZ3 | 216 | 0.818091 | 0.339658 | 41.52 | 0.32529 | 1.60998 |

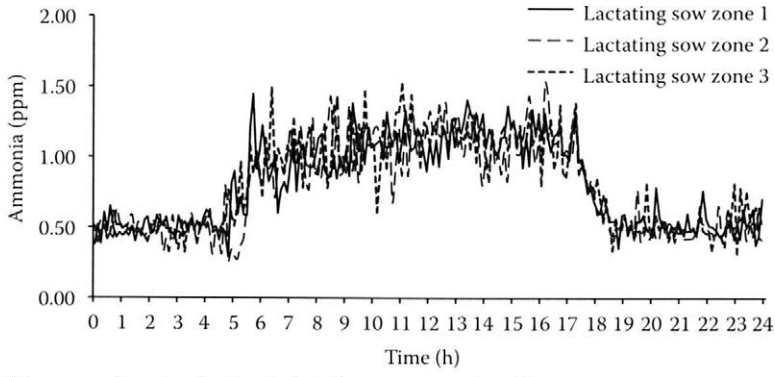


Fig. 1. Values of the ammonia concentration in lactating sows zones ($n$ = 5)

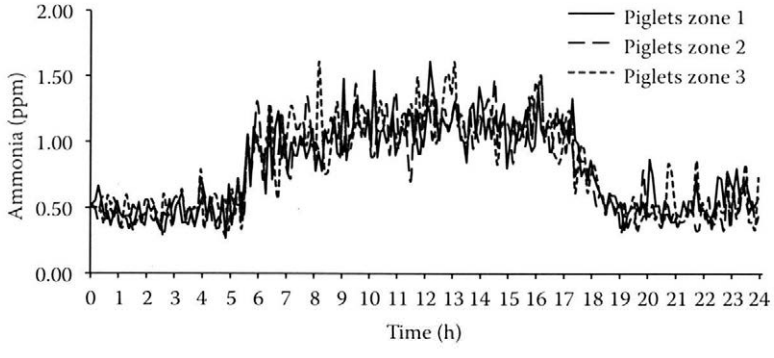


Fig. 2. Values of the ammonia concentration in piglets zones ($n$ = 5)

the use of optical filters. The detection limit is typically in the ppb (parts per bilion) region. The second part is INNOVA 1309 – multipoint sampler. This device is a 12 channel multiplexer, enabling gas samples to be drawn from up to 12 different sampling locations and delivered to the gas monitor INNOVA 1412. The third main part is a computer with the software supplied by the manufacturer, in which the data were saved (Dubeňová et al. 2012a, b).

**Statistical analysis**. The data were analysed by using Kruskal-Wallis test after the normality test using Kolmogorov-Smirnov procedure and the homogeneity of variance by using Levene's test. The software used was Statgraphics Centurion XVI.I (Statpoint Technologies, Inc., Warrenton, USA). Kruskal-Wallis test tests the null hypothesis that the medians within each of the six samples are the same. Since the $P$-value is greater than or equal to 0.05, no statistically significant difference occurs between the medians at 95.0% confidence level.

## RESULTS AND DISCUSSION

Three farrowing pens with permanent limited range of motion in the same barn were monitored. The monitoring was conducted during 24-h intervals with four repetitions. The samples of air were collected in each pen both in the lactating sow zone (LSZ, number) and in the piglets zone (PZ, number). The temperature and air humidity were measured every hour. The average value of temperature was 23.9°C and ranged from 20.3 to 27.1°C. The average value of air humidity was 58% and ranged from 44 to 67%.

The $P$-value in Kruskal-Wallis test was greater than 0.5 ($P$-value = 0.723974). No statistically significant difference was found between $NH_3$ concentrations in the lactating sows zones and piglets zones at the 95.0% confidence level.

The average values of $NH_3$ concentration ranged from 0.787738 ppm (0.547478 mg/m$^3$) to 0.818091 ppm (0.568573 mg/m$^3$)(Table 2). The min.

Table 3. Average values of ammonia concentration from 0 to 12 h/day in lactating sows zones (LSZ) and piglets zones (PZ), *n* (number of measurement repetitions) = 5

| Time range (h) | Ammonia concentration (ppm) | | | | | |
|---|---|---|---|---|---|---|
| | lactating sow zone | | | piglets zone | | |
| | 1 | 2 | 3 | 1 | 2 | 3 |
| 0–1 | 0.487478 | 0.498806 | 0.48815 | 0.51027 | 0.487723 | 0.502955 |
| 1–2 | 0.476792 | 0.498009 | 0.469214 | 0.425147 | 0.430193 | 0.432294 |
| 2–3 | 0.49537 | 0.453164 | 0.482297 | 0.452773 | 0.439877 | 0.473201 |
| 3–4 | 0.516359 | 0.492983 | 0.465278 | 0.448497 | 0.521809 | 0.5373 |
| 4–5 | 0.521271 | 0.442154 | 0.550766 | 0.478919 | 0.454481 | 0.482604 |
| 5–6 | 0.888893 | 0.626173 | 0.825715 | 0.730717 | 0.754871 | 0.732422 |
| 6–7 | 0.878973 | 0.902006 | 1.030439 | 0.964943 | 0.974023 | 0.94646 |
| 7–8 | 0.973921 | 1.016716 | 1.051974 | 0.945156 | 0.992164 | 1.125776 |
| 8–9 | 0.967766 | 1.085553 | 1.044719 | 0.954427 | 1.051929 | 1.062095 |
| 9–10 | 1.111477 | 1.106205 | 1.123325 | 1.144718 | 1.184368 | 1.111543 |
| 10–11 | 1.111386 | 1.064309 | 1.078154 | 1.087887 | 1.095204 | 1.165268 |
| 11–12 | 1.111491 | 1.097197 | 1.240652 | 1.099056 | 1.051559 | 1.156441 |

concentration of $NH_3$ was found in the second lactating sows zone (0.262535 ppm, 0.182462 mg/m$^3$) and the max. was detected in the piglets zone (1.61803 ppm, 1.124531 mg/m$^3$). The values measured met the requirements of the Decree of the Slovak Ministry of Agriculture No. 230/1998 which allows the max. concentration of $NH_3$ in the pig building of 20 ppm (13.9 mg/m$^3$). They also met the requirement of the reference document on best available techniques for intensive rearing of

Table 4. Average values of ammonia concentration from 12 to 24 h/day in lactating sows zones (LSZ) and piglets zones (PZ), *n* (number of measurement repetitions) = 5

| Time range (h) | Ammonia concentration (ppm) | | | | | |
|---|---|---|---|---|---|---|
| | lactating sow zone | | | piglets zone | | |
| | 1 | 2 | 3 | 1 | 2 | 3 |
| 12–13 | 1.095182 | 1.219488 | 1.19968 | 1.231693 | 1.182331 | 1.297738 |
| 13–14 | 1.253888 | 1.135958 | 1.148514 | 1.158282 | 1.111679 | 1.174325 |
| 14–15 | 1.145947 | 0.997191 | 1.078778 | 1.122504 | 1.216717 | 1.097822 |
| 15–16 | 1.153326 | 1.151786 | 1.174474 | 1.066754 | 1.092502 | 1.153028 |
| 16–17 | 1.134495 | 1.15721 | 1.053999 | 1.14801 | 1.163978 | 1.100929 |
| 17–18 | 0.947033 | 0.934847 | 0.980677 | 0.952193 | 0.882172 | 0.922263 |
| 18–19 | 0.577381 | 0.559231 | 0.571519 | 0.579131 | 0.562518 | 0.59465 |
| 19–20 | 0.513617 | 0.501596 | 0.524763 | 0.47322 | 0.468905 | 0.464848 |
| 20–21 | 0.53179 | 0.481313 | 0.489552 | 0.547354 | 0.437169 | 0.538188 |
| 21–22 | 0.539549 | 0.471461 | 0.492947 | 0.508673 | 0.438531 | 0.50466 |
| 22–23 | 0.483928 | 0.501226 | 0.50399 | 0.585442 | 0.443094 | 0.493801 |
| 23–24 | 0.530826 | 0.511125 | 0.563999 | 0.619535 | 0.514656 | 0.563569 |

poultry and pigs (IPPC Directive 2003) for ammonia the concentration with max. value of 10 ppm (6.95 mg/m$^3$). This result corresponds with our previous study where concentrations of the greenhouse gases (GHGes) $CO_2$, $N_2O$ (Dubeňová et al. 2012a), and $CH_4$ (Dubeňová et al. 2012b) were measured in farrowing pens with permanent limited range of motion for lactating sows. No differences occurred between the concentrations of GHGes in the zones of lactating sows and piglets. The differences between the min. and max. values were 0.062755 ppm (0.043615 mg/m$^3$) and 0.16906 ppm (0.1175 mg/m$^3$). They may be caused by an increased restlessness of the lactating sows.

The differences between the $NH_3$ concentrations during all day are shown in Figs 1 and 2 and Tables 3 and 4 (showing the average values from all the repetitions of the measurement). The changes in concentration are shown depending on the timetable of routine day works and animals activity. The feeding started at 6:30 a.m. However, the activity of the lactating sows started about one hour before feeding and the activity of piglets started about 30 min after increasing activity of the lactating sows increased. With the lactating sows it may have been caused by the feeding time habit. The activity of the piglets depended on the sows activity. The last daily control was at 4 p.m. upon which about one hour the concentration of $NH_3$ decreased. This may have been caused by the decreasing activity because the animals were not disturbed by personnel.

## CONCLUSION

The aim of this paper was the comparison of ammonia concentrations in the farrowing pens with permanent limited range of motion between the zones of lactating sows and piglets and the impact of the day hour on ammonia concentration in this place. There was no difference between the concentrations of GHGes in the zones of lactating sows and piglets. The average values of $NH_3$ concentration ranged from 0.787738 ppm (0.547478 mg/m$^3$) to 0.818091 ppm (0.568573 mg/m$^3$). The min. concentration of $NH_3$ was measured in the second lactating sows zone (0.262535 ppm, 0.182462 mg/m$^3$) while the max. concentration was measured in the piglets zone (1.61803 ppm, 1.124531 mg/m$^3$). The measured values found meet the requirements of the Decree No. 230/1998 of the Ministry of Agriculture and Rural Development of the Slovak Republic which allows the maximum concentration of $NH_3$ in the pig building to reach 20 ppm (13.9 mg/m$^3$). They also meet the requirement of the reference document on best available techniques for intensive rearing of poultry and pigs (IPPC Directive 2003) for ammonia concentration with max. value 10 ppm (6.95 mg/m$^3$).

## References


Cabaraux J.F., Philippe F.X, Laitat M., Canart B., Vandenheede M., Nicks B., 2009. Gaseous emissions from weaned pigs raised on different floor systems. Agriculture, Ecosystems and Environment, *130*: 86–92.

Clarisse L., Clerbaux C., Dentener F., Hurtmans D., Coheur P.-F., 2009. Global ammonia distribution derived from infrared satellite observations. Nature Geoscience, 2: 479–483.

Decree No. 230/1998 of the Ministry of Agriculture of the Slovak Republic. Collection of Laws on the breeding of farm animals and killing of slaughter animals.

Dubeňová M., Gálik R., Mihina Š., Šima T., 2012a. Nitrous oxide and carbon dioxide concentration in farrowing pens with permanent limited range of motion for lactating sows. Poljoprivredna tehnika, *37*: 101–109.

Dubeňová M., Gálik R., Mihina Š., Šima T., 2012b. Methane concentration in the place for lactating sows and piglets in the stall with the permanent limited range of motion. In: Proceedings MendelTech International, March 29–30, 2012. Lednice.

Ecim-Djuric O., Topisirovic G., 2010. Energy efficiency optimization of combined ventilation systems in livestock buildings. Energy and Buildings, *42*: 1165–1171.

Galloway J.N., Dentener F.J., Capone D.G., Boyer E.W., Howarth R.W., Seitzinger S.P., Asner G.P., Cleveland C.C., Green P.A., Holland E.A., Karl D.M., Michaels A.F., Porter J.H., Townsend A.R., Vorosmarty C.J., 2004. Nitrogen cycles: past, present and future. Biogeochemistry, *70*: 153–226.

Guingand N., Quiniou N., Courboulay V., 2010. Comparison of ammonia and greenhouse gas emissions from fattening pigs kept either on partially slatted floor in cold conditions or on fully slatted floor in thermoneutral conditions. Journées de la Recherche Porcine, *42*: 277–284.

IPPC Directive, 2003. Integrated Pollution Prevention and Control. Reference Document on Best Available Techniques for Intensive Rearing of Poultry and Pigs. Brussles, European Commission.

Krupa S.V., 2003. Effects of atmospheric ammonia ($NH_3$) on terrestrial vegetation: a review. Environmental Pollution, *124*: 179–221.

Mihina Š., Karandušovská I., Lendelová J., Boďo Š., 2011. Produkcia škodlivých plynov v objektoch pre výkrm

ošípaných s rôznym spôsobom odstraňovania hnoja. [Production of harmful gases and in the buildings for fattening pigs with different ways of manure removal.] In: Proceedings Rural Buildings 2011. Nitra: 84–92.

Olivier J.G.J., Bouwman A.F., Van der Hoek K.W., Berdowski J.J.M., 1998. Global air emission inventories for anthropogenic sources of $NO_x$, $NH_3$ and $N_2O$ in 1990. Environmental Pollution, *102*: 135–148.

Philippe F.X., Laitat M., Vandenheede M., Canart B., Nicks B., 2006. Comparison of zootechnical performances and nitrogen contents of effluent for fattening pigs kept either on slatted floor or on straw-based deep litter. Annales de Médecine Vétérinaire, *150*: 137–144.

Philippe F.X., Canart B., Laitat M., Wavreille J., Bartiaux-Thill N., Nicks B., Cabaraux J.F., 2010. Effects of available surface on gaseous emissions from group-housed gestating sows kept on deep litter. Animal, *4*: 1716–1724.

Philippe F.X., Cabaraux J.F., Nicks B., 2011a. Ammonia emissions from pig houses: Influencing factors and mitigation techniques. Agriculture, Ecosystems and Environment, *141*: 245–260.

Philippe F.X., Laitat M., Wavreille J., Bartiaux-Thill N., Nicks B., Cabaraux J.F., 2011b. Ammonia and greenhouse gas emission from group-housed gestating sows depends on floor type. Agriculture, Ecosystems and Environment, *140*: 498–505.

Philippe F.X., Laitat M., Nicks B., Cabaraux J.F., 2012. Ammonia and greenhouse gas emissions during the fattening of pigs kept on two types of straw floor. Agriculture, Ecosystems and Environment, *150*: 45–53.

Steinfield H., Gerber P., Wassenaar T., Castel V., Rosales C., de Haan C., 2006. Livestock's Long Shadow: Environmental Issues and Options. Rome, FAO: 375.

Topisirovic G., Radivojevic D., 2005. Influence of ventilation systems and related energy consumption on inhalable and respirable dust concentrations in fattening pigs confinement buildings. Energy and Buildings, *37*: 1241–1249.

Topisirovic G., Radojičic D., Dražic M., 2010a. Mogućnosti poboljšanja efektada rada ventilacionog sistema u odeljenjima prasilište i odgajalište na farmi svinja "Farkaždin". [Possibilities for improvement of ventilation systems efficiency in pig farm farrowing room and nursery.] Poljoprivredna tehnika, *35*: 5–16.

Topisirovic G., Radojičic D., Radivojevic D. 2010b. Predlog poboljšanja ambijentalnih uslov u objektima za tov svinja na farmi "Vizelj" [Possible improvement of ambient conditions in fattening pigs confinement building on the pig farm „Vizelj".] Poljoprivredna tehnika, *35*: 17–25.

Received for publication July 2, 2012
Accepted after corrections November 29, 2012

*Corresponding author*:

Ing. Monika Dubeňová, Slovak University of Agriculture in Nitra, Faculty of Engineering, Department of Production Engineering, Tr. A. Hlinku 2, 949 76 Nitra, Slovak Republic
phone: + 421 376 415 677, e-mail: monika.dubenova@post.sk

# Effect of crop residues on $CO_2$ flux in the CTF system during soil tillage by a disc harrow Lemken Rubin 9

T. Šima[1], M. Dubeňová[2]

[1]*Department of Machines and Production Systems, Faculty of Engineering, Slovak University of Agriculture in Nitra, Nitra, Slovak Republic*
[2]*Department of Production Engineering, Faculty of Engineering, Slovak University of Agriculture in Nitra, Nitra, Slovak Republic*

**Abstract**

Šima T., Dubeňová M., 2013. **Effect of crop residues on $CO_2$ flux in the CTF system during soil tillage by a disc harrow Lemken Rubin 9**. Res. Agr. Eng., *59* (Special Issue): S15–S21.

Carbon dioxide is one of the most important greenhouse gases. Agriculture, especially soil tillage, contributes to $CO_2$ emissions significantly. The aim of the paper was the comparison of the amounts of carbon dioxide emissions released from the soil into the atmosphere depending on the controlled traffic farming (CTF) and crop residues. Three variants of the experiment were realised: before the soil tillage, immediately after the soil tillage, and seven days after the soil tillage. The soil tillage was carried out after the harvest of winter wheat by disc harrow Lemken Rubin 9 with a tractor John Deere 8230 on the loamy soil. The monitoring points were selected in parts of the field with and without the crop residues and in trafficked and non-trafficked areas. The CTF system affects $CO_2$ flux, the amounts of emissions from the non-trafficked areas being higher than those from the trafficked areas. The crop residues left on the field cause a decrease of $CO_2$ flux. The incorporation of crop residues causes an increase of $CO_2$ flux.

**Keywords**: carbon dioxide; emissions from the soil; controlled traffic farming; soil compaction

Agriculture causes some environmental problems, mainly the greenhouse effect, contamination of water resources, and soil erosion. Carbon dioxide ($CO_2$) is one of the three most important greenhouse gases (Reicosky, Lindstrom 1993; Inselsbacher et al. 2011). Atmospheric concentrations of $CO_2$ are increasing at a rate of approximately 0.6% per year (IPCC 2007). Since this increase contributes to the changes in the Earth's climate, the interest in quantifying significant sources and sinks of $CO_2$ is growing and the international community has taken steps to reduce these emissions (Flessa et al. 2002; Reicosky e t al. 2005). The emissions released from the arable soil into the atmosphere are relatively small when compared with other sources, but the total area of the agricultural land is a source of a huge amount of emissions. The intensification of agriculture and continued upward pressure on the food production in sufficient quantity and adequate quality result in environmental aspects being side-lined (Šima et al. 2012). The controlled traffic farming is facilitated by the integration of information and communication technologies in farming (Auernhammer 2001; Chamen 2007) and that is a technology which minimises the compacted area of the field. It has the potential to increase the

Supported by the EU Operational Programme Research and Development, Project No. ITMS 26220220014.

economic (KINGWELL, FUCHSBICHLER 2011) and environmental benefits (ZHANG et al. 2002). The controlled traffic farming (CTF) confines all field traffic and compaction to permanent traffic lanes and reduces field trafficking (MAJDAN et al. 2011), improves the soil porosity and infiltration (KRIŠTOF et al. 2012; SMITH et al. 2012). The soil compaction is one of the most important factors which influences the aeration of the soil, nutrient uptake efficiency, emissions of greenhouse gases like $CO_2$ and $NO_x$, and affects the quality of the soil tillage (FRANČÁK et al. 2004; PÁLTIK et al. 2007; PONIČAN, KORENKO 2008; FINDURA et al. 2009). Precision agriculture increases the crop production efficiency (KRIŠTOF, HAŠANA 2007; LÍŠKA et al. 2008). The incorporation of the crop residues into the soil has been widely accepted to maintain soil fertility and enhance crop productivity. The incorporation of residues supplies additional C and N into the soil (ZOU et al. 2004) and affects $CO_2$ flux (REICOSKY et al. 2002). The soil tillage causes an accelerated flux of carbon dioxide emissions released from the soil into the atmosphere (REICOSKY 1997, 2001; BUC et al. 2010; KRIŠTOF et al. 2011; MACÁK et al. 2011).

The aim of this paper was the comparison of the amounts of carbon dioxide emissions released from the soil into the atmosphere depending on the controlled traffic farming and crop residues.

## MATERIAL AND METHODS

The experiment was carried out at the SUA University Farm Kolíňany Ltd., Kolíňany, Slovak Republic. The controlled traffic farming was implemented in a 16 ha field "Pri Jeleneckej ceste". The measurements of carbon dioxide emissions released from the soil into the atmosphere were realised after the harvest of wheat. The soil tillage was carried out by disc harrow Lemken Rubin 9 (Lemken GmbH & Co., Alpen, Germany) with the tractor John Deere 8230 (John Deere, Moline, USA).

There were three variants of the experiment:
- before the soil tillage,
- immediately after the soil tillage,
- seven days after the soil tillage.

Four monitoring points were selected:
- trafficked area with the crop residues (T-CR),
- trafficked area tracks without the crop residues (T-noCR),
- non-trafficked area tracks with the crop residues (nT-CR),
- non-trafficked area tracks without the crop residues (nT-noCR).

The amount of the crop residues was 0.897 kg/m$^2$. Loamy soil was studied. The soil bulk density for the trafficked and non-trafficked areas was 1.69 and 1.38 g/cm$^3$, respectively. The soil moisture content was measured by a gravimetric method and ranged from 11.54 to 12.31%, and pH in the trafficked area was 7.32 and 6.06 for $H_2O$ and KCl, respectively. The non-trafficked area pH reaction was 7.37 and 6.11 for $H_2O$ and KCl, respectively. The soil properties were analysed at the Department of Soil Science and Geology at the Slovak University of Agriculture in Nitra, Nitra, Slovak Republic.

**Methodical procedure**. The used method of measuring $CO_2$ emissions released from the soil into the atmosphere was that described by ŠIMA et al. (2012). The laboratory method consists of collecting soil samples from the field and their subsequent analysis in the laboratory. Big sampling probes were inserted into the soil at 150 mm depth, the surrounding soil was removed and the sampling probes were closed up from the bottom. INNOVA devices (LumaSense Technologies, Ballerup, Denmark) were used consisting of a photoacoustic field gas monitor INNOVA 1412 based on the photoacoustic infrared detection method, a multipoint sampler INNOVA 1309 used for the transport of the gas samples to the gas analyser INNOVA 1412, and a notebook with the operation software used for the control and setup of the analysis.

**Statistical analysis**. The data were analysed by using the ANOVA or Kruskal-Wallis test after normality test by using the Kolmogorov-Smirnov test and the homogeneity of variance by using the Levene's test. With ANOVA $P < 0.05$ we continued in the post-hoc LSD test. With Kruskal-Wallis test $P < 0.05$ we continued in the post-hoc Turkey's HSD test. We used the software Statgraphics Centurion XVI.I (Statpoint Technologies, Warrenton, USA). The graphic processing of the results was performed using the software Statistica 7 (Statsoft, Tulsa, USA).

## RESULTS AND DISCUSSION

The soil tillage, crop residues, and soil compaction affect carbon dioxide emissions released from the soil to the atmosphere (Fig. 1). A multifactor analysis of variance for $CO_2$ emissions was used. $P$-values for the time interval, variants and their

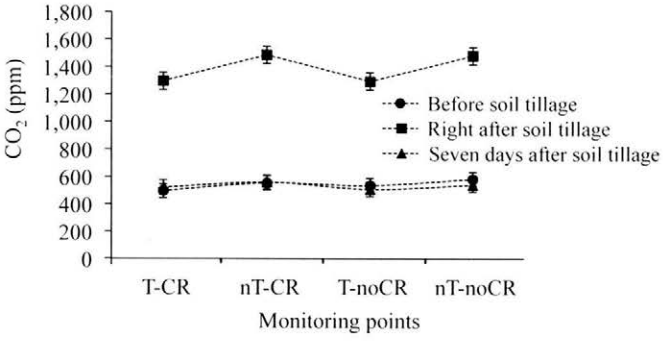


Fig. 1. Interactions and 95.0% confidence level for all variants of the experiment T-CR – trafficked area with crop residues; T-noCR – trafficked area without crop residues; nT-CR – non-trafficked area with crop residues; nT-noCR – non-trafficked area without crop residues

Table 1. Multiple Range tests 95.0% LSD for monitoring points

| Monitoring point | Count | LS Mean | LS Sigma | Homogeneous groups | |
|---|---|---|---|---|---|
| T-CR | 235 | 770.139 | 16.5052 | × | |
| T-noCR | 235 | 778.503 | 16.5052 | × | |
| nT-CR | 235 | 865.069 | 16.5052 | | × |
| nT-noCR | 235 | 868.655 | 16.5052 | | × |

LSD – least significant difference; LS – least squares; for abbreviations see Fig. 1

interaction were 0.0000, 0.0000 and 0.0083, respectively. Both factors had a statistically significant effect on $CO_2$ emissions at the 95.0% confidence level. Multiple Range tests for two factor affected $CO_2$ flux denote statistically significant differences between the trafficked and non-trafficked areas (Tables 1 and 2). The soil compaction significantly affects the flux of $CO_2$ released from the soil into the atmosphere at 95.0% confidence level. Tables 3 and 4 show that a statistically significant difference exists between the amounts of $CO_2$ emissions released from the soil into the atmosphere in the variant immediately after the soil tillage and those before the soil tillage and seven days after the soil tillage.

Table 2. Statistically significant difference for monitoring points

| Contrast | Significant | Difference | +/– Limits |
|---|---|---|---|
| T-CR – T-noCR | | –8.36405 | 45.7493 |
| T-CR – nT-CR | * | –94.9297 | 45.7493 |
| T-CR – nT-noCR | * | –98.5161 | 45.7493 |
| T-noCR – nT-CR | * | –86.5656 | 45.7493 |
| T-noCR – nT-noCR | * | –90.1521 | 45.7493 |
| nT-CR – nT-noCR | | –3.58647 | 45.7493 |

*denotes a statistically significant difference; for abbreviations see Fig. 1

### Before soil tillage

By using the Kolmogorov-Smirnov test, we did not find a normal distribution for any sets of values tested. The Kruskal-Wallis test was used. The *P*-value of the Kruskal-Wallis test ($P = 0$) was below 0.05 indicating that a statistically significant difference existed between the medians at 95.0% confidence level. To determine which means were significantly different, the Multiple Range test Turkey HSD was used (Table 5). The carbon dioxide emissions released from the soil into the atmosphere were affected by the crop residues on the soil surface and the trafficked and non-trafficked areas in the field. Table 5 shows that there were statistically significant differences between the monitoring points. Leaving the crop residues on the soil surface positively affected carbon dioxide flux from the soil into the atmosphere in the untilled soil with 8.24% and 5.60% in the trafficked and non-trafficked area, respectively. A positive environmental effect of the crop residues on the soil surface before the soil tillage was 2.42% higher in the trafficked area. The soil surface without the crop residues was a more

Table 3. Multiple Range tests 95.0% LSD for the variants of the experiment

| Variant | Count | LS Mean | LS Sigma | Homogeneous groups | |
|---|---|---|---|---|---|
| Seven days after soil tillage | 344 | 531.212 | 13.4008 | × | |
| Before soil tillage | 360 | 541.035 | 13.0997 | × | |
| Right after soil tillage | 236 | 1389.53 | 16.1791 | | × |

for abbreviations see Table 1

Table 4. Statistically significant difference for the variants of the experiment

| Contrast | Significant | Difference | +/– Limits |
|---|---|---|---|
| Before soil tillage – right after soil tillage | * | –848.492 | 40.8015 |
| Before soil tillage – seven days after soil tillage | | 9.82281 | 36.7296 |
| Right after soil tillage – seven days after soil tillage | * | 858.315 | 41.1755 |

*denotes a statistically significant difference

Table 5. Multiple Range test Turkey's HSD of samples before soil tillage

| Sample | Count | Mean | Homogeneous groups | | |
|---|---|---|---|---|---|
| T-CR | 90 | 494.214 | × | | |
| nT-CR | 90 | 552.04 | | | × |
| T-noCR | 90 | 534.952 | | × | |
| nT-noCR | 90 | 582.934 | | | × |

for abbreviations see Table 1

significant source of $CO_2$ emissions than the monitoring points with the crop residues. Emission flux from the trafficked area was lower than that from the non-trafficked area with 11.70 and 8.89% for the variants with and without the crop residues on the soil surface, respectively. These results (Fig. 2) are in agreement with the results obtained by Nozdrovický et al. (2011).

### Immediately after soil tillage

By using the Kolmogorov-Smirnov test, we found a normal distribution for all tested sets of values. The ANOVA test was used. The *P*-value of ANOVA was below 0.05 ($P = 0.036$). There was a statistically significant difference between the means of values at 95.0% confidence level. To determine which means were significantly different, the Multiple Range tests LSD test was used (Table 6). The soil tillage had an effect on carbon dioxide emissions flux. Table 6 shows no statistically significant difference between releasing $CO_2$ emissions from the monitoring points with and without the crop residues incorporated into the soil. A significant difference was found between the trafficked and non-trafficked areas in the field. The CTF system significantly affected carbon dioxide flux. The soil from the non-trafficked area released more emissions than the trafficked soil (Fig. 3), with 14.72 and 14.57% for the variants with and without the crop residues incorporated into the soil.

### Seven days after soil tillage

Using the Kolmogorov-Smirnov test, we found a normal distribution for all tested sets of values. The ANOVA test was used. The *P*-value of ANOVA was below 0.05 ($P = 0.0000$). A statistically significant difference existed between the means of values at the 95.0% confidence level. To determine which means were significantly different, the Multiple Range tests LSD test was used (Table 7). The measurement conducted seven days after the soil tillage showed a statistically significant difference in all variants of the experiment. The negative effect of the crop residues incorporated into the soil on carbon dioxide flux was 2.96 and 3.22% in the trafficked and non-trafficked areas, respectively. It may be have been caused by organic matter decomposition. The soil compaction affected $CO_2$ flux. There was a higher amount of $CO_2$ in the non-trafficked area, with 6.69 and 6.68% in the variants with and

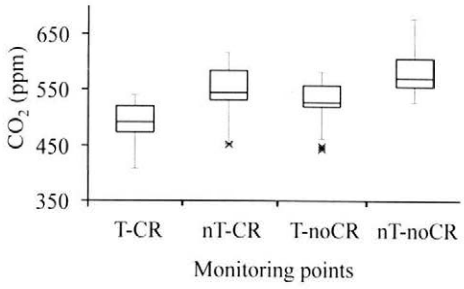


Fig. 2. Box-and-Whisker diagram of $CO_2$ concentration in monitoring points before soil tillage

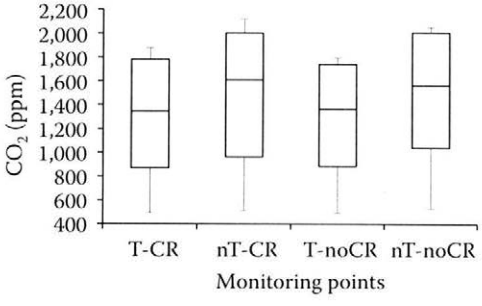


Fig. 3. Box-and-Whisker diagram of $CO_2$ concentration in monitoring points immediately after soil tillage

Table 6. Multiple Range test LSD of samples immediately after soil tillage

| Sample | Count | Mean | Homogeneous groups | |
|---|---|---|---|---|
| T-CR | 59 | 1,295.03 | × | |
| nT-CR | 59 | 1,485.72 | | × |
| T-noCR | 59 | 1,294.36 | × | |
| nT-noCR | 59 | 1,483.0 | | × |

for abbreviations see Fig. 1 and Table 1

Table 7. Multiple Range test LSD of samples seven days after soil tillage

| Sample | Count | Mean | Homogeneous groups | |
|---|---|---|---|---|
| T-CR | 86 | 521.176 | × | |
| nT-CR | 86 | 557.443 | | × |
| T-noCR | 86 | 506.199 | × | |
| nT-noCR | 86 | 540.029 | | × |

for abbreviations see Fig. 1 and Table 1

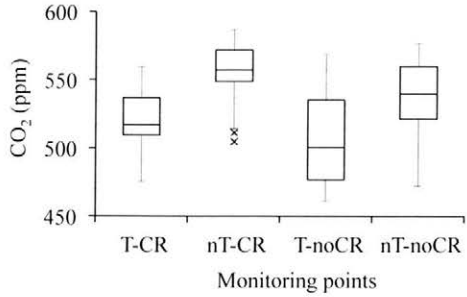


Fig. 4. Box-and-Whisker diagram of $CO_2$ concentration in monitoring points seven days after soil tillage

without the crop residues in the soil, respectively. The CTF system and crop residues in the soil affected carbon dioxide flux. These results (Fig. 4) are in agreement with the results obtained by Buc et al. (2011).

## CONCLUSION

Carbon dioxide emissions released from the soil into the atmosphere are one of the most important factors affecting the environment. The management of the crop production respecting environmental conditions may reduce carbon dioxide emissions in the global perspective. This study focused on analysing the effects of the crop residues left on the field and those incorporated into the soil in controlled traffic farming on releasing carbon dioxide emissions. The CTF system affects $CO_2$ flux, the amounts of emissions from the non-trafficked areas are higher than those from the trafficked areas. The crop residues left on the field decrease $CO_2$ flux. The effect of the crop residues on $CO_2$ emissions immediately after the soil tillage has not been shown. The incorporation of the crop residues causes an increasing $CO_2$ flux, which may be caused by organic matter decomposition.

## References

Auernhammer H., 2001. Precision farming – the environmental challenge. Computers and Electronics in Agriculture, *30*: 31–43.

Buc M., Nozdrovický L., Krištof K., 2010. Effect of the soil tillage practices on the $CO_2$ emissions from the soil to the atmosphere. In: A magyar megújuló energia stratégiai hangsúlyai, és kísérleti bemutatása: konferenciakiadvány.

[The Hungarian Renewable Energy Conference.] January 14, 2010. Gyöngyös: 67–70.

Buc M., Krištof K., Nozdrovický L., Šima T., 2011. Skúmanie vplyvu riadeného pohybu strojov na množstvo uvoľňovaných emisií $CO_2$ z pôdy do atmosféry. [Effect of controlled movement of machines to $CO_2$ flux.] In: Proceedings of the XIII$^{th}$ International Conference of Young Scientist 2011, September 19–20, 2011. Prague: 16–21.

Chamen W.C.T., 2007. Controlled-traffic farming as a complementary practice to no-tillage. In: Baker C.J., Saxton K.E., Ritchie W.R., Reicosky D.C., Ribeiro F., Justice S.E., Hobbs P.R., 2007. No-tillage and Seeding in Conservation Agriculture. FAO: 236–256.

Findura P., Buc M., Krištof K., Turan J., Ponjičan O., 2009. Hodnotenie kvality práce radličkového a tanierového kypriča. [Evaluation of the quality of work tine tiller and disc tiller.] In: Proceedings of the XIII$^{th}$ International Conference of Young Scientist 2009, June 17–19, 2009. Zvolen.

Flessa H., Ruser R., Dörsch P., Kamp T., Jimenez M.A., Munch J.C., Beese F., 2002. Integrated evaluation of greenhouse gas emissions ($CO_2$, $CH_4$, $N_2O$) from two farming systems in southern Germany. Agriculture, Ecosystems and Environment, *91*: 175–189.

Frančák J., Gálik R., Kováč Š., Korenko M., Simoník J., Zacharda F., 2004. Mechanizácia poľnohospodárskej výroby. [Machinery for Agriculture Production.] Nitra, Slovak University of Agriculture in Nitra: 201.

Inselsbacher E., Wanek W., Ripka K., Hackl E., Sessitsch A., Strauss J., Zechmeister-Boltenstern S., 2011. Greenhouse gas fluxes respond to different N fertilizer types due to altered plant-soil-microbe interactions. Plant & Soil, *343*: 17–35.

IPCC, 2007. Intergovernmental panel on climate change 2007. Synthesis report. IPCC, Geneva.

Kingwell R., Fuchsbichler A., 2011. The whole-farm benefits of controlled traffic farming: An Australian appraisal. Agricultural Systems, *104*: 513–521.

Krištof K., Hašana R., 2007. Presné poľnohospodárstvo ako prostriedok k efektívnej rastlinnej výrobe. [Precision agriculture as a tool for effective crop production.] Naše pole, *11*: 22–23.

Krištof K., Buc M., Nozdrovický L., Šima T., 2011. Vplyv technológie spracovania pôdy na množstvo uvoľňovaných emisií CO2 z pôdy do atmosféry. [Effect of the soil tillage technology on the amount of $CO_2$ emissions released from the soil to the atmosphere.] In: Proceedings of the XIII$^{th}$ International Conference of Young Scientist 2011, September 19–20, 2011. Prague: 111–115.

Krištof K., Smith E.K., Misiewicz P.A., Kroulik M., White D.R., Godwin R.J., 2012. Establishment of a long term experiment into tillage and traffic management. Part two: Evaluation of spatial heterogeneity for the design and layout of experimental sites. In: Proceedings of the International Conference of Agricultural Engineering, July 8–12, 2012. Valencia.

Líška E., Bajla J., Candráková E., Frančák J., Hrubý D., Ílleš L., Korenko M., Nozdrovický L., Pospíšil R., Špánik F., Žembery J., 2008. Všeobecná rastlinná výroba. [General Crop Production.] Nitra, Slovak University of Agriculture in Nitra: 421.

Macák M., Nozdrovický L., Buc M., 2011. Skúmanie účinkov náradia pre spracovanie pôdy na uvoľňovanie emisií $CO_2$ z pôdy do atmosféry. [Research of the soil tillage on $CO_2$ emissions released from soil to the atmosphere.] Mechanizace zemědělství, *61*: 31–38.

Majdan R., Tkáč Z., Kosiba J., Cvíčela P., Drabant Š., Tulík J., Stančík B., 2011. Zisťovanie súboru vlastností pôdy z dôvodu merania prevádzkových režimov traktora pre aplikáciu ekologickej kvapaliny. [The soil properties determination by reason of a measurement of tractor operating regimes for biodegradable fluid application.] In: Proceedings of Technics in Agrisector Technologies, November 3, 2011. Nitra, Slovak University of Agriculture in Nitra: 71–75.

Nozdrovický L., Macák M., Rataj V., Galambošová J., Buc M., 2011. Výskum účinkov technológií a techniky pre obrábanie pôdy s ohľadom na intenzitu uvoľňovania emisií $CO_2$ do atmosféry. [The Impacts of the Technologies and Machines for Soil Tillage on the $CO_2$ Flux from Soil to the Atmosphere.] Nitra, Slovak University of Agriculture in Nitra: 111.

Páltik J., Findura P., Maga J., Korenko M., Angelovič M., 2007. Poľnohospodárske stroje: skúšanie, konštrukcia, použitie – 1. Cast. [Agricultural Machines: Testing, Construction, Application – 1$^{st}$ Part.] Nitra, Slovak University of Agriculture: 190.

Poničan J., Korenko M., 2008. Stroje pre rastlinnú výrobu: stroje na zber krmovín, zrnín, ľanu, zemiakov, zeleniny a ovocia. [Machines for Crop Production: Machines for Forage, Grain, Flax, Potatoes, Vegetable and Fruit.] Nitra., Slovak University of Agriculture in Nitra: 248.

Reicosky D.C., 1997. Tillage-inducted $CO_2$ emission from soil. Nutrient Cycling in Agroecosystems, *49*: 273–285.

Reicosky D.C., 2001. Tillage-inducted $CO_2$ emissions and carbon sequestration: effect of secondary tillage and compaction. In: Garcia R. et al. (eds.), Conservation Agriculture: A Worldwide Challenge XUL. Cordoba: 265–274.

Reicosky D.C., Lindstrom M.J., 1993. Fall tillage method: effect on short term carbon dioxide flux from soil. Agronomy Journal, *85*: 1237–1243.

Reicosky D.C., Evans S.D., Cabardella C.A., Almaras R.R., Huggins D.R., 2002. Continuous corn with mouldboard tillage: residue and fertility effects on soil carbon. Journal of Soil and Water Conservation, *57*: 277–284.

Reicosky D.C., Lindstrom M.J., Schumacher T.E., Lobb D.E., Malo D.D., 2005. Tillage-inducted $CO_2$ loss across an eroded landscape. Soil and Tillage Research, *81*: 183–194.

Šima T., Nozdrovický L., Krištof K., Dubeňová M., Macák M., 2012. A comparison of the field and laboratory methods of measuring $CO_2$ emissions released from soil to the atmosphere. Poljoprivredna tehnika, *37*: 63–72.

Smith E.K., Kristof K., Misiewicz P.A., Chaney K., White D.R., Godwin R.J., 2012. Establishment of a long term experiment into tillage and traffic management. Part one: study background and experimental design. In: International Conference of Agricultural Engineering, July 8–12, 2012. Valencia.

Zhang N., Wang M., Wang N., 2002. Precision agriculture: a worldwide overview. Computers and Electronics in Agriculture, *36*: 113–132.

Zou J., Huang Y., Zong L., Zheng X., Wang Y., 2004. Carbon dioxide, methane and nitrous oxide emissions from a rice-wheat rotation as affected by crop residue incorporation and temperature. Advances in Atmospheric Sciences, *21*: 691–698.

Received for publication February 5, 2013
Accepted after corrections July 2, 2012

*Corresponding author*:

Ing. Tomáš Šima, Slovak University of Agriculture in Nitra, Faculty of Engineering,
Department of Machines and Production Systems, Tr. A. Hlinku 2, 949 76 Nitra, Slovak Republic
phone: + 421 376 414 351, e-mail: tomasko.sima@gmail.com

# Gyroscope calibration with the method of simulated identification

V. Cviklovič, D. Hrubý, M. Olejár, L. Priatková

*Department of Electrical Engineering, Automation and Informatics, Faculty of Engineering, Slovak University of Agriculture in Nitra, Nitra, Slovak Republic*

**Abstract**

Cviklovič V., Hrubý D., Olejár M., Priatková L., 2013. **Gyroscope calibration with the method of simulated identification**. Res. Agr. Eng., 59 (Special Issue): S22–S26.

The calibration of Micro-Electro-Mechanical System (MEMS) gyroscopes is important for the application in which an angle is measured. The equipment for the calibration of this sensor is not always available. In this case, the method of simulated identification can be used. Some of the conditions are: using different tracks with saving angular velocity measurements, knowledge of influencing variables with their monitoring, and knowledge of the initial and final states of the angle. Based on this information, an algorithm is designed for the correction of influencing parameters by computer equipment. In our case, offsets, gains, and cross coupling coefficients are calculated for each axis of a sensor ADIS16405BLMZ. The result is an error of up to 0.5°/min of movement. To obtain high accuracy results, it is necessary to reach the conditions which are described in this contribution.

**Keywords**: simulation; angular velocity; Simpson's rule; MEMS sensors

Nowadays, the science sometimes focuses on tasks in which it is not possible to calibrate sensors non-electrical values in real time for different reasons. The situation is complicated when the measured value is obtained indirectly – by computation and depends on previous states. This one is a typical example of angular displacement measuring and actual data position provided by accelerometers and gyroscopes in strap-down inertial navigations.

The gyroscopes used are mostly derivation ones, therefore it is necessary to calculate the current angle from the angular velocity data by integration. The integration errors increase with an increasing number of samples. Therefore, the sensor has to be precisely calibrated. The offset on the sensor output has the highest influence on the general error of the measured angle.

## MATERIAL AND METHODS

The measured angular velocity has to be compensated on the basis of the knowledge of the dependences which affect the operation of gyroscopes. The heading angle is calculated from the angular velocity by integration. The integration is connected with error increasing in time. Therefore, it is important to calibrate and compensate all influences at the highest rate.

The values influencing the angular velocity measurement are described in Eq. (1) (Titterton, Weston 2004):

$$\tilde{\omega}_x = (1+S_x)\omega_x + M_y\omega_y + M_z\omega_z + B_f + \\ + B_{gx}a_x + B_{gz}a_z + B_{axz}a_y a_z + n_x \quad (1)$$

where:

$\tilde{\omega}_x$ – compensated angular velocity (°/s)

$S_x$ – scale factor error which can be expressed as a polynomial in $\omega_x$ to represent scale-factor non-linearities

$M_y$, $M_z$ – cross coupling coefficients

$\omega_y$, $\omega_z$ – angular velocity of $y$ and $z$ axis (°/s)

$B_{f-g}$ – Earth gravity insensitive bias (°/s)

$B_{gx}$, $B_{gz}$ – g-sensitive bias coefficients in the axis $x$ and $z$ (s/m)

$a_x$, $a_y$, $a_z$ – accelerations in $x$, $y$ and $z$ axis (m/s$^2$)

$B_{axz}$ – anisoelastic bias coefficient (s$^3$/m$^2$)

$n_x$ – zero mean random bias in the axis $x$ (°/s)

Analogically, it is necessary to compensate the angular velocity measurements in the three axes of the coordinate system.

The identification has generally a double meaning (Ondráček, Janíček 1990):

- knowledge about any object as the object identification,
- ideal identification with more or less different objects – system identification.

Under the term identification we can understand the identification of an idea which has begun with the advent of the computer technology and its aftermath of the system theory genesis. The main part of identification is an identification experiment with characteristic attributes. Its results must be objectivised input data for the identification solution. The next part of the identification consideration is the advisement, the values of which will be determined by the identification experiment and which require the measurement accuracy. The realisation "trial-error" is not acceptable (Ondráček, Janíček 1990).

A simulated identification consists of these steps (Ondráček, Janíček 1990):

- creation of an algorithm and active program of the current task, allowing to determine the correction parameters in the selected limits of the current task solution for the input data,
- the values of the correction parameters will be estimated,
- on the basis of experience and knowledge, intervals will be estimated to show in which range the measured values can be,
- correction in simulation according to the measurement error,
- the analysis of the identification solution and determination of the correction parameters,
- errors calculation for the selected correction parameters,
- analysis of the identification extent of initial and final values.

The input data of identification are the measured angular velocities in the axes $x$, $y$, and $z$. The output is the final heading angle of the inertial sensor in comparison with the initial position in all the three axes of the coordinate system. This is because of the fact that the precise angle cannot be measured in time. The determination of angles is done on the basis of information and is calculated from the gravity vector and magnetic induction vector of the Earth in the final position of a navigation unit. The output parameters are calculated from the differences between the initial and final angles of the measurement in simulation.

We chose the inertial sensor ADIS16405BLMZ (tri-axis inertial sensor with magnetometer) with a digital output developed by Analog Devices (Norwood, USA) for the demonstration of the designed method. It is a tri-axial accelerometer, gyroscope, and magnetometer developed by the Micro-Electro-Mechanical Systems (MEMS) technology. The dynamic range of the gyroscope is ±300 °/s and the initial sensitivity is 0.05 °/s/LSB. The absolute value of the magnetic induction vector is 45.8 μT, and during the measurement its value and direction were constant. The dynamic range of the accelerometer is ±18 g (176.59 m/s$^2$), and the initial sensitivity is 3.33 mg/LSB (0.03267 m/s$^2$). Other important parameters are described in the datasheet of the sensor.

We used a unit INU 1.0 designed by ourselves for the measurement data saving, which is based on a 32 bit microprocessor LM3S3748 developed by Texas Instruments Company (Dallas, USA). The measured data are saved on the flash memory of a USB mass storage device. The sample frequency used was 816.6598 Hz. The temperature was also monitored during the measurements. All input data for the sensor are measured at the temperature of 34°C which is important for easy data processing.

The temperature causes the offset fluctuation in MEMS gyroscopes. The effect of temperature on the offset is specified for individual gyroscopes and is considerably non-linear. The temperature effect brings an error into the measurement. ADIS16405BLMZ contains a temperature sensor for the compensation of the temperature influence on the measured values. The sensor datasheet refers to the temperature dependence of the gyroscope, which is ±40 ppm/K. Non-linearity is up to 0.1% in the

full range. The influence of the power supply voltage is minimalized with using a precision voltage regulator. The voltage waveform is watched during the measurements realised currently with the inertial sensor. Therefore, the dependence mentioned is not interesting for our work.

The output samples obtained from MEMS gyroscopes are disturbed by white noise. Let $N_i$ be the $i^{th}$ random variable in the white noise sequence. Each $N_i$ is identically distributed with the mean $E(N_i) = E(N) = 0$ and finite variance $Var(N_i) = Var(N) = \sigma^2$. By the definition of the white sequence $Co_iv(N_i, N_j) = 0$ for all $i \neq j$. The result of using the rectangular rule to integrate the white noise signal $\varepsilon(t)$ over a timespan $t = n \times \delta t$ is (Woodman 2007):

$$\int_0^t \varepsilon(\tau)d\tau = \delta t' \sum_{i=1}^{n} N_i \quad (2)$$

where:

$n$ – number of samples received from the device during the period

$\delta t'$ – time between successive samples

The expected error is:

$$E(\int_0^t \varepsilon(\tau)d\tau) = \delta t' \times n \times E(N) = 0 \quad (3)$$

and the variance is:

$$Var(\int_0^t \varepsilon(\tau)d\tau) = \delta t^2 \times n \times Var(N) = \delta t \times t \times \sigma^2 \quad (4)$$

Hence, the noise introduces a zero-mean random walk error into the integrated signal, whose standard deviation (Woodman 2007)

$$\sigma_\theta(t) = \sigma \times \sqrt{\delta \times t} \quad (5)$$

grows in proportion to the square root of time. Since we are usually interested in how the noise affects the integrated signal, it is common for manufacturers to specify the noise using an angle random walk ($ARW$) measurement

$$ARW = \sigma_\theta(1) \quad (6)$$

with units °/sqrt(hour). The random walk is given for the used sensor. The random walk is one of the parameters which cannot be compensated by the designed method. The effect on the accuracy of the measurement is negative.

The angle was calculated according to Simpson's rule with six nodes (Chapra 2002):

$$\alpha_{xn+1} = \alpha_{xn} + \frac{1}{3f}(\omega_{xi-6} + 4\omega_{xi-5} + 2\omega_{xi-4} + 4\omega_{xi-3} + 2\omega_{xi-2} + 4\omega_{xi-1} + \omega_{xi}) \quad (7)$$

where:

$\alpha_{xn+1}$ – new value of angle in the $x$ axis (°)

$\alpha_{xn}$ – previous value of angle in the $x$ axis (°)

$f$ – sample frequency (Hz)

$\omega_x$ – actual sample of angular velocity (°/s)

## RESULTS AND DISCUSSION

Fig. 1 illustrates the time waveform of the noise in the individual axes of the gyroscope. On the basis of its distribution, it is possible to determine approximately the offset limits of identification and to speed up the whole calculation. The averages of the individual axes were –0.0447 °/s in the $x$ axis, –0.3754 °/s in the $y$ axis, and 0.151 °/s in the $z$ axis. In simulation, we obtained the offset limits from –0.1 °/s to 0 °/s for the $x$ axis, from –0.45 °/s to –0.3 °/s for the $y$ axis, and from 0.1 °/s to 0.2 °/s for the $z$ axis of the values described. We calculated with 0.001 °/s step for all offsets.

Gain calibration has a condition that the initial and final angles of simulation must be different, namely the more the better. In supposition that the angles should be equal, the simulation results would always have initial values of the calibration parameters for gains in each axis. For all the axes, the limits are in a 5% tolerance, from –0.05 to 0.05 with 0.001 steps. We did not suppose that the deviations in gain would overreach the setup tolerance.

In the next step, we were interested in finding the calibration constants for cross coupling coefficients ($M$). The developer specifies the accuracy of this parameter being ±0.05°. Based on this description, we set the simulation limits at ±0.0009 with 0.0001 steps for each axis.

We did not pay attention to g-sensitive bias correction. In the case of its inclusion among the calibration parameters, we must ensure the accel-

Table 1. Calibration parameters found

| | B | S | $M1$ | $M2$ |
|---|---|---|---|---|
| $x$ axis | –0.012 | 0.002 | –0.0002 ($y$) | 0.0001 ($z$) |
| $y$ axis | –0.396 | 0.011 | 0.0001 ($x$) | 0.0004 ($z$) |
| $z$ axis | 0.196 | 0.014 | –0.0003 ($x$) | –0.0001 ($y$) |

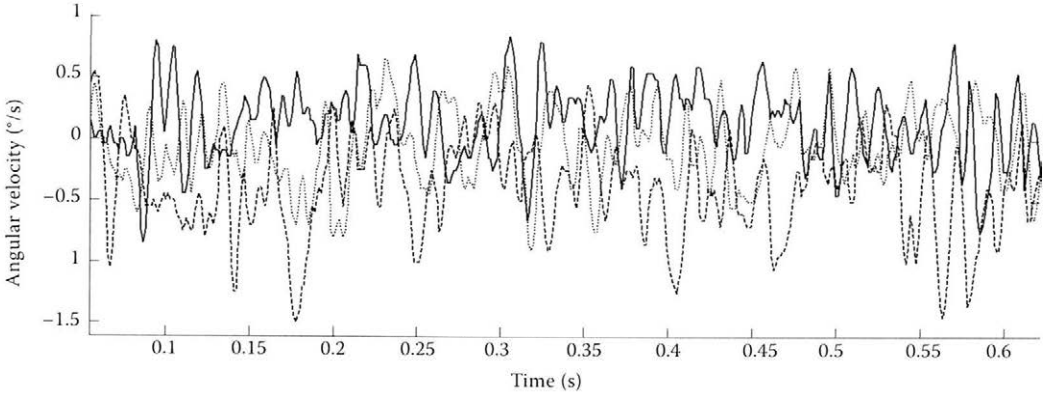


Fig. 1. Angular velocity noise example

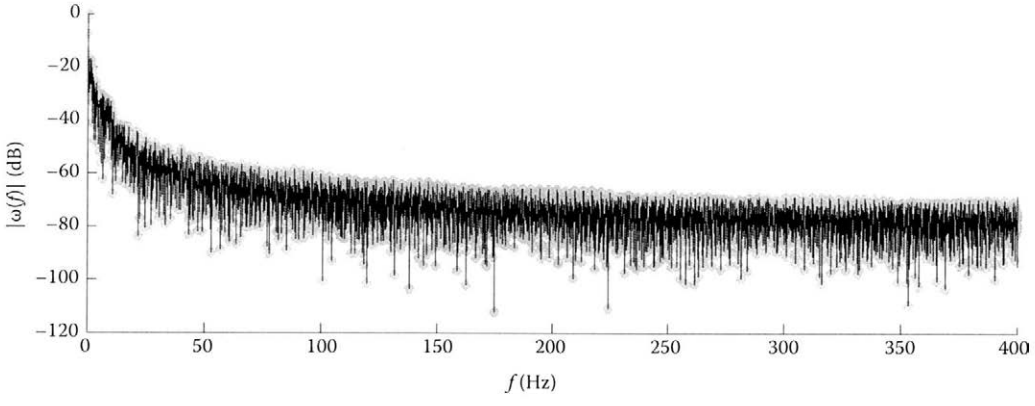


Fig. 2. Fast Fourier Transform (FFT) of angular velocity measurements
$\omega(f)$ – single-sided amplitude spectrum of angular velocity in time; $f$ – frequency

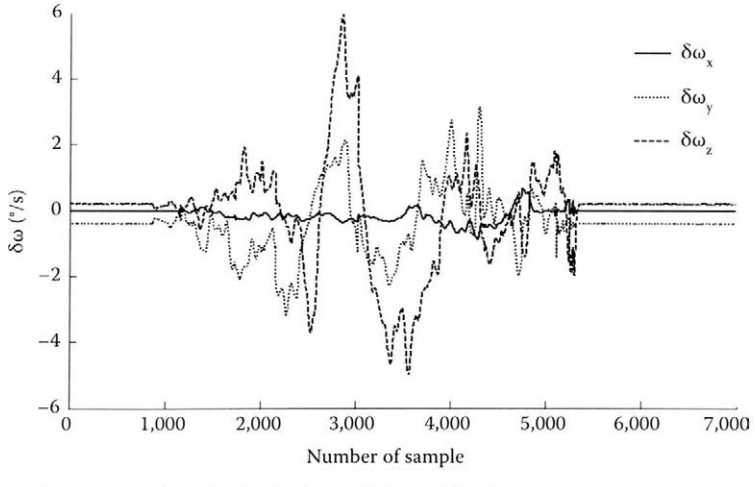


Fig. 3. Difference between angular velocities before and after calibration
$\delta\omega_x$, $\delta\omega_y$, $\delta\omega_z$ – angular velocity difference before and after calibration in axis $x$, $y$ and $z$ (°/s)

eration values of at least 4 g; otherwise, it is not possible to find precise values of the correction parameters with the method described. For the used sensor, g-sensitive bias is up to 0.05 °/s/g.

With using one waveform, the results may be markedly distorted. As a rule, the results will be more precise with the increasing number of paths. A disadvantage is in an increased complication of the results. In our case, we chose three different time waveforms in the range of 15 seconds. The optimal coefficients were considered to be those with which the sum of deviations in each axis of all waveforms was minimal. In the next step, it is necessary to check the waveforms of angular velocity before simulation if the values do not overreach the dynamic range of the sensor. In the case of the angular velocity waveform limitation, errors would occur in the identification. The resulting correction parameters would be useless. The result of simulation is shown in Table 1.

Fig. 2 proved that the frequency components in the time measurement were deeply below half the sample frequency value. Nyquist-Shannon sampling theorem was thus fulfilled.

The designed algorithm of the described method was created in the Matlab application (MathWorks, Natick, USA). All data are in a data array form. The consequential algorithm for finding optimal correction parameters consists of six nested loops for each axis of the coordinate system. Fig. 3 shows the difference between angular velocities before and after calibration.

## CONCLUSION

The main disadvantage of MEMS gyroscope error sources is the error specification in individual sensors. Therefore, each sensor requires an individual approach as regards the calibration and correction. Conventional methods for the calibration of gyroscopes require a special workplace, which is difficult to be available. For the development of simple applications with gyroscopes, the sensors can be calibrated by the described method. A disadvantage is just the time which is necessary for the calculation of the correction parameters. In our case, we have obtained sensor accuracy of up to 0.5° (up to 15° without calibration) during one min in the working time of the device. However, the accuracy has an influence also on the dynamic range of angular velocity where the resolution of the sensor plays an important role.

## References

Chapra S.C., 2002. Numerical Methods for Engineers: With Software and Programming Applications. 4th Ed. New York, McGraw-Hill.

Ondráček E., Janíček P., 1990. Výpočtové modely v technickej praxi. [Computational Models in Technical Practice.] Prague, SNTL.

Titterton H.D., Weston J.L., 2004. Strapdown Inertial Navigation Technology, 2nd Ed. Stevenage, Institution of Engineering and Technology.

Woodman O., 2007. An introduction to Inertial Navigation. Technical report No. 696. Cambridge, University of Cambridge.

Received for publication July 2, 2012
Accepted after corrections Jaunary 1, 2013

*Corresponding author:*

Ing. Vladimír Cviklovič, Ph.D., Slovak University of Agriculture in Nitra, Faculty of Engineering, Department of Electrical Engineering, Automation and Informatics, Tr. A. Hlinku 2, 949 76 Nitra, Slovak Republic
phone: + 421 376 415 783, e-mail: vladimir.cviklovic@uniag.sk

# The operation of agricultural tractor with universal ecological oil

J. Kosiba, Z. Tkáč, Ľ. Hujo, B. Stančík, I. Štulajter

*Department of Transport and Handling, Faculty of Engineering, Slovak University of Agriculture in Nitra, Nitra, Slovak Republic*

**Abstract**

Kosiba J., Tkáč Z., Hujo Ľ., Stančík B., Štulajter I., 2013. **The operation of agricultural tractor with universal ecological oil**. Res. Agr. Eng., 59 (Special Issue): S27–S33.

This contribution presents the results of the research into the characteristics of ecological oil labelled MOL Farm UTTO Synt in the tractor operating conditions. Biodegradable fluid was applied in the gear and hydraulic circuits of the tractor Zetor Forterra 114 41. The fluid was assessed for contamination and lubrication properties by its effect on the wear of tractor hydraulic pump during the application. The hydraulic pump was removed from the tractor at specified time intervals because of its technical condition relating to the flow efficiency. The measurements were calculated as flow efficiency with minimum environmental impact of oil on the hydraulic pump wear.

**Keywords**: synthetic oil; hydraulic pump; flow characteristic

At the present time, hydrostatic systems are widely spread in the industry. They provide various types of motion. The power transmission is realised by hydraulic fluid. Hydraulic fluid needs servicing and requires the control of operating parameters (Majdan et al. 2008; Belovič, Majdan 2011). Almost 50% of all the oils sold in the world finish at the present time as forfeits during the operation in nature (Jakob, Theissen 2006). Therefore, it is extremely important to replace mineral oils with vegetable oils or plant-based synthetic oils (Tkáč et al. 2010).

Agricultural technology has a negative impact on all elements of the environment. As to air, it is affected by the exhaust emissions, and the soil respectively water by oil and for fuel components (Jablonický et al. 2007; Kučera, Pršan 2008; Kučera, Rédl 2008). This paper presents the results of a long-term operational test of the biodegradable synthetic oil MOL Farm UTTO Synt (Slovnaft a.s., Bratislava, Slovak Republic), which is currently under development. The operational test was performed on one of the most used tractors, the tractor Zetor Forterra 114 41 (Zetor Tractors a.s., Brno, Czech Republic) in the conditions of Slovak farms. The hydraulic pump was removed from the tractor in the time intervals; the pump was mounted onto the experimental laboratory device for measuring the flow characteristics at the Department of Transport and Handling, Faculty of Engineering, University of Agriculture in Nitra, Nitra, Slovak Republic.

Subsequently, the oil samples were collected for the analysis and detection of iron and copper contamination by means of infrared spectra. In view of the utilization of hydraulic fluid in a machine, it is the most important to know the running properties of the fluid, i.e. to know the influence of the fluid

Supported by the Scientific Grant Agency VEGA of the Ministry of Education of the Slovak Republic and the Slovak Academy of Sciences, Grant No.1/0857/12.

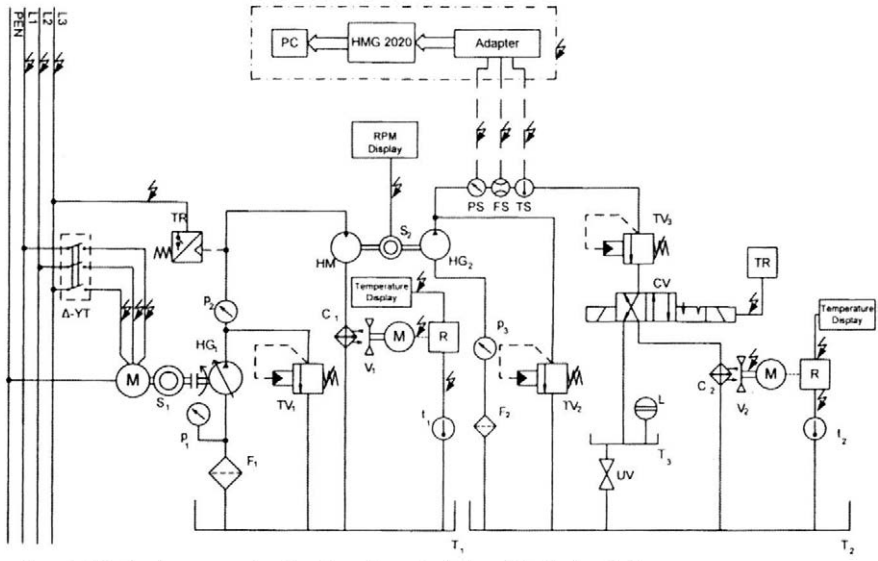


Fig. 1. Experimental device for measuring the flow characteristics of the hydrostatic pump
PEN – neutral; $L_1$ – phase 1; $L_2$ – phase 2; $L_3$ – phase 3; Δ-YT – delta-wye transformer; M – electric motor; $HG_1$ – regulating hydrostatic pump; $TV_1$, $TV_2$ – insured valve; $S_1$, $S_2$ – coupler; HM – hydrostatic motor; $HG_2$ – tested hydrostatic pump; $TV_3$ – valve for adjusting pressure; PS – pressure sensor; FS – flow sensor; TS – temperature sensor; CV – control valve; TR – trigger; T – oil temperature controllers; L – flowmeter; $p_1$, $p_2$, $p_3$ – pressure sensors; $t_1$ – temperature sensor for tank $T_1$; $t_2$ – temperature sensor for tank $T_2$; $T_1$, $T_2$, $T_3$ – tank; $F_1$, $F_2$ – filter; $V_1$, $V_2$ – ventilator; $C_1$, $C_2$ – cooler; UV – spherical plug valve (Tkáč et al. 2008)

on the technical state of the hydraulic system parts (Žikla, Jablonický 2006; Jablonický et al. 2007; Tkáč et al. 2008).

## MATERIAL AND METHODS

The experimental device for measuring the flow characteristics is shown in Fig. 1. It was designed at the Department of Transport and Handling, Technical Faculty of Slovak University of Agriculture in Nitra, Nitra, Slovak Republic.

This device allows to measure the following characteristics:

$Q = f(p)_n$ dependence of the flow rate on the pressure at constant speeds and $Q = f(n)_p$ dependence of the flow rate on the speed at constant pressure.

The test stand consists of two hydraulic circuits. The left hydraulic circuit is used to drive the hydraulic pump $HG_2$ in the measurement. The output line of the hydraulic pump $HG_1$ is directly connected to the hydraulic motor output HM ($HG_1$ is a regulatory axial piston pump). To set the speed of the measured hydraulic pump $HG_2$, the flow change is used made by the hydraulic pump $HG_1$. The pressure valves $TV_1$ and $TV_2$ have the function of the safety valve. The pressure valve $TV_3$ is designed to set the values of pressure (from zero to the nominal value). We measure the flow $Q = f(p)_n$ at the set pressure value, or the pressure to measure $Q = f(n)_p$.

Before measuring the flow characteristics of the hydraulic pump, we set the speed at the nominal value (measured by the hydraulic pump $HG_2$) by changing the flow hydraulic pump ($HG_1$). In the measurement of the characteristics, a gradual increase in pressure is created by the pressure valve $TV_3$ (to the nominal value of the pressure measured by hydraulic pump

Table 1. Specifications of oil MOL Farm UTTO Synt

| Property | Unit | Amount |
|---|---|---|
| Density at 15°C | g/cm³ | 0.8681 |
| Kinetic viscosity at 40°C | mm²/s | 58.14 |
| Kinetic viscosity at 100°C | mm²/s | 10.22 |
| Viscosity index | | 165 |
| Pour point | °C | –42 |
| Flash point | °C | 232 |
| Calcium | % | 0.318 |

$HG_2$). Based on these data, we can determine the flow characteristics of the hydraulic pump (Drabant et al. 2010; Majdan 2010; Tkáč et al. 2010).

During the operation of the tractor, the following physico-chemical properties of the ecologic oils were monitored:

- contamination of liquid admixtures, by IR spectroscopy,
- iron content,
- copper content important factors for obtaining high quality representative samples are: the correct choice of the delivery points; mixing and heating the fluid at the operating temperature. The analysis of the pollution samples of iron and copper was performed in the accredited laboratory WearCheck, Hungary.

**Ecological oil**. Ecological oil is made from the synthetic fluid and is marked as MOL Farm UTTO Synt. It belongs to the type of oil UTTO (Universal Tractor Transmission Oil). This oil is destined for the common gear-hydraulic circuits of agricultural tractors. Table 1 shows the basic technical parameters of the synthetic oil tested.

Before operating, the test tractor was equipped with a new hydraulic pump type UD 25 (Jihostroj a.s., Velešín, Czech Republic). At the same time, the gear-hydraulic circuit of the tractor was mounted and also a new oil filter was installed. At the start of the operational testing of the synthetic oil MOL Farm UTTO Synt the temperature regimes were tested of the tractor working with a gear-hydraulic circuit. The measurements were performed by placing the temperature sensor using a coupling flange on the output line of hydraulic pump.

Operations, and types of auxiliary equipment for measuring the thermal regime:

- disc cultivator LBD 4.5,
- plow Kverneland LD 100,
- drill SE 1073 M.

## RESULTS AND DISCUSSION

The measuring system consisted of the digital recording unit HMG 2020 (Hydac GmbH, Sulzbach/Saar, Germany) and temperature sensor (ETS 4144-A-000; Hydac GmbH). The digital recording unit HMG 2020 recorded temperatures at one second intervals. The measurement of the thermal regime lasted 50 minutes. The temperature modes of the tractor gear-hydraulic circuit operation during the work operations are shown in Fig. 2. The highest temperature was reached in the tractor with seeder SE 1073 M (Agroplus s.r.o., Hlohovec, Slovak Republic). The oil temperature was stabilised at approximately the same time with all measurements (Kosiba et al. 2011a, b).

The work operations conducted during the synthetic oil performance test are shown in Table 2.

The oil temperature is the most important parameter for the use of biodegradable oils in the gear-hydraulic circuits of tractors. The measured values of the oil temperature can not reduce an operating test of MOL Farm UTTO synthetic oil. The oil is applied into the gear-hydraulic circuit Zetor Forterra 114 41 tractor. The hydraulic pump type UD 25 was removed from the tractor at intervals of 450 engine hours and 900 engine hours. Then an experimental laboratory device was installed for measuring the flow characteristics. The measurement of the flow characteristics is used to determine the impact of the synthetic oil on the hydraulic pump life. The flow hydraulic pump efficiency was calculated from the measured flow characteristics (Cvíčela et al. 2008):

$$\eta_{pr} = \frac{Q}{V_G \times n} \times 100 \quad (1)$$

where:

$Q$ – output flow rate ($dm^3$.rpm)

$V_G$ – geometrical volume of hydrostatic pump ($dm^3$)

$n$ – nominal rotation speed of hydrostatic pump (rpm)

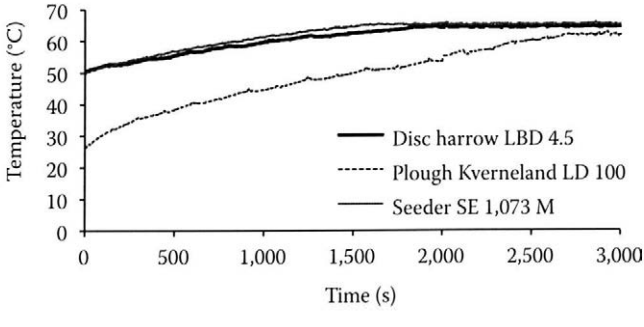


Fig. 2. Temperature modes of Zetor Forterra 114 41 tractor

Table 2. Working operations performed with Zetor Forterra 114 41 tractor during operating test

| Work | Machinery type (producer) | Engine hours | |
|---|---|---|---|
| | | 0–450 | 450–900 |
| Stubble cultivation | LBD 4,5 (Chervona Zirka, Kirovograd, Ukraine) | 86 | 95 |
| Transport | BSS-9 (Brandýrske strojírny, Senice na Hané, Czech Republic) | 46 | 70 |
| Ploughing | Kverneland LD 100 (Kverneland Group, Kverneland, Norway) | 105 | 149 |
| Seeding | 1 073 M (Pneusej – Accord, Hlahovec, Slovak Republic) | 191 | 118 |
| Plant protection | Forrás 2006/18 (Interat ZRT., Bicske, Hungary) | 20 | 19 |
| Summary | | 448 | 451 |

The flow efficiency was determined with a new hydraulic pump, after completing 450 engine hours and after completing 900 engine hours. The measurement of the flow characteristics was performed at speeds $n$ = 800 rpm, $n$ = 1200 rpm, and $n$ = 1,500 rpm. Figs 3, 4, and 5 show the flow efficiency of the hydraulic pump UD 25 at different speeds.

The greatest decrease in the hydraulic pump flow efficiency was detected at a speed $n$ = 800 rpm and a pressure of 20 MPa. The flow efficiency of the hydraulic pump type UD 25 dropped from $\eta_0$ = 89.8% to $\eta_{900}$ = 87.75%. Under the nominal speed of the hydraulic pump $n$ = 1500 rpm and a pressure of 20 MPa, the flow efficiency of the hydraulic pump declined from $\eta_0$ = 96.89% to 95.73% = $\eta_{900}$.

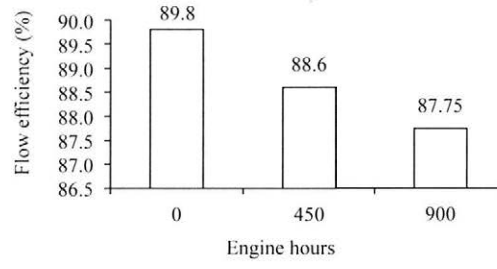


Fig. 3. The flow efficiency of UD 25 hydraulic pump at rotation speed $n$ = 800 rpm

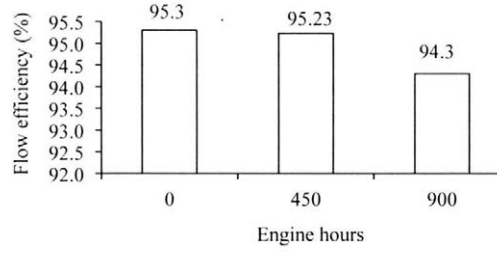


Fig. 4. The flow efficiency of UD 25 hydraulic pump at rotation speed $n$ = 1,200 rpm

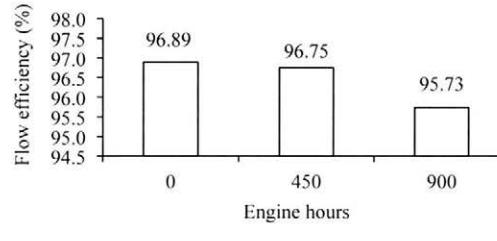


Fig. 5. The flow efficiency of UD 25 hydraulic pump at rotation speed $n$ = 1,500 rpm

### Basic parameters of descriptive statistics

Table 3 presents the basic descriptive statistics indicators, which were determined by statistical data analysis module in a MS Excel 2007 (Microsoft Corp., Redmond, USA). The graphic processing of the results was performed using software Statistica 7 (Statsoft, Inc., Tulsa, USA).

$$V = \frac{1}{N} \times \sum_{i=1}^{N} (x_i - x)^2 \quad (2)$$

where:

$N$ – statistical file size

$x_i$–$x_i$ – values of the units

$x$ – average

Standard deviation:

$$SD = \sqrt{V^2} \quad (3)$$

The differences in the range between the min. and max. values are relatively small. The outliers and

Table 3. Basic parameters of descriptive statistics at pressure $p$ = 20 MPa

| | Average | Median | Modus | Min. | Max. | Variance | Standard deviation |
|---|---|---|---|---|---|---|---|
| Output flow rate – 0 engine hours ($dm^3$.rpm) | 36.335 | 36.32 | 36.29 | 35.741 | 36.865 | 0.057 | 0.239 |
| Output flow rate – 450 engine hours ($dm^3$.rpm) | 36.282 | 36.368 | 36.423 | 34.516 | 36.988 | 0.243 | 0.493 |
| Output flow rate – 900 engine hours ($dm^3$.rpm) | 35.902 | 35.903 | 35.778 | 34.91 | 36.595 | 0.112 | 0.334 |

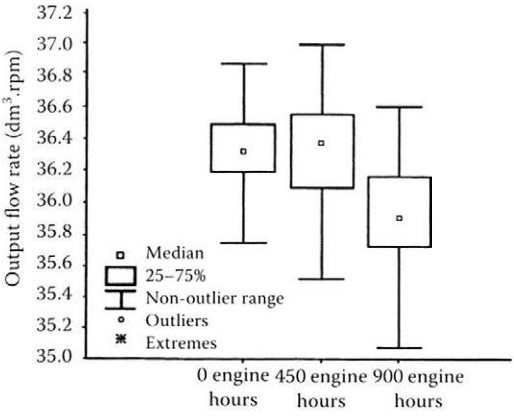


Fig. 6. Box-and-Whisker diagram of the output flow rate

extreme points on the Box-and-Whisker diagram of the output flow rate were not found (Fig. 6).

## Evaluation of oil pollution

The analysis of oil pollution by chemical elements (iron and copper) was performed in the accredited laboratory WearCheck, Hungary. The test was performed by ASTM D 4951-02 (standard test method for the determination of additive elements in lubrication oils by inductively coupled plasma atomic emission spectrometry). New oil was evaluated after completing 450 and 900 engine hours. The course of oil contamination by the chemical elements is shown in Fig. 7.

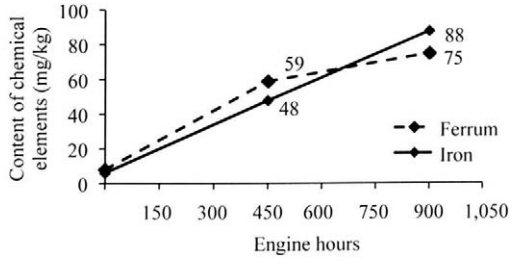


Fig. 7. Contents of chemical elements

The level of oil MOL Farm UTTO Synt pollution with admixtures (Cu, Fe) has reached a critical level after completing 450 engine hours. The limit values of oil pollution were exceeded in the gear-hydraulic circuit of the tractor Zetor Forterra 114 41 after completing 900 engine hours.

## Analysis of the origin of synthetic oil pollution

The evaluation of the analysis of the origin of synthetic oil pollution by IR spectroscopy is shown in Fig. 8. The change in the synthetic oil MOL Farm UTTO Synt can be seen in the areas of 1,650 $cm^{-1}$ and 1,600 $cm^{-1}$. On the $x$ axis are shown the wavelengths that correspond to the individual chemical compounds. In the case of new oil, the absorbance reflects the chemical compounds concentration in the oil produced. The increase of absorbance after 450 and 900 engine hours reflects the increase of the chemical compounds concentrations. The additives are characterised precisely by the wavelengths from 1,500–1,700/cm. The changes of absorbance at these wavelengths expressing the oil degradation were not identified.

## CONCLUSION

The performance test has shown that the new biodegradable oil MOL Farm UTTO Synt is very beneficial for our lives. We look forward to the possibility of greening the agricultural tractors used in Slovak agriculture. This contribution proves minimal effect of the synthetic oil on the decrease of the flow efficiency during the performance test and hydraulic pump wear. The experimental device was constructed at the Department of Transport and Handling, Faculty of Engineering, Slovak University of

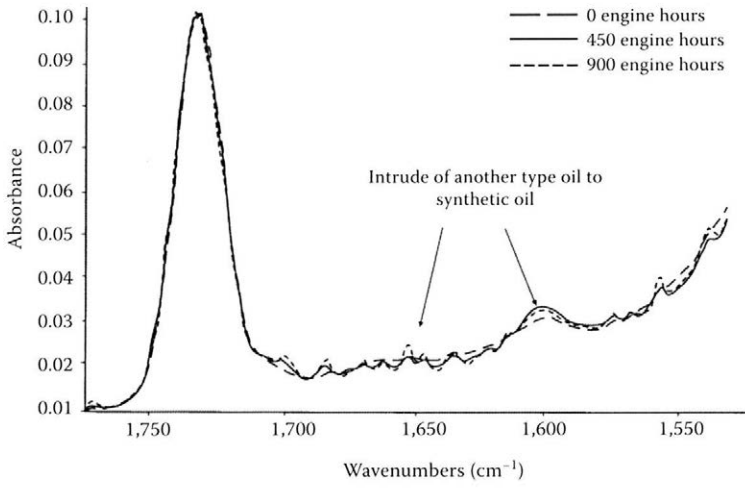


Fig. 8. Evaluation of oil contamination by IR spectroscopy

Agriculture in Nitra. The ecological fluid meets the requirements for the operation of agricultural tractors in terms of a low impact on the wear of hydraulic components. The results show good lubricating properties of the organic oil to ensure a reliable operation of the tractor. The operational test had to be stopped prematurely for increased contents of impurities (chemical elements Fe and Cu), after a consultation with the producer of the synthetic oil. Using IR spectroscopy, it was found that the impurities got into the hydraulic circuit of the tractor Zetor Forterra 114 41. These contaminants get into the hydraulic circuit through external hydraulic outlets admixture of mineral oil. We can say that the new developing biodegradable synthetic oil MOL Farm UTTO Synt does not affect the construction or operation of the tractor Zetor Forterra 114 41. MOL Farm UTTO Synt has no negative influence on the rubber components in the hydraulic circuit of the tractor Zetor Forterra 114 41. The price of the oil is higher than that of standard mineral oils.

## References


Belovič R., Majdan R., 2011. Hodnotenie znečistenia ekologickej kvapaliny. [The evaluation of biodegradable fluid cleanliness] In: Recent Advances in Agriculture, Mechanical Engineering and Waste Policy. Nitra, Slovak University of Agriculture in Nitra.

Cvíčela P., Majdan R., Abrahám R., Jablonický J., 2008. Monitoring the operating loading of a hydrostatic pump UD 25. In: Conference Proceedings from X. International Conference of Young Scientists 2008. Prague, Czech University of Life Sciences Prague.

Drabant Š., Kosiba J., Jablonický J., Tulík J., 2010. The durability test of tractor hydrostatic pump type UD 25 under operating load. Research in Agricultural Engineering, *56*: 116–121.

Jablonický J., Abrahám R., Majdan R., Cvíčela P., 2007. Skúšky traktora s biologicky odbúrateľným olejom. [Tests of the tractor with biodegradable oil.] In: Assurance – Quality – Responsibility, 3rd International Scientific Conference. Košice, Technical University: 123–127.

Jakob H., Theissen H., 2006. Bio-based Oils in Hydraulics – Experience from Five Years of Market Introduction in Germany. Institute for Fluid Power Drives and Controls (IFAS), RWTH Aschen University, Germany.

Kosiba J., Tkáč Z., Hujo Ľ., Bureš Ľ., 2011a. Operating modes of hydraulic circuit of tractor Zetor Forterra 114 41. Acta Technologica Agriculturae, *2*: 46–49.

Kosiba J., Tkáč Z., Hujo Ľ., Tulík J., 2011b. Application of synthetic oil in tractor hydraulic circuit. Machines, technologies, materials. MTM: International Virtual Journal for Science, Technics and Innovations for the Industry, *4*: 57–59.

Kučera M., Pršan J., 2008. Analýza trecích stôp a produktov opotrebenia. [Analysis of friction marks and wear products.] Acta Technologica Agriculturae, *2*: 43–49.

Kučera M., Rédl J., 2008. Vplyv podmienok experimentu na tribologické vlastnosti vybraných materiálov. [Effects of experimental conditions on tribologic properties of selected materials.] Acta Technologica Agriculturae, *1*: 98–104.

Majdan R., 2010. Simulácia tlakového rázu v hydraulickom obvode. [Simulation of pressure surge in hydraulic circuit.] In: Proceedings International XII. Conference of Young Scientists. Nitra: 119–123.

Majdan R., Cvíčela P., Bohát M., Ivanišová K., 2008. The observation of hydrostatic pump deterioration during the

durability test according to hydraulic fluids contamination. In: Proceedings X. International Conference of Young Scientists 2008. Prague, Czech University of Life Sciences Prague: 147–153.

Tkáč Z., Drabant Š., Majdan R., Cvíčela P., 2008. Testing stands for laboratory tests of hydrostatic pumps of agricultural machinery. Research in Agricultural Engineering, *54*: 183–191.

Tkáč Z., Majdan R., Drabant Š., Abrahám R., Vozárová V., Jablonický J., 2010. Hodnotenie vlastností hydraulických kvapalín na základe skúšok s použitím hydrogenerátora. [Evaluation of the Properties of Hydraulic Fluids Based Tests with Using Hydrostatic Pump.] Nitra, Slovak University of Agriculture in Nitra: 112.

Žikla A., Jablonický J., 2006. Kopírujúca regulácia trojbodového závesu traktorov. [Copying control of tractor three-hitch point.] Hydraulika a pneumatika, *4*: 42–46.

Received for publication July 2, 2012
Accepted after corrections January 16, 2013

*Corresponding author*:

Ing. Ján Kosiba, Slovak University of Agriculture in Nitra, Faculty of Engineering, Department of Transport and Handling, Tr. A. Hlinku 2, 949 76 Nitra, Slovak Republic
phone: + 421 376 414 128, e-mail: jan.kosiba@gmail.com

# Application of differential geometry in agricultural vehicle dynamics

J. Rédl, V. Váliková

*Department of Machine Design, Faculty of Engineering, Slovak University of Agriculture in Nitra, Nitra, Slovak Republic*

**Abstract**

Rédl J., Váliková V., 2013. **Application of differential geometry in agricultural vehicle dynamics**. Res. Agr. Eng., 59 (Special Issue): S34–S41.

This paper deals with the application of differential geometry methods to a precise calculation of the length of trajectory of an agricultural mechanism that moves on a sloping terrain. We obtained technical exciting function from experimental measurements, out of which we obtained the function of Euler's parameters by using computer processing. The processing of these parameters provided translational and angular velocities of the gravity centre of the systemic vehicle MT8-222, which performed the determined mounted manoeuvres. We obtained differential equations that describe the function of a spatial curve by the application of differential geometry methods. The length of the curve is obtained by a numerical solution of the differential equations formed. We used Dormand-Prince numerical method for the numerical solution. Next, we evaluated the error of the numerical integration for every calculation by reason of the stability of computation. We also addressed the geometric characteristics of the curves such as the radius of curvature. The mounted manoeuvres as well as the corresponding velocities, trajectories, and radiuses of curvature were processed in a graphic way.

**Keywords**: trajectory modelling; numerical integration; radius of curvature

The analysis, planning, and optimisation of the vehicle trajectory are nowadays intensively examined problems not only in the field of the agricultural mechanisms movement in relation to precision agriculture but also in the modelling and simulation of the vehicle motion and in the research into the dynamic effects on the vehicle. The research into the trajectory of the vehicle motion focuses also on the fields of development and design of the set mechanisms capable of autonomous decision and generation of the trajectory according to the input values from the sensors. Such a design is preceded by a simulation process which is based on differential moving equations of a rigid body as well as of a system of rigid bodies. Euler's parameters are used for the spatial dislocation of the vehicle and spatial transformation based on orthogonal matrices as well as the principles of differential geometry. To define the tire – ground relationship, the principles of terramechanics are advantageously used. An intensive research is realised also in the fields of the analysis of the vehicle trajectory in different reference coordinate axes, when the dynamics of transport is investigated as introduced in Punzo et al. (2011). They point out the possibility of obtaining the exact vehicle trajectory with the help of GPS or using the simulation programme NGSIM (Next Generation SIMulation; Federal Highway Administration, Washington DC, USA). It is possible to obtain precise values of the trajectory length by utilisation of GPS data, but a high risk exists of the loss of signal in mountain-

ous areas. Purwin and D'Andrea (2006) dealt with the generation and planning of the vehicle trajectory to provide its exact motion and minimise its trajectory to the accurately specified destination. The analysis of the stability of motion and the compliance of the specified trajectory of the vehicle motion are processed in the works of Ailona et al. (2005) and Yoon et al. (2009). Yoon et al. (2009) designed a dynamic model for the generation of the vehicle trajectory following the properties of the terrain and dislocation of a terrain barrier where there it is not possible to pass through it. Antos and Ambrósio (2004) presented strategies of the control of vehicle motion pursuant to the dynamics of rigid bodies. They realised simulations in the environment of the program Matlab® (MathWorks, Natick, USA). For spatial transformations, Euler's parameters were used advantageously. The result was the design of a driver which is able to provide vehicle motion according to the trajectory generated before. Under the authority of the differential geometry, model and real trajectories were evaluated. Almost in every work, the trajectory was generated by dynamic equations that had been generalised by Pacejka (2005).

## MATERIAL AND METHODS

**The length of the curve.** Šalát (1981) as well as Ivan (1989) describes the length of the curve by means of differential geometry in the identical way. Parameterisation of the curve is addressed also by Agoston (2005).

Let $K$ be a curve, which is defined by parameterisation:

$$\boldsymbol{r} = \boldsymbol{r}(t);\ t \in \langle \alpha, \beta \rangle \quad (1)$$

where:

$\boldsymbol{r}$ – denomination of function for parameterisation

$\boldsymbol{r}(t)$ – parameterisation of curve $K$ in point $t$

$\alpha, \beta$ – initial and end point of the curve

Denote $\boldsymbol{R}(\alpha) = A$, $\boldsymbol{R}(\beta) = B$. The point $A$ is the original point and point $B$ is the final one of the curve $K$ when its orientation is induced by parameterisation. Let $D = \{t_0, t_1, t_2, \dots, t_r\}$, where $\alpha < t_0 < t_1 < t_2 \dots < t_r = \beta$ is a certain division of the interval $\langle \alpha, \beta \rangle$.

where:

$\boldsymbol{R}(\alpha)$ – parameterisation of curve $K$ in point $\alpha$

$\boldsymbol{R}(\beta)$ – parameterisation of curve $K$ in point $\beta$

$D$ – set of points, which divides interval $\langle \alpha, \beta \rangle$ into $r$-divisions

$t_0$–$t_r$ – $r$-divisions of interval $\langle \alpha, \beta \rangle$

Denote $M_i = \boldsymbol{R}(t)$, for $i = 0, 1, 2, \dots, r$. Points $M_0, M_1, \dots, M_r$ follow gradually one after another in the orientation of the curve accordant with parameterisation (1), thus:

$$A = M_0 < M_1 < M_2 < \dots < M_r = B \quad (2)$$

These points divide the curve $K$ into $r$ partial curves (arcs) $\widehat{M_{i-1}M_i}$. We substitute each of them by an abscissa (subtense) $M_{i-1}M_i$. We denote the broken line consisting of abscissas $M_{i-1}M_i$ $(i = 1, 2, \dots, r)$ as $K(D)$. We say that the broken line $K(D)$ is inscribed into the curve $K$.

Let's $(D)$ denote the length of the broken line $K$(D). Hence:

$$s(D) = \sum_{i=1}^{r} d(M_{i-1}, M_i) = \sum_{i=1}^{r} |r(t_i) - r(t_{i-1})| \quad (3)$$

where:

$d$ – length of the partial curves

It can happen (if the curve is not simple) that the point $M_{i-1}$ is identical with the point $M_i$ for some $i$. In this case, it holds that $d(M_{i-1}, M_i) = 0$.

Using the foregoing way, every division $D$ of the interval $\langle \alpha, \beta \rangle$ is assigned a positive number $s(D)$, which presents the length of the corresponding inscribed break line $K(D)$. To every sequence $\{D_n\}$ of the division of the interval $\langle \alpha, \beta \rangle$ appertains the sequence of number $\{s(D_n)\}$. It is evident that, if there exists a number, that $d(D_n) \leq s$ for every division $D_n$ and the lower the difference $d(D_n) \leq s$ the smoother the division $D$, then the non-negative number s is called the length of the curve $K$. We establish a definition:

If the corresponding sequence $\{s, D_n\}$ for every regular sequence $\{D_n\}$ of the division of the interval $\langle \alpha, \beta \rangle$ is convergent and the limit does not depend on the selection of sequence $\{D_n\}$, we say that the curve $K$ is rectifiable and we name the number $s = \lim_{n \to \alpha} s(D_n)$ its length.

According to this definition and knowledge of the transformation of the parameter of the curve, it can be relatively easy to prove that the length of the curve does not depend on its parameterisation. From the geometric point of view, it is an obvious requirement for the definition of the curve length.

From the definition of the curve length and theorems about the limit of numeric sequence follows the veracity of the next theorem.

**Theorem 1** (monotony property)

If the curve $K$ is rectifiable and its length is $s$, then its each part $K'$ is rectifiable too and for its length s' holds: $s \leq s'$.

By the help of this theorem, the theorem about other important property of the curve length (additive property) can be proved.

**Theorem 2** (additive property)

(a) If the curve $K$ is rectifiable, then for its optional division into the final number of partial curves $K_1, K_2, \ldots, K_n$ each from parts $K_1$ is rectifiable and it holds:

$$s = s_1 + s_2 + \ldots + s_i + \ldots + s_n \tag{4}$$

where:

$s$ – length of the curve $K$

$s_i$ – length of its parts $K_i$, $i = 1, 2, \ldots n$

(b) The curve $K$, which is the connection of the final number of rectifiable curves $K_1, K_2, \ldots, K_n$, is also rectifiable and for its length s holds the equality (4).

The following theorem speaks out about a sufficient condition of the curve rectifiability.

**Theorem 3**

Let $\boldsymbol{r} = \boldsymbol{r}(t)$, $t \in \langle\alpha, \beta\rangle$ be parameterisation of the curve $K$. If the function $\boldsymbol{r}$ has a continuous derivative $\boldsymbol{r}'$ in the interval $\langle\alpha, \beta\rangle$ (in the point A from the right, in the point B from the left), then the curve $K$ is rectifiable and for its length s holds:

$$s = \int_\alpha^\beta \left|\frac{dr(t)}{dt(t)}\right| dt \tag{5}$$

that is:

$$s = \int_\alpha^\beta \sqrt{\left[\frac{dx(t)}{dt}\right]^2 + \left[\frac{dy(t)}{dt}\right]^2 + \left[\frac{dz(t)}{dt}\right]^2}\, dt \tag{6}$$

$$\text{if } \boldsymbol{r}(t) = x(t)\mathbf{i} + y(t)\mathbf{j} + z(t)\mathbf{k} \tag{7}$$

where:

$\mathbf{i}, \mathbf{j}, \mathbf{k}$ – unity vectors

$x, y, z$ – coordinates

This corollary follows from the definition of the regular and partly regular curves and from theorems 2 and 3.

When we utilise the parameterisation of the curve $K$, we obtain a flexion of the curve. For the regular curve $K$ holds that for every point the flexion equals:

$$\varkappa = \sqrt{[x''(t)]^2 + [y''(t)]^2 + [z''(t)]^2} \tag{8}$$

Using Eq. (7) and its first and second derivation leads to the relation for the curvature of the curve. We establish determinants A, B, C as:

$$A = \begin{vmatrix} y', & z' \\ y'', & z'' \end{vmatrix}, B = \begin{vmatrix} z', & x' \\ z'', & x'' \end{vmatrix}, C = \begin{vmatrix} x, & y' \\ x'', & y'' \end{vmatrix} \tag{9}$$

For the curvature in every point of the curve $K$ then holds:

$$K = \frac{\sqrt{A^2 + B^2 + C^2}}{\sqrt{[(x(t)')^2 + (y(t)')^2 + (z(t)')^2]^3}} \tag{10}$$

From the preceding relations we can define the radius of curvature as the reciprocal of the curvature:

$$\rho = \frac{1}{K} \tag{11}$$

**Numerical integration**. In the created application, the numerical method is implemented for integration of Runge-Kutta methods, especially Dormand-Prince method. This method is analysed in the paper of its authors Dormand and Prince (1980). They presented this method thanks to Butcher's table, in which the coefficients of the individual terms in the equations are described. Butcher's table was used also by Hoppensteadt (2007). The equations for Dormand-Prince method have the following forms:

$$\begin{aligned}
k_1 &= h_n f(x_n, y_n) \\
k_2 &= h_n f\left(x_n + \frac{1}{5}h_n, y_n + \frac{1}{5}k_1\right) \\
k_3 &= h_n f\left(x_n + \frac{3}{10}h_n, y_n + \frac{3}{40}k_1 + \frac{9}{40}k_2\right) \\
k_4 &= h_n f\left(x_n + \frac{4}{5}h_n, y_n + \frac{44}{45}k_1 - \frac{56}{15}k_2 + \frac{32}{9}k_3\right) \\
k_5 &= h_n f\left(x_n + \frac{8}{9}h_n, y_n + \frac{19{,}372}{6{,}561}k_1 - \frac{25{,}360}{2{,}187}k_2 + \frac{64{,}448}{6{,}561}k_3 - \right. \\
&\quad \left. - \frac{212}{729}k_4\right) \\
k_6 &= h_n f\left(x_n + h_n, y_n + \frac{9{,}017}{3{,}168}k_1 - \frac{355}{33}k_2 - \frac{46{,}732}{5{,}247}k_3 + \right. \\
&\quad \left. + \frac{492}{176}k_4 - \frac{5{,}103}{18{,}656}k_5\right) \\
k_7 &= h_n f\left(x_n + h_n, y_n + \frac{35}{384}k_1 - \frac{500}{1{,}113}k_3 + \frac{125}{192}k_4 - \right. \\
&\quad \left. - \frac{2{,}187}{6{,}784}k_5 + \frac{11}{84}k_6\right) \\
y_{n+1} &= y_n + \frac{35}{284}k_1 + \frac{500}{1{,}113}k_3 + \frac{125}{192}k_4 - \frac{2{,}187}{6{,}784}k_5 + \frac{11}{84}k_6
\end{aligned} \tag{12}$$

where:
$k_1$–$k_7$ – Runge-Kutta koefficients
$h_n$ – step of the numerical integration
$y_n$, $y_{n+1}$ –the value in the points $x_n$, $x_{n+1}$

**Quaternion feedback control.** Wie (2008) considers the attitude dynamics of a rigid vehicle described by Euler's rotational equation of the motion:

$$\mathbf{J}\dot{\boldsymbol{\omega}} + \boldsymbol{\omega} \times \mathbf{J}\boldsymbol{\omega} = \mathbf{u} \tag{13}$$

where:
$\mathbf{J}$ – inertia matrix
$\boldsymbol{\omega} = (\omega_1, \omega_2, \omega_3)$ – angular velocity vector
$\mathbf{u} = (u_1, u_2, u_3)$ – control torque input vector

The cross product of two vectors is represented in the matrix notation as

$$\boldsymbol{\omega} \times \mathbf{h} = \begin{bmatrix} 0 & -\omega_3 & \omega_2 \\ \omega_3 & 0 & -\omega_1 \\ -\omega_2 & \omega_1 & 0 \end{bmatrix} \begin{bmatrix} h_1 \\ h_2 \\ h_3 \end{bmatrix} \tag{14}$$

where:
$\mathbf{h} = \mathbf{J}\boldsymbol{\omega}$ – angular momentum vector

It is assumed that the angular velocity vector components $\omega_i$ along the body/fixed control axes are measured by rate gyros.

Euler's rotational theorem states that the rigid body attitude can be changed from any given orientation to any other orientation by rotating the body around an axis, called the Euler axis, which is fixed to the rigid body and is stationary in inertial space. Such a rigid body rotation around the Euler axis is often called the eigenaxis rotation.

Let a unit vector along the Euler axis be denoted by $\mathbf{e} = (e_1, e_2, e_3)$, where $e_1$, $e_2$ and $e_3$ are direction cosines of the Euler axis relative to either an inertial reference frame or the body – fixed control axes. The four elements of quaternions ($q_1$–$q_4$) are then defined as:

$$\begin{aligned} q_1 &= e_1 \sin(\theta/2) \\ q_2 &= e_2 \sin(\theta/2) \\ q_3 &= e_3 \sin(\theta/2) \\ q_4 &= \cos(\theta/2) \end{aligned} \tag{15}$$

where:
$\theta$ – denotes the rotation angle around the Euler axis

and we have:

$$q_1^2 + q_2^2 + q_3^2 + q_4^2 = 1 \tag{16}$$

The quaternion kinematic differential equations are given by:

$$\begin{bmatrix} \dot{q}_1 \\ \dot{q}_2 \\ \dot{q}_3 \\ \dot{q}_4 \end{bmatrix} = \frac{1}{2} \begin{bmatrix} 0 & \omega_3 & -\omega_2 & \omega_1 \\ -\omega_3 & 0 & \omega_1 & \omega_2 \\ \omega_2 & -\omega_1 & 0 & \omega_3 \\ -\omega_1 & -\omega_2 & -\omega_3 & 0 \end{bmatrix} \begin{bmatrix} q_1 \\ q_2 \\ q_3 \\ q_4 \end{bmatrix} \tag{17}$$

Like the Euler-axis vector $\mathbf{e} = (e_1, e_2, e_2)$, defining a quaternion vector $\mathbf{q} = (q_1, q_2, q_2)$ as:

$$\mathbf{q} = \boldsymbol{e} \sin(\theta/2) \tag{18}$$

we rewrite Eq. (17) as

$$\begin{aligned} 2\dot{\mathbf{q}} &= q_4\boldsymbol{\omega} - \boldsymbol{\omega} \times \mathbf{q} \\ 2\dot{q} &= -\boldsymbol{\omega}^T\mathbf{q} \end{aligned} \tag{19}$$

where:

$$\boldsymbol{\omega} \times \mathbf{q} = \begin{bmatrix} 0 & -\omega_3 & \omega_2 \\ \omega_3 & 0 & -\omega_1 \\ -\omega_2 & \omega_1 & 0 \end{bmatrix} \begin{bmatrix} q_1 \\ q_2 \\ q_3 \end{bmatrix} \tag{20}$$

Because quaternions are well-suited for on-board real-time computation, the vehicle orientation is nowadays commonly described in terms of quaternions, and a linear state feedback controller of the following form can be considered for real-time implementation:

$$\boldsymbol{u} = -\boldsymbol{K}\mathbf{q}_\mathbf{e} - \boldsymbol{C}\boldsymbol{\omega} \tag{21}$$

where $\mathbf{q}_\mathbf{e} = (q_{1e}, q_{2e}, q_{3e})$ is the attitude error quaternion vector and $\mathbf{K}$ and $\mathbf{C}$ are controller gain matrices to be properly determined. The attitude error quaternions ($q_{1e}$, $q_{2e}$, $q_{3e}$, $q_{4e}$) are computed using the desired or commanded attitude quaternions ($q_{1c}$, $q_{2c}$, $q_{3c}$, $q_{4c}$) and the current attitude quaternions ($q_1$, $q_2$, $q_3$, $q_4$) as follows:

$$\begin{bmatrix} q_{1e} \\ q_{2e} \\ q_{3e} \\ q_{4e} \end{bmatrix} = \begin{bmatrix} q_{4c} & q_{3c} & -q_{2c} & -q_{1c} \\ -q_{3c} & q_{4c} & q_{1c} & -q_{4c} \\ q_{2c} & -q_{1c} & q_{4c} & -q_{3c} \\ q_{1c} & q_{2c} & q_{3c} & q_{4c} \end{bmatrix} \begin{bmatrix} q_1 \\ q_2 \\ q_3 \\ q_4 \end{bmatrix} \tag{22}$$

If the commanded attitude quaternion vector is simply the origin defined as

$$(q_{1c}, q_{2c}, q_{3c}, q_{4c}) = (0, 0, 0, +1) \tag{23}$$

then the control logic (21) becomes:

$$\boldsymbol{u} = -\boldsymbol{K}\mathbf{q} - \boldsymbol{C}\boldsymbol{\omega} \tag{24}$$

On the other hand, if the origin is chosen as (0, 0, 0, –1), then the control logic (21) becomes:

$$\boldsymbol{u} = +\boldsymbol{K}\mathbf{q} - \boldsymbol{C}\boldsymbol{\omega} \tag{25}$$

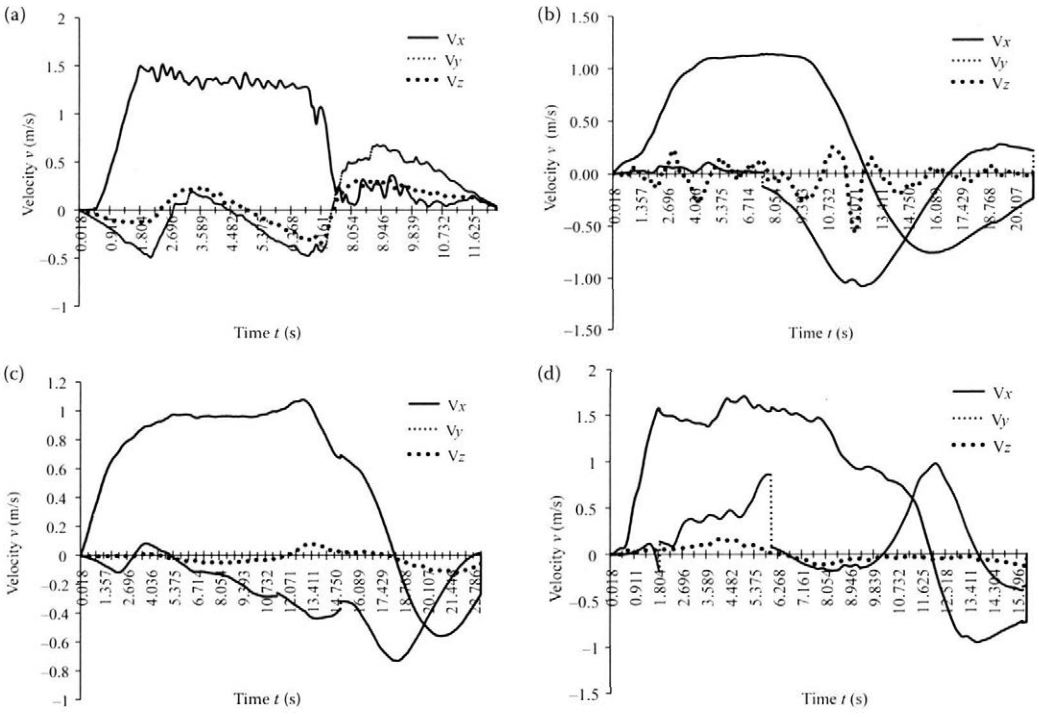


Fig. 1. Translational velocities of the centre of gravity: (a) Manoeuvre 1, (b) Manoeuvre 2, (c) Manoeuvre 3, (d) Manoeuvre 4
Vx, Vy, Vz – velocities in the direction of $x$, $y$, $z$ axis, respectively

**Agricultural machine and determination of manoeuvres**. The agricultural machine used in these experiments was the systemic vehicle MT8-222 (ZTS Obchodný podnik, Slovenská Ľupča, Slovak Republic) that is designated for working on the sloping terrain. The design of this machine is addressed by PÁLTIK et al. (2007). The average value of the slope gradient was 30–33 degrees. Experimental measurements were done from which we got the functions of the acceleration of the centre of gravity. When we processed these functions with a computer, we obtained Euler's parameters. The processing of these parameters yielded the translational and angular velocities of the centre of gravity of the systemic vehicle MT8-222, which performed the determined mounted manoeuvres. The moments of inertia of the vehicle with respect to the $x$, $y$, $z$ axes were $J_x$ = 240 kg.m$^2$, $J_y$ = 520 kg.m$^2$, and $J_z$ = 950 kg.m$^2$. The weight of the vehicle was 1.356 kg.

Four different manoeuvres were executed:

**Manoeuvre 1**: moving on the slope along the down-grade slope with braking.

**Manoeuvre 2**: moving on the slope along the down-grade slope with turning to the down-grade slope.

**Manoeuvre 3**: moving on the slope along the hillside with turning to the hillside.

**Manoeuvre 4**: moving on the slope along the down-grade slope with 45 degree yaw angle with turning to the down-grade slope.

The real trajectories executed during the manoeuvres are shown below. We assume that all of the discreet functions used by us were in the given interval <0, $t$>, where $t$ is the time of the manoeuvre execution, continuous. We suppose the existence of the position vector of the vehicle centre of gravity towards the origin of inertial coordinate system in every instant of time. During the manoeuvres execution, there was no overturn of the vehicle.

We respected the standard SAE J670 200801 (1976) as for the terminology of the vehicle dynamics.

## RESULTS AND DISCUSSION

We recommend for use in practice that curves, obtained by this approach, were approximate by polynomial functions owing to the achievement of better smoothness of the function continuance,

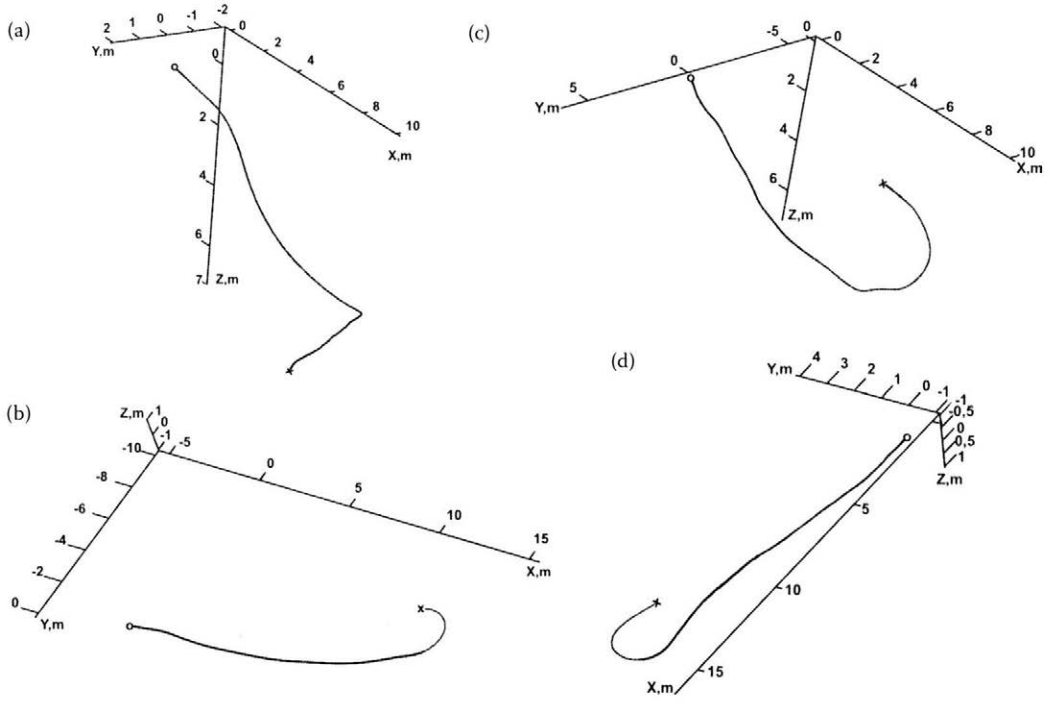


Fig. 2. Vehicle manoeuvres: (a) Manoeuvre 1; (b) Manoeuvre 2; (c) Manoeuvre 3; (d) Manoeuvre 4

whereas our functions have a stochastic character. The algorithm we formed uses also characteristic parameters of the curve such as flexion, torsion, and curvature, but their exposure would surpass the size of this contribution. That is why we present only the radius of curvature ρ. We substitute the values of translational accelerations, velocities, and the dislocations of the centre of gravity into the corresponding parameters in Eqs (6), (7), (9) and (10). The coordinates of the centre of gravity towards the inertial reference frame were obtained by utilisation of Eq. (16) to (25), similarly to Šesták et al. (1993) and Schaub et al. (2002). Using Eq. (16), we determined the stability of the evaluation of Euler's parameters and also the error of the evaluation, which was in the range of $3.10^{-13}$–$4.10^{-13}$. To solve the system of simultaneous differential equations (Eq. 17), we used Dormand-Prince method in the form of Eq. (12) for the computation of Euler's parameters. By means of Euler's parameters, we created the transformation matrix in the form:

$$[M_T]_i = \prod_{i=1}^{n} \begin{bmatrix} q_1^2 + q_2^2 - q_3^2 - q_4^2 & 2(q_2q_3 + q_1q_4) & 2(q_2q_3 - q_1q_3) \\ 2(q_2q_3 - q_1q_4) & q_1^2 + q_3^2 - q_4^2 - q_2^2 & 2(q_3q_4 + q_1q_2) \\ 2(q_4q_2 + q_1q_3) & 2(q_3q_4 - q_1q_2) & q_1^2 + q_4^2 - q_2^2 - q_3^2 \end{bmatrix}_i^T \quad (26)$$

whereas in every $i$-cycle the matrix is transposed. The components of the vectors of the translational and angular velocities of the centre of gravity in the inertial system were determined from the transformation equations as follows:

$$\begin{bmatrix} v_{XE} \\ v_{YE} \\ v_{ZE} \end{bmatrix}_i = [M_T]_i \times \begin{bmatrix} \frac{dx(t)}{dt} \\ \frac{dy(t)}{dt} \\ \frac{dz(t)}{dt} \end{bmatrix}_i, \begin{bmatrix} \omega_{XE} \\ \omega_{YE} \\ \omega_{ZE} \end{bmatrix} = [M_T]_i \times \begin{bmatrix} \frac{d\theta_x(t)}{dt} \\ \frac{d\theta_y(t)}{dt} \\ \frac{d\theta_z(t)}{dt} \end{bmatrix}_i \quad (27)$$

In Fig. 1, the translational velocities are shown for Manoeuvres 1, 2, 3, and 4.

The coordinates of the centre of gravity in the inertial system were obtained by integration:

$$\begin{bmatrix} x_E \\ y_E \\ z_E \end{bmatrix}_i = \int_0^t \begin{bmatrix} v_{XE} \\ v_{YE} \\ v_{ZE} \end{bmatrix}_i dt \quad (28)$$

Table 1. The lengths of the trajectories for Manoeuvres 1, 2, 3, and 4

| Manoeuvre | Trajectory (s, m) | Error of numerical integration |
|---|---|---|
| 1 | 11.076 | −8.515E-14 |
| 2 | 17.996 | −4.689E-13 |
| 3 | 18.744 | −4.026E-13 |
| 4 | 18.169 | −1.197E-12 |

Real trajectories of Manoeuvres 1, 2, 3, and 4 were obtained by solving Eq. (28) and are shown in Fig. 2.

To obtain the length of each trajectory of Manoeuvres 1, 2, 3, and 4, we used Eq. (6). The application of the methods of differential geometry gives us differential equations that describe the function of the spatial curve, in this case the trajectory. To solve these differential equations, we used the application created in the Delphi development environment. This application implements the numerical method Dormand-Prince (Eq. 12) and enables us to obtain the results of differential equations by numerical integration. The results achieved are given in Table 1. Also listed are the errors of numerical integration for each evaluation of the length of the vehicle trajectory.

According to Eq. (11), we evaluated the values of the radius of curvature for each manoeuvre. Fig. 3 shows the continuances of the radiuses of curvature for Manoeuvres 1 to 4. Due to limpidity, we reduced the number of the displayed points in Manoeuvres 1 and 2 in Fig 3a, b. We used the logarithmic scale to display the graphs. For the evaluation of parameters in Eqs (8), (9), and (10), we substitute x, y, z, x′, y′, z′, x″, y″, z″ by $x_E$, $y_E$, $z_E$, $v_{xE}$, $v_{yE}$, $v_{zE}$, $a_{xE}$, $a_{yE}$, $a_{zE}$, respectively.

As shown in Fig. 3, the shapes of the curves have a stochastic continuance. From the realised simulation computation it follows that the acceleration function has a deforming influence on the continuance of the radius of curvature. It is possible to obtain a smoother continuance of the acceleration functions by reverse derivation, but we do not recommend it because of a high inaccuracy. The results of the length of trajectory obtained by the approach mentioned seem highly evidentiary in comparison with the real experiment.

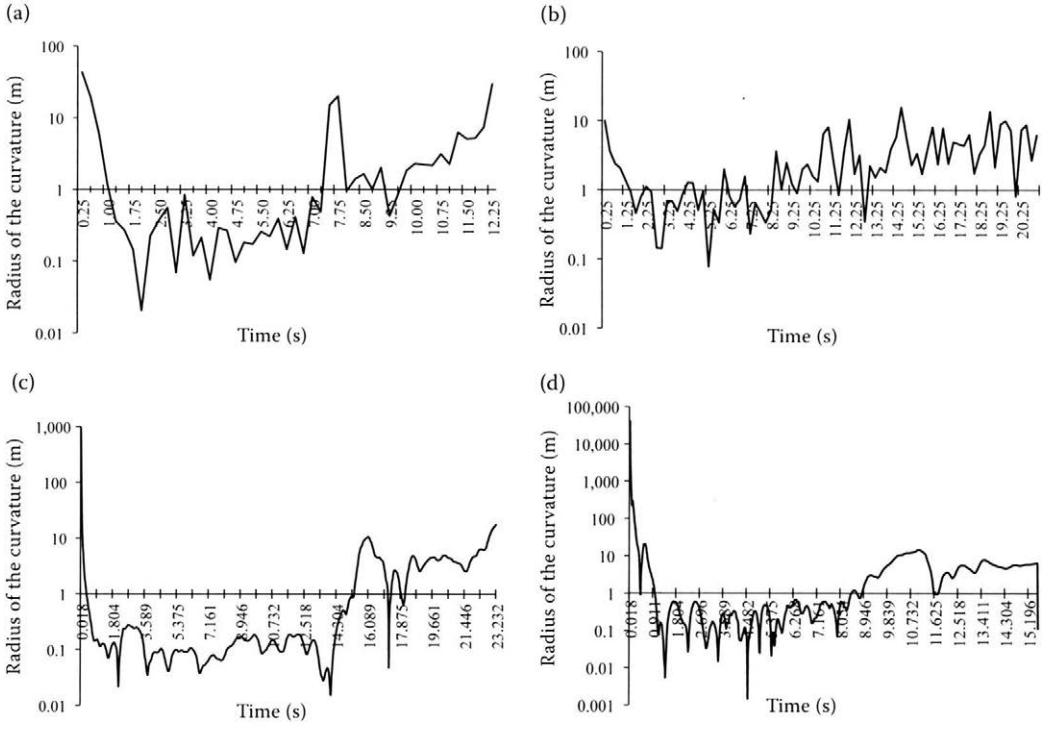


Fig. 3. Radius of curvature of the vehicle trajectory: (a) Manoeuvre 1; (b) Manoeuvre 2; (c) Manoeuvre 3; (d) Manoeuvre 4

## CONCLUSION

In this contribution, we addressed the application of differential geometry in the determination of the trajectory followed by the systemic vehicle MT8-222 in executing four different manoeuvres on the sloping terrain. We also dealt with the evaluation of the radius of curvature for each manoeuvre. The length of the trajectory was 11.076 m for Manoeuvre 1, 17.996 m for Manoeuvre 2, 18.744 m for Manoeuvre 3, and 18.169 m for Manoeuvre 4. The radiuses of curvature for each manoeuvre are interpreted in a graphic way. The described methodology using Euler's parameters has been published also by Šesták et al. (1993), as well as by Schaub et al. (2002), Rédl (2007), and Wie (2008). The stability of the numerical integration was provided by the determination of the error of the numerical integration. The step of the numerical integration was determined as $h_n$ = 1/56, which corresponds with the experimental measurement on the agricultural machine. The methods and approaches presented are utilisable in the case of the determination of the specified trajectory and required manoeuvres of automatic mobile devices in the field of precision agriculture, as well as in the modelling and simulation of the vehicle motion or in the research into dynamic effects on the vehicle.

### References


Agoston M.K., 2005. Computer Graphics and Geometric Modeling. London, Springer-Verlag: 959.

Ailona A., Berman N., Arogeti S., 2005. On controllability and trajectory tracking of a kinematic vehicle model. Automatica, *41*: 889–896.

Antos P., Ambrósio J.A.C., 2004. A control strategy for vehicle trajectory tracking using multibody models. Multibody System Dynamics, *11*: 365–394.

Dormand J.R., Prince P.J., 1980. A family of embedded Runge-Kutta formulae. Journal of Computational and Applied Mathematics, *6*: 19–26.

Hoppensteadt F.C., Jackiewicz Z., Zubik-Kowal B., 2007. Numerical solution of volterra integral and integro – differential equations with rapidly vanishing convolution kernels. BIT Numerical Mathematics, *47*: 325–350.

Ivan J., 1989. Matematika 2. [Mathematics 2.] Bratislava, Alfa: 632.

Pacejka H.B., 2005. Tire and Vehicle Dynamics, 2nd Ed. SAE International: 642.

Páltik J., Findura P., Maga J., Korenko M., Angelovič M., 2007. Poľnohospodárske stroje. [Agricultural Machines.] Nitra, Slovak University of Agriculture in Nitra: 190.

Punzo V., Borzacchiello M.T., Ciuffo B., 2011. On the assessment of vehicle trajectory data accuracy and application to the Next Generation SIMulation (NGSIM) program data. Transportation Research Part C, *19*: 1243–1262.

Purwin O., D'Andrea R., 2006. Trajectory generation and control for four wheeled omnidirectional vehicles. Robotics and Autonomous Systems, *54*: 13–22.

Rédl J., Kročko V., 2007. Analýza stability výpočtu Euler – Rodriguesových parametrov. [Solving stability analysis of Euler – Rodrigues parameters.] Acta Facultatis Technicae, *11*: 125–133.

SAE J670 2008-01, 2008. Vehicle Dynamics Terminology. Warrendale, SAE International.

Šalát T., 1981. Malá encyklopédia matematiky. [Little Encyclopedia of Mathematics.] 3rd Ed. Bratislava, Obzor: 856.

Šesták J., Sklenka P., Škulavík L., 1993. Matematické modely terénnych vozidiel určené na popis ich správania pri práci na svahu. [Mathematical Models of Terrain Vehicles Designated for Description of the Behaviour When Operating on the Slope.] Nitra, VES VŠP: 91.

Schaub H., Junkins J.L., 2002. Analytical Mechanics of Space Systems. Virginia, American Institute of Aeronautics and Astronautics: 558.

Wie B., 2008. Space Vehicle Dynamics and Control. 2nd Ed. Virginia, American Institute of Aeronautics and Astronautics: 985.

Yoon Y., Shin J., JinKim H., Park Y, Sastry S., 2009. Model – predictive active steering and obstacle avoidance for autonomous ground vehicles. Control Engineering Practice, *17*: 741–750.


Received for publication July 3, 2012
Accepted after corrections January 31, 2013

*Corresponding author*:

doc. Ing. Jozef Rédl, Ph.D., Slovak University of Agriculture in Nitra, Faculty of Engineering, Department of Machine Design, Tr. A. Hlinku 2, 949 76 Nitra, Slovak Republic
phone: + 421 376 415 670, e-mail: redl@is.uniag.sk

# Hard machining of agricultural machines parts

R. Drlička, J. Žarnovský, R. Mikuš, I. Kováč, M. Korenko

*Department of Quality and Engineering Technologies, Faculty of Engineering, Slovak University of Agriculture in Nitra, Nitra, Slovak Republic*

**Abstract**

Drlička R., Žarnovský J., Mikuš R., Kováč I., Korenko M., 2013. **Hard machining of agricultural machines parts**. Res. Agr. Eng., 59 (Special Issue): S42–S48.

For the renovation and/or improvement of the surface properties of machine elements, hard facing is often used. Hard structures obtained in layers or by heat treatment achieve a hardness of up to 68 hardness (HRC) or even more. The grinding of these surfaces demands the use of processing fluids and causes sometimes changes in the surface layers structure. Hard turning can replace grinding when certain requirements are fulfilled, particularly tough machining system. Hard deposits of two weld-on materials on a sample of steel grade S235JRG1 have been turned using cemented carbide inserts with a TiAlN coating of PVD type. The surface roughness measurements along with the observation of insert wear have been conducted to find proper machining parameters and conditions for this application. Cutting inserts manufacturer guidelines for special application could be insufficient or even not provided. Besides that, it is necessary in the experiments to take into account and examine the cutting ceramics and cubic boron nitride (CBN)/ polycrystalline cubic boron nitride (PCBN).

**Keywords**: hard turning; tool wear; surface quality; roughness; hardness

One of the main advantages of hard turning resides in the effectiveness potential of the machining of the tribological nodes elements.

Hard machining can be applied in many typical machining operations, but extremely demanding tribological conditions causing relatively rapid tool wear, which results in the tool dimension and shape accuracy loss, limit its use to such applications where tools made of a suitable cutting material are available.

Hard turning is generally defined as rotating and taper parts machining with a hardness of more than 45 hardness (HRC) using a lathe or turning centre. Allowing to achieve surface roughness $R\max/Rz$ = 1.6 μm, it can replace grinding or can be used as roughing in the case of finishing grinding. Currently, it is most used for the turning of heat-treated parts with a hardness of 45 HRC to 68 HRC and more.

The reduction or removal of the cutting fluids from the process is recommended due to two main reasons. The lifecycle cost of the cutting fluid (filtration, cleaning, residues removal) influences significantly the manufacturing costs level (Baránek, Janáč 2006). According to many sources, the cutting fluid costs can achieve in automotive industry 16–20% of the total manufacturing costs. The coming definition of quality emphasises the environmental aspects of the products and processes. The restrictions in the application of dangerous materials by law made the fluids manufacturers improve fluid formulas and evolve new fluid types. The user's reaction is a change in preferences of the fluid type and processes (Žitňanský et al. 2002, 2011).

Three types of cutting tool materials are suitable for the hard turning technology, taking its application and characteristics into account:

Table 1. Basic characteristics of Fluxofilcord 58 and Fluxodur 62

| | Chemical composition (%) | | | | Hardness (HRC) |
|---|---|---|---|---|---|
| | C | Mn | Cr | other | |
| Fluxodur 62 | 4 | 0.5 | 30 | Si: 1.2 | 57–62 |
| Fluxofilcord 58 | 0.5 | 1.5 | 5.5 | Mo: 0.6 | 56–58 |

- cemented carbides,
- cutting ceramics based on $Al_2O_3$ and $Si_3N_4$,
- hard materials – polycrystalline diamond (PCD), cubic boron nitride (CBN)/polycrystalline cubic boron nitride (PCBN).

Hard turning technology advantages in comparison to finish grinding:

- machining in one fixture/clamping maintaining the highest concentricity and perpendicularity,
- lower initial investment costs related to the turning machining centre purchase,
- use of a lower number of machines to achieve the required surface quality,
- at least one order shorter set up times and production cycles (total time saving in comparison with grinding of more than 60% in some cases),
- less time for the manipulation and cutting tool exchange,
- the possibility to produce the radius and curves using common tools with inserts,
- higher material removal rate,
- easy chip disposal.

Finish grinding also has some advantages when compared to hard turning:

- cheaper abrasive cutting tools,
- high level of shape accuracy (cylindricity, roundness),
- machined surface quality – rare and not regular white layer presence,
- half level of the residual stress in the surface layer (Majerčík 2008).

The hard turning technology applied to hard-to-machine materials leads to many problems in the surface quality achieved. Surface changes affecting the mechanical, stress-corrosion, and fatigue properties of the finished parts may occur. The highest demands are made on the surface and near-surface layers quality of hard-to-machine material parts along with the economic and environmental requirements (cutting tool life) (Czán, Neslušan 2005).

## MATERIAL AND METHODS

The aim of this paper is to evaluate the possibilities of hard layers machining, created by welding-on hard facing flux-cored wire of two constitutions, using the TIG (Tungsten Inert Gas) method.

The objective is to find the possibilities of hard machining application in the function surface obtaining for tribological joints with high demands on the finishing quality. The applicability is reviewed in terms of not only the final surface quality but also the machining process basis.

Two of flux wires different chemical compositions and strength properties were used as the filler material, namely Fluxodur 62 (Oerlikon, Zurich, Switzerland) and Fluxofilcord 58 (Air Liquide Welding, Lužianky, Slovak Republic). Their chemical composition and effective hardness are described in Table 1.

Fluxodur 62 application: worn parts of worm conveyor, mixers blades, pump parts, gravel stirrer, and other parts of mixing devices. The structure of the deposit is overeutectoid with chrome carbides addition.

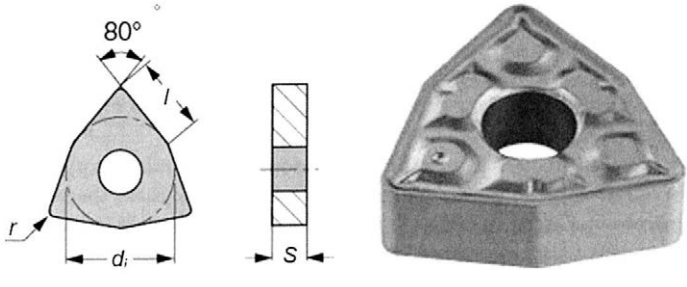


Fig. 1. Cutting insert WNMG 06T308-TF dimensions (mm): $l = 6.52$, $d_i = 9.52$, $S = 3.9$, $r = 0.8$

Table 2. Measured values of the arithmetic average of absolute values (*Ra*)

| Weld-on material | Fluxofilcord 58 | | | Fluxodur 62 | | |
|---|---|---|---|---|---|---|
| $f_n$ (mm) | 0.12 | 0.23 | 0.35 | 0.12 | 0.23 | 0.35 |
| Measuring planes | *Ra* (μm) | | | | | |
| 1 | 0.34 | 0.9 | 1.08 | 0.28 | 0.52 | 0.36 |
| 2 | 0.37 | 0.97 | 1.01 | 0.49 | 0.66 | 0.47 |
| 3 | 0.28 | 0.73 | 1.14 | 0.17 | 0.65 | 0.52 |
| 4 | 0.30 | 0.78 | 1.08 | 0.41 | 0.46 | 0.49 |
| Mean value | 0.32 | 0.85 | 1.08 | 0.34 | 0.57 | 0.46 |
| $\sigma_{Ra}$ | 0.04 | 0.11 | 0.05 | 0.14 | 0.10 | 0.07 |

$f_n$ – feed per revolution; $\sigma_{Ra}$ – standard deviation of *Ra*

Table 3. Comprehensive roughness measurement in one of the measuring planes

| Weld-on material | Fluxofilcord 58 | | | Fluxodur 62 | | |
|---|---|---|---|---|---|---|
| $f_n$ (mm) | 0.12 | 0.23 | 0.35 | 0.12 | 0.23 | 0.35 |
| No. | 4 | 5 | 6 | 1 | 2 | 3 |
| *Rq* (μm) | 0.31 | 0.90 | 1.27 | 0.14 | 1.22 | 0.84 |
| $\sigma_{Rq}$ (μm) | 0.08 | 0.09 | 0.11 | 0.03 | 0.10 | 0.12 |
| *Rt* (μm) | 1.3 | 3.6 | 5.2 | 0.9 | 4.1 | 3.3 |
| $\sigma_{Rt}$ (μm) | 0.10 | 0.25 | 0.42 | 0.07 | 0.31 | 0.35 |
| *Rz* (μm) | 0.8 | 1.6 | 3.2 | 0.6 | 3.6 | 0.8 |
| $\sigma_{Rz}$ (μm) | 0.06 | 0.17 | 0.21 | 0.06 | 0.37 | 0.11 |
| *Rp* (μm) | 0.6 | 1.6 | 2.5 | 0.4 | 2.4 | 2.2 |
| $\sigma_{Rp}$ (μm) | 0.04 | 0.17 | 0.13 | 0.02 | 0.14 | 0.23 |

$f_n$ – feed per revolution; No. – sample number; *Rq* – root mean squared; *Rt* – max. height of the profile; *Rz* – average distance between the highest peak and lowest valley in each sampling length; *Rp* – max. peak height; $\sigma_{Rq}$, $\sigma_{Rt}$, $\sigma_{Rz}$, $\sigma_{Rp}$ – standard deviations of *Rq*, *Rt*, *Rz*, *Rp*, respectively

Fluxofilcord 58 application: parts exposed to strong abrasion: excavator, digger, dredger, conveyor, hammer, shatter parts. The deposit has no cracks, pores, and it is resistant to impact load.

The testing sample was a cylindrical shaft of diameter 45 mm and length 200 mm, steel grade S235JRG1. Welding was realised using the machine Cemont Smarty TX 160alu (Air Liquide Welding, Lužianky, Slovak Republic). Pure argon was used as the shielding gas in both cases with a flow of 7.5–8.0 l/min. Based on the flux-cored wire diameter and material, the welding current was set to 140 A.

The deposits were turned on the CNC lathe Doosan LYNX 220 A (Doosan Infracore Co., Seoul, South Korea). The tool holder MWLNR 2525M-06W (ISCAR Ltd., Tefen, Israel) with $\kappa_r$ = 95° was used. The cutting insert WNMG 06T308-TF (Fig. 1) (ISCAR Ltd.) was used with a negative cutting part geometry and nose angle 80° with respect to the not evenly deposited weld-on. It has a submicron substrate with the TiAlN coating of Physical Vapor Deposition (PVD) type, designed for machining heat resistant alloys, austenitic stainless steels, carbide steels at medium to high cutting speeds, interrupted cut and severe cutting conditions. It is resistant to notch creation on the main edge and build-up.

**Machining conditions**. The sample was prepared for hard turning using the lathe to make the surface smoother after manual welding on. It is very important to set the depth of the cut to prevent the in-

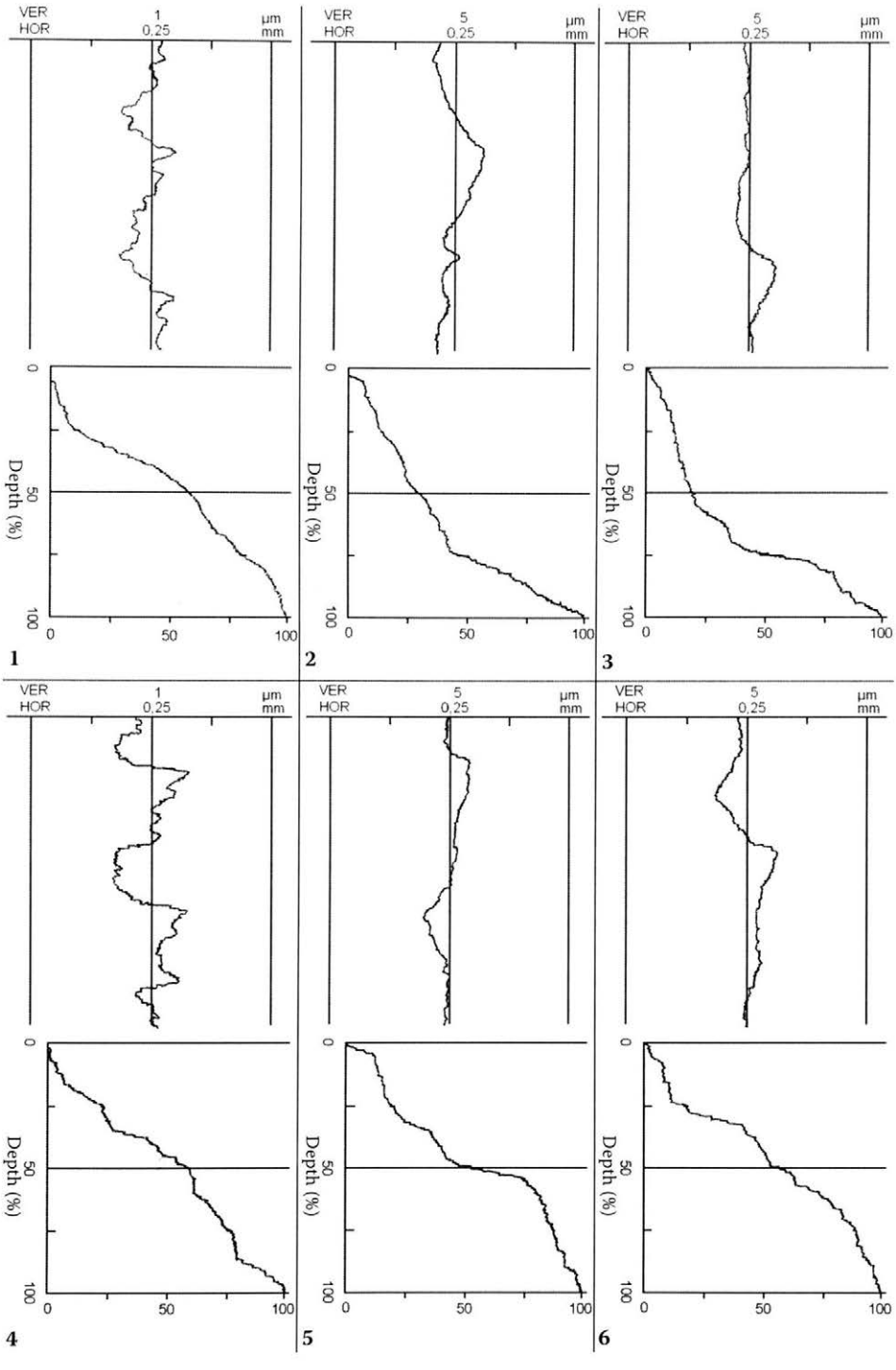


Fig. 2. *Ra* (average of absolute values) measurement record (first and third row graphs: VER (vertical), HOR (horizontal) – axes units) and carrier surface on section level graphs (second and fourth row)

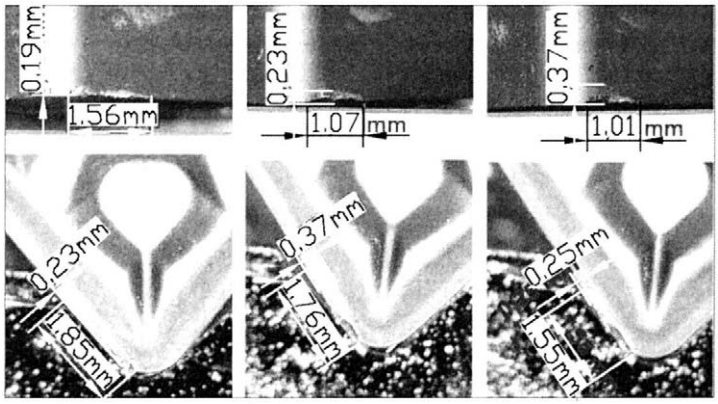


Fig. 3. Tool inserts wear in turning Fluxofilcord 58

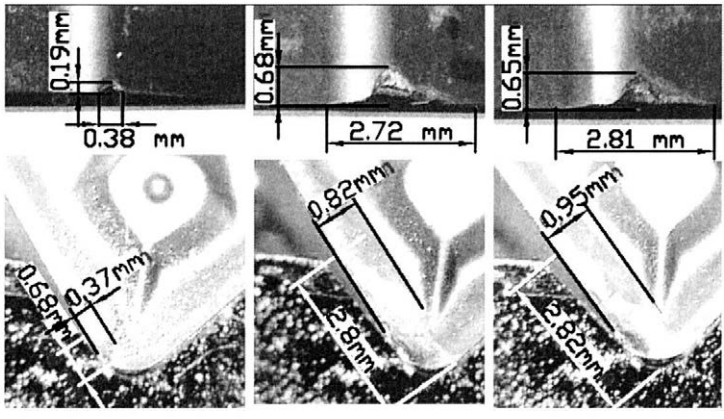


Fig. 4. Tool inserts wear in turning Fluxodur 62

terrupted cutting as a main reason of rapid wear of the cutting insert. It is not possible to achieve non-interrupted cutting in the first pass due to craters and small pits on the surface as a result of welding and roughing.

The parameter allowing changes in some range was fed. It was chosen from the low, middle, and high limits of the manufacturer's recommended range. The cutting speed selected was in the middle of the manufacturer's recommended range, while the depth of the cut considering the weld properties was set lower:

- spindle rotation: $n$ = 1.537/min,
- cutting speed: $v_c$ = 200 m/min,
- feed per revolution: $f_n$ = 0.12–0.35 mm,
- depth of cut: $a_p$ = 0.2 mm.

**Measurement of cutting insert wear**. The digital microscope BBCGROUP DA-70350 (BBC Tools, Nitra, Slovak Republic) was used to measure the cutting insert wear. It was connected to the PC via USB and allowed a real-time screen display, 10–200× magnification, LED assistant light, VGA resolution, video capture at 30 fps, a holder with easy positioning and capturing, user-friendly environment.

The Carl-Zeiss application AxioVison LE (Carl Zeiss AG, Oberkochen, Germany) was used to measure the common reference and obtain the real-scale factor. The dimensioned lengths in pixels were then converted to millimetres automatically. The maximal error occurring due to operator's error in the reference setting was 0.01 mm.

## RESULTS AND DISCUSSION

The measured results of roughness show a relation to machining parameters in the case of Fluxofilcord 58 weld-on, less trends in the case of Fluxodur 62 weld-on.

Besides the *Ra* value in Table 2, Table 3 shows the values of parameters *Rz*, *Rt*, *Ry*, and others. In the case of *Rz*, the relation is similar to *Ra*. More than the numerical values, the graphical record of the measurement expresses the surface character.

Table 4. Dimensions of tool wear in turning Fluxofilcord 58

| Fluxofilcord 58 | $f_n$ (mm) | | |
|---|---|---|---|
| | 0.12 | 0.23 | 0.35 |
| $VB_{max}$ | 0.19 | 0.23 | 0.37 |
| $KB$ | 0.23 | 0.37 | 0.25 |
| Rake face wear length | 1.85 | 1.76 | 1.55 |

$VB_{max}$ – maximal width of flank wear land; $KB$ – crater centre distance; $f_n$ – feed per revolution

Steadily growing carrier profile, appears in measurement 1 Fluxodur 62 (feed per revolution 0.12 mm) and in measurements 4 and 6 Fluxofilcord (feed per revolution 0.12 and 0.35 mm) (Fig. 2).

### Cutting insert wear evaluation

The images of cutting inserts wear were processed in the graphical application mentioned above and dimensioned. The wear snapshots are placed in Figs 3 and 4 from the left to the right according to the increasing feed values. The tables with the wear values at the rake face and flank face are provided to make the comparison easier (Tables 4 and 5). The width of the wear on the flank face $VB_{max}$ had the main influence on the tool life. The width increased with the feed in both cases, with a small exception in the case of Fluxodur 62 feed change from 0.23 to 0.35 mm.

As for the rake face, the tool wear measured according to standard STN ISO 3685 (1999) as the $KB$ parameter showed an increasing trend in the case of Fluxodur 62, but not in the case of Fluxofilcord 58. The rake face wear area length decreased slightly when turning the first weld-on material, but increased in the case of Fluxodur 62. These materials differ in hardness (57–60 HRC for Fluxofilcord 58 when compared to 61–64 HRC for Fluxodur 62) due to the nature of the material structure.

Table 5. Dimensions of tool wear in turning Fluxodur 62

| Fluxodur 62 | $f_n$ (mm) | | |
|---|---|---|---|
| | 0.12 | 0.23 | 0.35 |
| $VB_{max}$ | 0.19 | 0.68 | 0.65 |
| $KB$ | 0.37 | 0.82 | 0.95 |
| Rake face wear length | 0.68 | 2.80 | 2.82 |

$VB_{max}$ – maximal width of flank wear land; $KB$ – crater centre distance; $f_n$ – feed per revolution

Based on the previous, it can be stated generally that the wear grows with the feed in the inspected range of the cutting parameters. Despite the manufacturer's guidelines, the wear values did not respond to the machined area and reduced the tool life significantly.

## CONCLUSION

The application of innovation in machining technologies, that is the improvement of advanced technologies, is a desirable trend in industry today. The economic, environmental, and legislative reasons may accelerate this effort, resulting in the cost and production time reduction and environment protection.

This research needs to be coupled with wear resistance tests simulating real operation conditions as well as the structures after the machining study in terms of residual stress and microhardness distribution.

To prove proper friction properties of the surface created in machining, quantitative evaluation of the surface roughness proceeds in tribological tests. The tool wear exceeds the prior expectations. The TiAlN coated cemented carbide showed quite a poor wear resistance although it should withstand the interrupted cut of hard materials. Besides the weld structure character, the removal of the coating layers, leaving the substrate unprotected, as observed e.g. by Nabhani (2001), should be considered in the cutting edge wear mechanism evaluation. Based on the results of other authors (Dawson et al. 2001; Brookes et al. 2002), in the following research the CBN tool insert needs to be examined as well as cemented carbide with different types of coating.

The manual type of welding-on technology has been chosen in relation to the testing purposes. In some cases, the mechanised welding-on can be used instead of the former, resulting likely in a smoother deposit surface. Keeping the process type, the TOPTIG (Air Liquide Welding patented) technology could be adopted to examine this.

Regardless of the problems mentioned above, it can be concluded that the hard turning with a properly selected parameter and suitable machining system has a great potential as concerns the time reduction and productivity increase.

## References


Baránek I., Janáč A., 2006. Vývojové smery v technológií obrábania. [Trends in machining technology.] Strojárstvo, 2: 76.

Brookes E.J., James R.D., Shutt C., Taylor C.J., 2002. Machining abrasion-resistant hard-facings with PCBN tools. In: Kuljanic E. (ed.), Proceedings AMST 02 – Advanced Manufacturing Systems and Technology, June 2002, Udine: 113–120.

Czán A., Neslušan M., 2005. Trieskové obrábanie ťažkoobrobiteľných materiálov. [Machining of Hard-to-Machine Materials.] Žilina, EDIS: 156.

Dawson G., Ty G., Kurfess R.T., 2001. Hard turning, tool life, and surface quality. Manufacturing Engineering, 4: 88–98.

Majerčík J., 2008. Náhrada brúsenia kalených ocelí tvrdým sústružením. [Replacing of hardened steels grinding by hard turning.] Strojárstvo, 5: 4–14.

Nabhani F., 2001. Wear mechanisms of ultra-hard cutting tools materials. Journal of Materials Processing Technology, 3: 402–412.

STN ISO 3685, 1999. Skúšanie trvanlivosti sústružníckych nástrojov s jednou reznou hranou [Tool-life testing with single-point turning tools.] Bratislava, SUTN: 30.

Žitňanský J, Tomáš J., Kročko V., 2002. Energetická náročnosť pri sústružení za sucha. [Power consumption in dry turning.] Acta Mechanica Slovaca, 2: 367–372.

Žitňanský J., Žarnovský J., Mikuš R., Kováč I., Andrássyová Z., 2011. Material machining for friction of moving parts for agricultural machines. Research in Agricultural Engineering, 57: S61–S68.


Received for publication July 7, 2012
Accepted after corrections January 1, 2013

*Corresponding author*:

Ing. Róbert Drlička, Slovak University of Agriculture in Nitra, Faculty of Engineering,
Department of Electrical Engineering, Automation and Informatics, Tr. A. Hlinku 2, 949 76 Nitra, Slovak Republic
phone: + 421 376 414 101, e-mail: robert.drlicka@uniag.sk

# I-x-w diagram of wet air and wheat grain

I. Vitázek, J. Havelka

*Department of Transport and Handling, Faculty of Engineering, Slovak University of Agriculture in Nitra, Nitra, Slovak Republic*

**Abstract**

Vitázek I., Havelka J., 2013. **I-x-w diagram of wet air and wheat grain**. Res. Agr. Eng., 59 (Special Issue): S49–S53.

The authors have been working for 50 years in the research and development of drying in agriculture. In the way of drying applied, warmed air is used as the drying medium. The thermodynamics of wet air is used for the analysis of these processes of drying in the calculations and in graphic demonstrations applying an i-x diagram of wet air. This diagram does not include any information about the state of the dried material. The authors therefore enlarged this i-x diagram with the equilibrium moisture contents of the dried material. In their work, the authors present a method using this enlarged diagram and, as an example, the i-x-w diagram of wet air and equilibrium moisture of wheat grain.

**Keywords**: drying in agriculture; equilibrium moisture; thermodynamics; sorption isotherm

The majority of agricultural products are harvested with a high moisture content. Therefore, it is necessary to reduce the moisture content by drying to an optimal value for long-term storage, i.e. to the standard moisture content. Warmed atmospheric air is used as the drying medium for the energy input and moisture output.

The thermodynamics of wet air elaborated by Chyský (1977) is used for the process analysis of drying. The thermodynamics of drying has been presented in several basic publications (Pabis 1966, 1982; Maltry, Pötke 1966; Imre 1974). Equilibrium moisture contents in the form of sorption isotherms are presented in these publications and also in a detailed publication by Nikitina (1963), and also in the recent publications by Štencl (2000a, b).

A disadvantage of all methods published is that the process of drying consists of two parts:
- thermodynamics of wet air,
- thermodynamics of humid material.

In their research works from 1970 up to the present day, the authors therefore elaborated a new complex diagram of wet air with inserted moisture information on the dried material (Havelka 1973; Vitázek 1996, 2011). The graphic description of the process of drying is significantly better.

In this paper, the authors present their most recent alternative of the method of importing the equilibrium moisture content into the i-x diagram of wet air.

Also in this paper, some specific parameters are used of wet air and humid material. Therefore, a brief description of them is introduced in the following section.

## MATERIAL AND METHODS

**Wet air**. Wet air is used as a drying medium for delivering the necessary heat for humidity evaporation and taking away this evaporated humidity. Wet air is a mixture of several over-heated vapours. An exception is water vapour which condenses in the working temperatures area. Therefore, the thermodynamics of wet air was elaborated.

Relative humidity of wet air φ:

$$\varphi = p_p/p'' \quad (1)$$

where:

$p_p$ – partial pressure of water vapour (Pa)

$p''$ – pressure of saturated water vapour at the temperature of the air concerned (Pa)

Specific humidity of wet air ($x$):

$$x = M_W/M_M \quad \text{(kg/kg)} \quad (2)$$

where:

$M_W$ – mass of water vapour (kg)

$M_M$ – whole mass of the wet air (kg)

The enthalpy of wet air is calculated with a specific mass unit $(1 + x)$ kg:

$$i_{(1+x)} = i_a + x \times i_p \quad (3)$$

where:

$i_{(1+x)}$ – enthalpy of wet air

$i_a$ – enthalpy of dry air

$i_p$ – enthalpy of water vapour

$x$ – humidity ratio

The following numerical equation is used for wet air of temperature 0–100°C and pressure 100 kPa:

$$i_{(1+x)} = 1.02t + x(2{,}500 + 1.84t) \quad \text{(kJ)} \quad (4)$$

where:

$t$ – temperature of wet air

Using these relations, Mollier constructed his i-x diagram of wet air. In the coordinates $i$, $x$, are demonstrated straight lines of $t$ = const., with curves φ = const., and with the curve of saturated wet air φ = 1. These parameters are used in the modelling of the process of drying.

**Humid material**. The humidity of the material $u$ can be described by means of two parameters STN 12 6000 (1996).

Moisture content dry basis $u$, which is predominantly used in the theory of drying:

$$u = M_W/M_{dM} \quad \text{(kg/kg)} \quad (5)$$

where:

$M_W$ – mass of humidity (kg)

$M_{dM}$ – mass of dry basis of the material (kg)

Moisture content wet basis $w$ is used in the practice of drying:

$$w = (M_W/M_M) \times 100 \quad (\%) \quad (6)$$

where:

$M_W$ – mass of humidity (kg)

$M_M$ – whole mass of the material (kg)

Bilateral relations of this are as follows:

$$w = 100 \times u/(1 + u), \quad u = w(100 - w) \quad (7, 8)$$

**Process of drying**. The process of drying is divided into three sections. Schematic demonstration of these sections in graphic description in curve of drying is shown in Fig. 1. The three sections:

(1) section of the growing rate of drying,

(2) section of a permanent rate of drying, in which the evaporation of free moisture from the surface prevails, the decrease of moisture being directly proportional to time,

(3) section of a falling rate of drying, in which the decrease of the bound moisture is not proportional to time. The evaporation from the inside of the material, the section ends with the equilibrium moisture content.

The equilibrium moisture is the moisture relevant to the state of thermodynamic equilibrium of the material parameters and ambient atmosphere.

**Sorption**. Sorption isotherm is the graphic demonstration of the equilibrium moisture of the material $u_r$, in relation to the relative humidity $w_r$ of ambient air at the given temperature and pressure.

The literature contains tables of $u_r$ for various $\varphi_r$ (relative humidity of wet air) at a constant temperature, which were investigated with the use of laboratory experiments.

A great number of authors have presented also analytic relations $\varphi_r = f(u_r, t)$ in various forms.

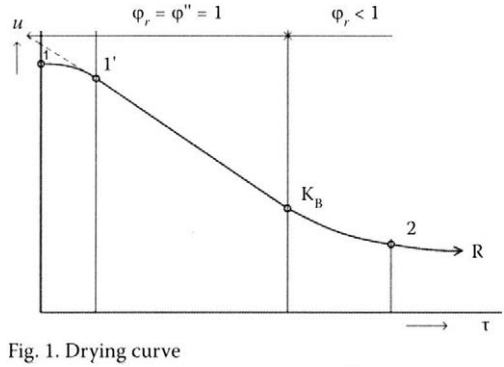


Fig. 1. Drying curve

1 – start of drying; 2 – end of drying; $K_B$ – critical point; R – point of equilibrium humidity, in the theory in infinity; 1–1' – section of increasing rate of drying; 1'–$K_B$ – section of permanent rate of drying; $K_B$–R – section of falling rate of drying; $u$ – moisture content dry basis; τ – time

The best form for agricultural materials is the relation from HENDERSON (1952), which was brought into Europe by PABIS (1982):

$$1 - \varphi_r = \exp(-a \times T \times u_r^n) \quad (9)$$

where:

$\varphi_r$ – equilibrium relative humidity of wet air
$u_r$ – equilibrium moisture content dry basis
$T$ – absolute temperature ($K$)
$a, n$ – coefficients, individual for every material

**Regression**. The authors adapted Eq. (9) for regression to obtain coefficients $a, n$ with regression values.

The authors took from the literature the tabulated values of the isotherm of the given material and, using regression, they calculated the coefficients of Henderson's relation.

By adaptation, Eq. (9) is transformed to logarithm and multiplied with –1:

$$-\ln (1 - \varphi_r) = a \times T \times u_r^n \quad (10)$$

and the logarithm of this Eq. (10) is:

$$\ln (-\ln (1 - \varphi_r)) = \ln a + \ln T + n \times \ln u_r \quad (11)$$

This equation is transformed to the linear form and used for linear regression of the tabulated values of the given material. The linear form of Eq. (11) is:

$$Y = A + B \times X \quad (12)$$

where:

$$Y = \ln(-\ln(1-\varphi_r)) \quad (13)$$

$$A = \ln a + \ln T \quad (14)$$

$$X = \ln u_r = \ln (w_r/(100 - w_r)) \quad (15)$$

where:

$Y, A, X$ – coefficients of linear equation

By means of the linear regression of the tabulated values of the given material, we obtain the values of $A$ and $B$, from which we deduce:

$$N = B \quad (16)$$

$$A = \exp (A - \ln T) \quad (17)$$

These new coefficients $a, n$ are used in a modified equation of Henderson:

$$\varphi_r = 1 - \exp (a \times T \times u_r^n) \quad (18)$$

where:

$n$ – coefficient of Henderson's modified equation
$T$ – thermodynamic temperature of given material

## RESULTS AND DISCUSSION

### Wheat

From the tables specified by PABIS (1982), the authors took the values of the isotherm for wheat, i.e. equilibrium moisture contents $w_r$ at the temperature of 20°C and pressure of 101.325 kPa (Table 1).

This isotherm is presented in a graphic form in Fig. 2 in the coordinates $w_r$, $\varphi_r$.

Using the regression of these values, we obtained the constants for Henderson's analytical relation for this wheat:

$$\varphi = 1 - \exp (-0.2053 \times T \times u^{2.2376}) \quad r = 0.994 \quad (19)$$

where:

$\varphi$ – relative humidity of wet air
$T$ – thermodynamic temperature of given material
$u$ – moisture content dry basis
$r$ – correlation coefficient

With this Eq. (19) the authors calculated the equilibrium moisture contents (w.b.) $w_r$ = 8, 10, 12, 14, 16, 18, 20, 24% course for temperatures of 10 to 50°C and drew these curves $w_r$ = const. into the i-x diagram of wet air using lines $t$ = const. and curves $\varphi$ = const. as new coordinates.

The authors propose this new form of diagram to be designated as i-x-w diagram of wet air and humid wheat grain.

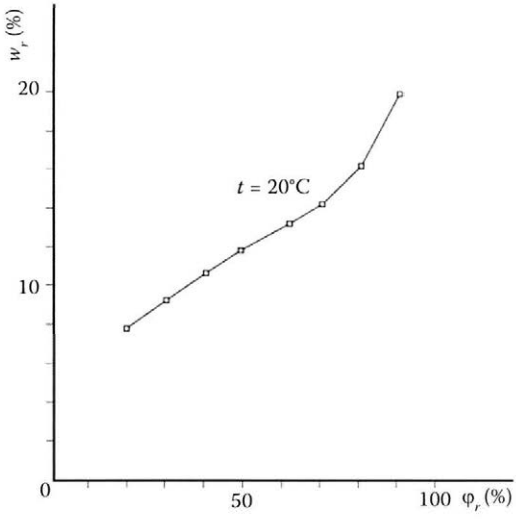


Fig. 2. Sorption isotherm of wheat grain
$w_r$ – equilibrium moisture content wet basis; $\varphi_r$ – equilibrium relative humidity of wet air

Table 1. Wheat equilibrium moisture content wet basis for temperature 20°C

| φ (%) | 20 | 30 | 40 | 50 | 60 | 70 | 80 | 90 |
|---|---|---|---|---|---|---|---|---|
| $w_r$ (%) | 7.80 | 9.24 | 10.68 | 11.84 | 13.10 | 14.30 | 16.02 | 19.95 |

φ – relative humidity of wet air; $w_r$ – equilibrium moisture content wet basis

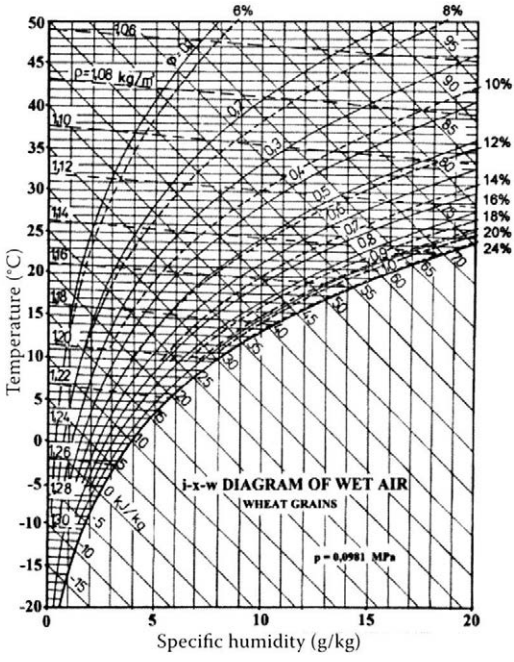


Fig. 3. I-x-w diagram of wet air and equilibrium moisture of wheat grain
$p$ – atmospheric pressure

The application of wet air thermodynamics is a significant method for the analysis of the drying processes in agriculture. Since 1970, the authors have developed the thermodynamics of drying in agriculture. In this work, they refer to their improvement on this thermodynamics with a combination of i-x diagram of wet air and with the equilibrium moisture values of the given material, which were confirmed with laboratory experiments.

In Fig. 2 is presented the sorption isotherm of wheat grains at 20°C. Information in this diagram is short for its utilisation in the thermodynamics of drying.

The i-x diagram of wet air is used advantageously for the graphic demonstration of the state changes of the drying medium in the drying process, without any information on the state changes of the dried material.

In Fig. 3 is shown a new i-x-w diagram of wet air and equilibrium moisture of wheat grains. This new diagram is able to demonstrate, in graphic form, parallel state changes of the drying medium and of the dried material. This diagram enables therefore an improved thermodynamic analysis of the drying process.

## CONCLUSION

The i-x-w diagram of wet air and equilibrium moisture of a given material is a new type of diagram, which is unknown in the specialised literature. This diagram enables the most suitable analysis of the drying process.

The authors used this diagram in their works with a great success. They will continue in the development of the thermodynamic analysis of drying processes through modelling the process in research, and in the evaluation of drying processes in practice.

### References

HAVELKA J., 1973. Optimalizácia sušenia sena s prihrievaním vzduchu. [Optimal process of hay drying with heated air.] In: Proceedings Súčasná teória a prax sušenia zrnovín a krmovín. [Current Theory and Practice of Drying of Grain and Forage Plants.] Bratislava, DT SVTS: 229–238.

HENDERSON S.M., 1952. A basic concept of equilibrium moisture. Agricultural Engineering, 33: 29–32.

CHYSKÝ J., 1977. Vlhký vzduch. [Wet Air.] Prague, SNTL: 160.

IMRE I., 1974. Száritási közikönyv. [Manual of Drying.] Budapest, Müszaki Könyvkiado: 1122.

MALTRY W., PÖTKE E., 1966. Technika poľnohospodárskeho sušiarenstva. [Technics of Drying in Agriculture.] Bratislava, SVPL: 490.

NIKITINA L.M., 1963. Tablicy ravnovesnogo udelnogo vlagosoderžanija i energii svjazi vlagi s materialama. [Tables of Equilibrium Moisture Vontents and Binding Energy of Moisture with Material.] Moscow, Gosenergoizdat: 174.

PABIS S., 1965. Suszenie plodów rolnych. [Drying of Agricultural Products.] Warszawa, PWRiL: 316.

PABIS S., 1982. Teoria konwekcionogo suszenia produktov rolniczuych. [Theory of Heat Conduction Drying of Agricultural Products.] Warszawa, PWRiL: 229.

STN 12 6000, 1996. Sušiarenstvo. Technika sušenia. [Slovak Technical Norm – Drying technics.] Bratislava, Slovak Office of Standard, Metrology and Testing.

Štencl J., 2000a. Equilibrium moisture content of *Festuca pratensis* in near ambient air drying conditions. Acta Technologica Agriculturae, *3*: 21–26.

Štencl J., 2000b. Equilibrium moisture content as a control parameter for a meadow grass drying process in a barn. Acta Technologica Agriculturae, *3*: 27–31.

Vitázek I., 1996. Modifikovaný i-x diagram vlhkého vzduchu. [Modified i-x diagram of wet air.] Poľnohospodárstvo, *8*: 645–651.

Vitázek I., 2011. Technika sušenia v teórii a v praxi – Obilniny. [Drying Technics in Theory and Practice – Cereals.] Nitra, Slovak University of Agriculture in Nitra: 102.

Received for publication July 9, 2012
Accepted after corrections February 1, 2012

*Corresponding author:*

doc. Ing. Ivan Vitázek, CSc., Slovak University of Agriculture in Nitra, Faculty of Engineering, Department of Transport and Handling, Tr. A. Hlinku 2, 949 76 Nitra, Slovak Republic
phone: + 421 376 414 756, e-mail: ivan.vitazek@uniag.sk

# Verification of agro-production building structures affecting the quality of indoor environment in the summer season

Š. Pogran[1], T. Reichstadterová[1], J. Lendelová[1], D. Páleš[1], W. Bieda[2], M. Bošanský[1]

[1]*Department of Structures, Faculty of Engineering, Slovak University of Agriculture in Nitra, Nitra, Slovak Republic*

[2]*Department of Rural Buildings, Faculty of Environmental Engineering and Land Surveying, University of Agriculture in Kraków, Kraków, Poland*

**Abstract**

Pogran Š., Reichstadterová T., Lendelová J., Páleš D., Bieda W., Bošanský M., 2013. **Verification of agro-production building structures affecting the quality of indoor environment in the summer season**. Res. Agr. Eng., 59 (Special Issue): S54–S59.

This contribution focuses on the evaluation of the effect of aerated concrete external wall of a hall falling within the category of special-purpose agricultural buildings in terms of the phase shift of temperature oscillation. The assessment was performed by precise and approximate calculation procedures and was then compared with the results obtained from the values actually measured under the operating conditions.

**Keywords**: phase shift of temperature oscillation; temperature damping; external cladding

The building energy balance is affected by different thermo-physical phenomena generated by the interaction between solar radiation and different parts of the building envelope. These components should be closely linked with a unified aim to provide an improvement on the energy balance of the building (Fuliotto et al. 2010). Internal air temperature is influenced by variations in outdoor conditions such as temperature, solar radiation or meteorological situation. Other important parameters are wall overall heat transfer coefficient, internal heat gains or losses caused by devices such as lighting, occupancy, etc. Many articles related to this topic are focused on energy storage using heat accumulation in purpose-designed structures (Khudhair, Farid 2004; Heim 2010). At the present time, the phase shift of temperature oscillation is a lack in understanding thermal characteristic of buildings, which can present the semblance of a considerable influence on the thermal comfort of interior users during the summer period. The surface of the building envelope is heated by exposure to the increased external air temperature or direct sunlight, and at the same time the increased temperature from the surface is gradually spread towards the interior. Heat conduction occurs due to the exchange of energy

Supported by the Scientific Grant Agency VEGA of the Ministry of Education of the Slovak Republic and the Slovak Academy of Sciences, Grant No. 1/0609/12.

between micro-particles in solids but also in the air (Řehánek 2002). The phase shift expresses the time during which the max. external air temperature increases the max. temperature on the inner surface of the building structure. This means that the phase shift of temperature oscillation in individual parts of the building envelope Ψ indicates the level of thermal stability of the internal environment. The higher its value, the greater thermal stability will exist in the internal space. The objective of the presented research was to verify the computing methods for determining the temperature damping of the external cladding in the agricultural manufacturing building in relation to the actually reached parameters obtained during summer "tropical days".

## MATERIAL AND METHODS

The selected part of the external wall of the hall in a special-purpose agricultural building was assessed in terms of the phase shift of temperature oscillation in the summer season. Computational models were used to validate the results under practical operating conditions.

The external wall of the building is designed with light-weight aerated concrete blocks with a thickness of 300 mm and both of its sides are of lime-cement plaster 15 mm thick. The composition of the envelope structure and thermal properties of the wall layers are shown in Table 1.

The assessment in the computing part was done by precise calculations according to Šklover et al. (1966) and Halahyja et al. (1985), the output of which are relationships presented in a complex form. The results of this calculation are compared with a commonly used approximate equation (Chmúrny 2003; Vaverka 2006), followed by the assessment.

During the verification of the phase shift of the temperature oscillation, seven consecutive "tropical days" (from August 19, 2011 to August 26, 2011) were taken into account. Such a long period can already be considered sufficiently substantiated in terms of the exposure of the considered building to high temperatures. During the verification of the phase shift of the temperature oscillation in the selected east-oriented external wall, the period from August 24, 2011 (from 2.00 p.m.) to August 26, 2011 (till 2.00 p.m.) was taken into account due to the assumed time delay between the achievement of max. waveform ambient temperatures and inner surface temperatures. The actual assessment of the phase shift of the temperature oscillation was carried out only for the interval of one day (August 25, 2011 from twelve midnight to twelve midnight). Numerous results obtained were compared with the actually measured values. The measurements were made with a temperature and relative humidity logger Comet 3121 (Comet System Ltd., Rožnov pod Radhoštěm, Czech Republic) and a surface temperature logger DS 18 B20 (Department of Electrical Engineering, Automation and Informatics, Slovak University in Nitra, Nitra, Slovak Republic).

## RESULTS AND DISCUSSION

### Numerous expression of the phase shift of temperature oscillation

#### Precise calculation

(1) Temperature damping of a three-layer construction in a complex form (Šklover 1966)

$$\Theta_3 = \frac{s_2}{s_3}\left[\frac{s_1}{s_2}\times N\times\cosh\left(\frac{\bar{s}_2}{\lambda_2}\times d_2\right)+M\times\sinh\left(\frac{\bar{s}_2}{\lambda_2}\times d_2\right)\right]\times$$
$$\times\left[\sinh\left(\frac{\bar{s}_3}{\lambda_3}\times d_3\right)+\frac{\bar{s}_3}{h_e}\times\cosh\left(\frac{\bar{s}_3}{\lambda_3}\times d_3\right)\right]+$$
$$+\left[\frac{s_1}{s_2}\times N\times\sinh\left(\frac{\bar{s}_2}{\lambda_2}\times d_2\right)+M\times\cosh\left(\frac{\bar{s}_2}{\lambda_2}\times d_2\right)\right]\times$$
$$\times\left[\cosh\left(\frac{\bar{s}_3}{\lambda_3}\times d_3\right)+\frac{\bar{s}_3}{h_e}\times\sinh\left(\frac{\bar{s}_3}{\lambda_3}\times d_3\right)\right] \quad (1)$$

where:

$\lambda_1, \lambda_2, \lambda_3$ – thermal conductivity of the layers (W/m.K)

$s_1, s_2, s_3$ – heat absorption capacity of the wall structure layers (W/m$^2$.K)

$d_1, d_2, d_3$ – thickness of the layers (m)

$h_e$ – surface coefficient of heat transfer on the external side of the structure (W/m$^2$.K)

$M, N$ – parameters indicating the ratio of heat flows and thermal amplitudes

whereby

$$s_j = 0.00853\times\sqrt{\lambda_j c_j \rho_j} \quad (2)$$

$$\bar{s}_j = s_j\times\sqrt{i} \quad (3)$$

where:

$s_j$ – heat absorption capacity (W/m$^2$.K)

$c_j$ – specific heat capacity (J/kg.K)

$\rho_j$ – bulk density (kg/m$^3$)

Table 1. Thermo-technical properties of building materials (STN 73 0540-3 2002)

| Layer | Material | Thickness of layer (m) | Bulk weight (kg/m$^3$) | Thermal conductivity (W/m.K) | Specific heat capacity (J/kg.K) |
|---|---|---|---|---|---|
| 1. | lime-cement plaster | 0.015 | 2,000 | 0.99 | 790 |
| 2. | light-weight aerated concrete block | 0.300 | 550 | 0.19 | 840 |
| 3. | lime-cement plaster | 0.015 | 2,000 | 0.99 | 790 |

(2) Phase shift of temperature oscillation $\Psi_1^\circ$

$$\psi_1^\circ = \text{argum}(\Theta) = \text{arctg}\frac{b}{a} + k\pi \quad (4)$$

where: $k = 0$ at $a > 0, b > 0$
$k = 1$ at $a < 0, b < 0$
$k = 2$ at $a > 0, b < 0$

where:

argum ($\Theta$) – complex shape of the phase shift of temperature oscillation (–)

$k$ – coefficient (–)

$a$ – abscissa of a complex number (–)

$b$ – ordinate of a complex number (–)

Then,
$\Psi_1^\circ$ = 10.09 (h).

**Approximate calculation**

We determined the phase shift of temperature oscillation $\Psi_2^\circ$ by an approximate calculation in a time scale through the equation

$$\psi_2^\circ = \frac{1}{15}\left[40.5\sum_{j=1}^{n} D_j - \text{arctg}\frac{\alpha_i}{h_i + U_{si}\sqrt{2}} + \text{arctg}\frac{U_{se}}{U_{se} + h_e\sqrt{2}}\right] \quad (5)$$

where:

$$D_j = R_j s_j \quad (6)$$

where:

$R_j$ – thermal resistance of a layer (m$^2$.K/W)

$U_{si}$, $U_{se}$ – heat absorption capacity of individual surface layers (W/m$^2$.K)

$h_i$ – heat transfer coefficient at internal surface (W/m$^2$.K)

$h_e$ – heat transfer coefficient at external surface (W/m$^2$.K)

$D_j$ – thermal inertia (–)

$s_j$ – heat absorption capacity (W/m$^2$.K)

Then,
$\Psi_2^\circ$ = 11.63 (h).

Temperature harmonic fluctuation is schematically described in Fig. 1.

**Phase shift of temperature oscillation expressed according to actually measured values**

After the time period of six consecutive tropical days (from August 19, 2011 to August 24, 2011) during which the temperature value exceeded 30°C, the courses of external and internal temperatures as well as temperatures of the circumferential wall on the internal surface were measured during the next 48 hours.

Based on the values measured during the first interval of 24 h (from August 24, 2011 from 2.00 p.m. to August 25, 2011 till 2.00 p.m.) and the second interval of 24 h (from the August 25, 2011 from 2.00 p.m. to August 26, 2011 to 2.00 p.m.), the following data were evaluated.

(1) Average daily temperature of external air $\theta_{eDm}$ according to the equation

$$\theta_{eDm} = \frac{1}{144}\left(\theta_{e1} + \theta_{e2} + \ldots\right) \quad (7)$$

where:

$\theta_{e1}$, $\theta_{e2}$ – daily temperatures of external air (measured in the intervals of 10 min, it means 144 measurements in 24 h)

Average daily temperature of external air measured from the registered records:

$\theta_{eD1m}$ = 27.16°C (first interval of 24 h)
$\theta_{eD2m}$ = 26.50°C (second interval of 24 h)

(2) Average daily temperature of the internal surface on the considered wall $\theta_{si,m}$ according to the equation

$$\theta_{si,Dm} = \frac{1}{144}\left(\theta_{si,1} + \theta_{si,2} + \ldots\right) \quad (8)$$

where:

$\theta_{si,1}$, $\theta_{si,2}$ – daily temperatures on the internal surface (measured in the interval of 10 min, it means 144 measurements in 24 h)

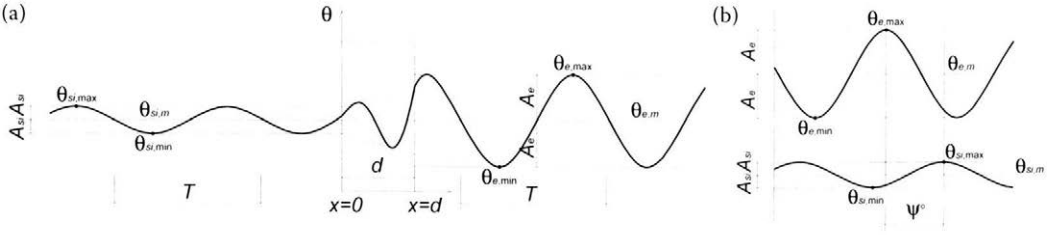


Fig. 1. Schematic description of temperature harmonic fluctuation:
(a) thermal damping; (b) phase shifts of thermal oscillations Ψ in the wall structure
$A_{si}$ – temperature amplitude on the internal surface of the structure (K); $A_e$ – external air temperature amplitude (K); $T$ – time (h); $\theta_{si,min}$ – min. internal surface temperature (°C); $\theta_{si,max}$ – max. internal surface temperature (°C); $\theta_{si,m}$ – medium internal surface temperature (°C); $\theta_{e,min}$ – min. external air temperature (°C); $\theta_{e,max}$ – max. external air temperature (°C); $\theta_{e,m}$ – medium external air temperature (°C); $\psi°$ – phase shift of temperature oscillation (–); $d$ – wall thickness in the $x$-direction (mm)

The average daily temperature of the internal surface on the considered wall measured from the registered records:

$\theta_{si,D1m}$ = 28.24°C (first interval of 24 h)
$\theta_{si,D2m}$ = 28.58°C (second interval of 24 h)

(3) Temperature of internal air $\theta_{i,m}$ was found by a similar procedure:

$\theta_{i,D1m}$ = 28.85°C (first interval of 24 h)
$\theta_{i,D2m}$ = 29.17°C (second interval of 24 h)

For illustration, the courses of the measured values with a subsequent definition of the assessed area are shown in Fig. 2.

The phase shift of temperature oscillation was determined from the measured data $\Psi = t_2 - t_1 = 3.30$ h (Fig. 3).

A number of researches focused on the impact of the building envelopes on heating and cooling loads of the buildings assuming the indoor air temperature is constant (Bojic et al. 2001; Li, Chen 2003). According to Gong et al. (2005), even though a building is naturally ventilated in summer, its mean indoor air temperature is considered as a constant, being only 1.5°C higher than the outdoor air temperature. However, when a building is naturally ventilated, the indoor air temperature also varies periodically because of the impact of the outdoor air temperature and ventilation rate (Yam et al. 2003). Therefore, it cannot be considered as a constant in analysing air-conditioned buildings. In summers, non-air-conditioned interiors of halls in special-purpose agricultural buildings cause considerably non-stationary conditions that negatively affect qualitative parameters of the work environment. According to Zhou et al. (2007), the use of a heavy wall with external insulation is predicted to have the lowest amplitude of indoor air temperature and such wall is

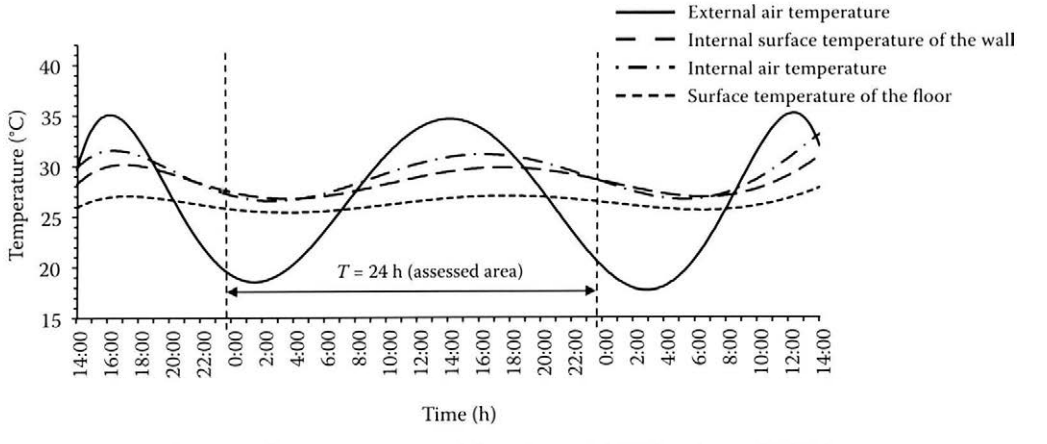


Fig. 2. Trend lines of courses of parameters measured from August 24, 2011 to August 26, 2011

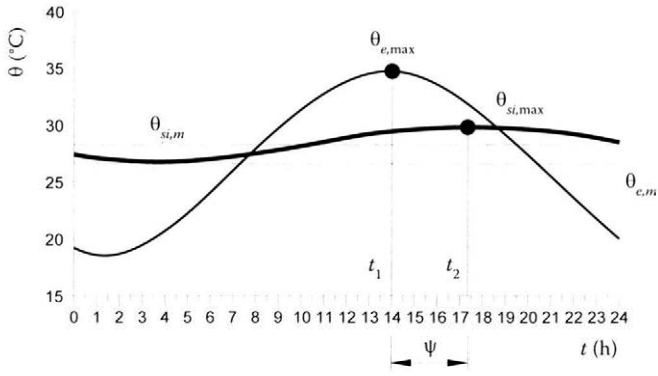


Fig. 3. Scheme of the course of measured external temperatures $\theta_e$ and internal surface temperatures of the wall $\theta_{si}$ $t$ – time (h); $t_1$ – time to reach the max. external air temperature (h); $t_2$ – time to reach the max. internal surface temperature (h); for abbreviations see Fig. 1

suitable for naturally ventilated buildings. The fluctuation of internal air temperature decreases, and the time needed to reach the max. temperature extends with a decreasing amount of internal thermal mass. But the effect becomes negligible when the time constant of the system is more than 20 hours.

In the case of the structure considered in this study, the mean temperature of the inner surface of the outer thermally uninsulated wall was higher than the average ambient temperature. For that reason, considerably different results were obtained of the phase shift of temperature oscillation between the calculation methods and direct measurements in operating conditions. The reasons for this finding can be analysed as follows:

(1) A direct effect was observed of sunlight on the external wall. In the case of the assessed east-oriented wall, intense solar radiation is evident from the morning hours already. Sun rays fall on the wall plane almost at a 90° angle, which causes a fast increase of external surface temperature. The effect of solar radiation is combined with a very important role of the cloud occurrence.

(2) A high average internal air temperature was observed. In this case, the average internal air temperature was higher than the average external air temperature. In terms of the heat balance, especially the size of areas of transparent elements, their inclination from the horizontal plane and their orientation towards the compass points participates in the increase of internal air temperature.

(3) Furthermore, another important factor is the quality of the storage capacity in the upper parts of the building structure envelope and the intensity of natural ventilation during high daily temperature of the outside air. In terms of the heat balance, only the floor structure can be assigned to a greater cooling effect if it is placed directly on the ground (Fig. 2).

## CONCLUSION

The results of our measured values significantly distort non-stationary effects difficult to predict (the variability of external climatic conditions, method, and ventilation rate). This has been demonstrated by a multiple difference between the results obtained from the precise calculation procedure and the results obtained from the values measured under the operating conditions.

The phase shift of temperature oscillation indicates the thermal stability of the interior of the building as well as the justification of the need to install an air conditioner to cool the interior ("summer energy buildings").

More accurate results in assessing the quality of the envelope in terms of thermal technology, and in assessing the effect of the phase shift of temperature oscillation on the thermal stability of the indoor environment in individual parts of buildings can be achieved by advanced computational methods (e.g. Computational Fluid Dynamics – CFD), which enable the calculation of airflow with respect to the complexity and non-linearity of the radiation changes. This being the case, the difference between the air and surface temperatures computed and the data measured is generally less than 1 K.

### References

Bojic M., Yik F., Sat P., 2001. Influence of thermal insulation position in building envelope on the space cooling of

high-rise residential buildings in Hong Kong. Energy and Buildings, *33*: 569–581.

Chmúrny I., 2003. Thermal Protection of Buildings. 1st Ed. Bratislava, Jaga: 214.

Fuliotto R., Cambuli F., Mandas N., Bacchin N., Manara G., Chen Q., 2010. Experimental and numerical analysis of heat transfer and airflow on interactive building facade. Energy and Buildings, *42*: 23–28.

Gong M., Ji Z., Bai G., 2005. Calculation and analysis on inner surface temperature of envelope of natural ventilated buildings in Guangzhou. Heating Ventilating & Air Conditioning, *35*: 20–23.

Halahyja M., Beťko B., Bloudek K., Puškáš J., Tomašovič P., 1985. Building Thermal Technology, Acoustics and Lighting. 1st Ed. Bratislava, ALFA: 752.

Heim D., 2010. Isothermal storage of solar energy in building construction. Renewable Energy, *35*: 788–796.

Khudhair A.M., Farid M.M., 2004. A review on energy conservation in building applications with thermal storage by latent heat using phase change materials. Energy Conversion and Management, *45*: 263–275.

Li Y., Chen G., 2003. Influence of envelops on energy consumption of central air-conditioning system. Journal of Wuhan University of Science & Technology (Natural Science Edition), *26*: 256–258.

Řehánek J. 2002. Thermal Accumulation of Buildings. Prague, ČKAIT: 276.

STN 73 0540-3, 2002. Thermal performance of buildings and components. Thermal protection of buildings. Part 3: Properties of environments and building products. Bratislava, Slovak Office of Standards, Metrology and Testing.

Šklover A.M., Vasiljev B.F., Uškov F.V., 1966. Fundamentals of Heat Transfer Process in livestock production buildings. Moscow, Strojizdat.

Vaverka J., 2006. Building Thermal Technology and Buildings Energetics. Brno, VUTIUM: 648.

Yam J., Li Y., Zheng Z., 2003. Nonlinear coupling between thermal mass and natural ventilation in buildings. International Journal of Heat and Mass Transfer, *46*: 1251–1264.

Zhou J., Guoqiang Z., Lin Y., Li Y., 2007. Coupling of the thermal mass and natural ventilation in buildings. Energy Buildings, *40*: 979–986.

Received for publication July 9, 2012
Accepted after corrections November 7, 2012

*Corresponding author*:

doc. Ing. Štefan Pogran, CSc., Slovak university of Agriculture in Nitra, Faculty of Engineering, Department of Structures, Tr. A. Hlinku 2, 949 78 Nitra
phone: + 421 376 415 691, e-mail: stefan.pogran@uniag.sk

# Selected properties of agricultural biomass

V. Kažimírová[1], T. Brestovič[2], R. Opáth[1]

[1]*Department of Production Engineering, Faculty of Engineering, Slovak University of Agriculture in Nitra, Nitra, Slovak Republic*
[2]*Department of Power Engineering, Faculty of Mechanical Engineering, Technical University of Košice, Košice, Slovak Republic*

**Abstract**

Kažimírová V., Brestovič T., Opáth R., 2013. **Selected properties of agricultural biomass**. Res. Agr. Eng., 59 (Special Issue): S60–S64.

The presented contribution deals with the quantification of moisture, combustible matter content, ash content and higher heating value of the selected types of biomass used for the heat production by direct combustion. The moisture, combustible matter, and ash contents were determined by gravimetric analysis in accordance with the established standards. The average moisture of the materials examined varied from 4.35 to 9.17%; the combustible matter content in the original samples ranged from 79.46 to 93.51%; the ash content ranged from 2.14 to 11.28%. Higher heating values of the examined types of biomass varied from 14,996 to 17,641 kJ/kg. The main contribution of the thesis is the acquisition of values usable in subsequent theoretical and practical efforts to increase the efficiency of the heat production by direct combustion of biomass. The results are useable in biomass boiler design and in identifying suitable conditions for combustion, including the service parameters of biomass boilers.

**Keywords**: gravimetry; dry mass; combustible matter; ash; higher heating value

Combustion is one of the possible biomass uses, resulting in the production of heat utilisable for the household heating, heating of industrial and agricultural structures, and as processing heat. The products of combustion are combustion gases, solid combustion products, and heat.

The goal of this paper is to determine the proportions of combustible matter and ash in the dry mass and the higher heating value of several materials produced in agriculture and landscape design that could be used as biofuels utilised in energy production by their direct combustion.

The dry mass of solid fuels consists of ash and combustible matter. The energy content of a fuel is not characterised by the content of combustible matter in that fuel because each fuel has a different higher heating value depending on its chemical composition. The amount of ash produced by combustion of a certain type of fuel can be estimated by means of the known composition of the dry mass of this fuel.

## MATERIAL AND METHODS

Fuel samples that were subjected to analysis (wheat screenings, hay, cane, Japanese knotweed, and poppy screenings) belong to a wide group of the agricultural waste biomass and biomass obtained from the landscape maintenance. The other examined sample was wheat not used for feeding purposes.

**Measuring of moisture and percentages of combustible matter, and ash**. A muffle furnace Nabetherm L9/11/SW (Nabertherm GmbH, Lilienthal, Germany) (Fig. 1) with the heating device

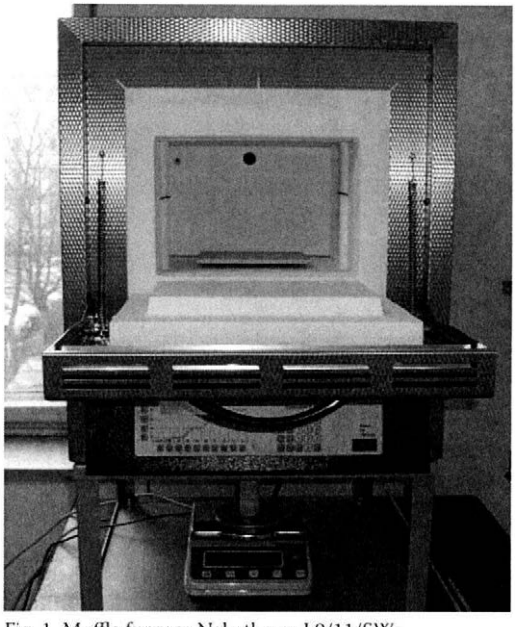

Fig. 1. Muffle furnace Nabetherm L9/11/SW

power of 3.0 kW was used in the measuring of moisture, combustible matter, and ash contents. The muffle furnace was equipped with a Controller P 320 (Nabertherm GmbH, Lilienthal, Germany) control unit and digital scales Kern EW 420-3NM (Kern & Sohn GmBb, Balingen, Germany) with the accuracy of ±0.001 g. The furnace enables the heating of the samples examined up to 1,100°C while recording the weight of the sample.

Moisture is measured in accordance with the standard STN 44 1377 (1978). The sample is heated up to a temperature of 105–110°C and is dried until the difference between the subsequently measured weights (measurements are made in 30 min intervals) is less than 0.1% of the sample weight determined in the previous measurement.

The ash content was determined according to the standard STN ISO 1171 (2003). The samples were annealed at the temperature of 815°C.

The combustible content can be either established from the gravimetric analysis or calculated using the known values of humidity and ash contents.

The sample of the analysed fuel kept in a ceramic bowl was placed in the muffle furnace. The temperatures and time periods of the application (Fig. 2, Table 1) were adjusted on the control unit.

The moisture, ash, and combustible matter contents in the original samples of the examined fuels were determined according to the following equations:

– moisture content:

$$W = \frac{m_1 - m_2}{m_1} \quad (-) \tag{1}$$

– ash content:

$$A = \frac{m_3}{m_1} \quad (-) \tag{2}$$

– combustible content:

$$h = \frac{m_2 - m_3}{m_1} \quad (-) \tag{3}$$

or

$$h = 1 - (A + W) \quad (-) \tag{4}$$

where:

$m_1$ – original weight of sample (g)

$m_2$ – weight of dry mass (g)

$m_3$ – weight of ash (g)

For better comparability of the fuels, ash and combustible matter contents in the dry mass of the individual fuels were calculated using the gathered results:

– ash content in dry mass:

$$A_s = \frac{m_3}{m_2} \quad (-) \tag{5}$$

– combustible matter content in dry mass:

$$h_s = \frac{m_4}{m_2} \quad (-) \tag{6}$$

where:

$$m_4 = m_2 - m_3 \quad (g) \tag{7}$$

where:

$m_4$ – weight of combustible matter (g)

**Estimation of higher heating value**. The higher heating value is estimated by the combustion of a small fuel sample in the calorimeter in accordance with the standard STN ISO 1928 (2003). The higher

Table 1. Temperatures used in gravimetric measurements

| Period | Time of temperature application (min) | Temperature (°C) |
|---|---|---|
| 1 | 60 | 20–107 |
| 2 | 120 | 107 |
| 3 | 60 | 107–500 |
| 4 | 60 | 500 |
| 5 | 60 | 500–815 |
| 6 | 60 | 815 |

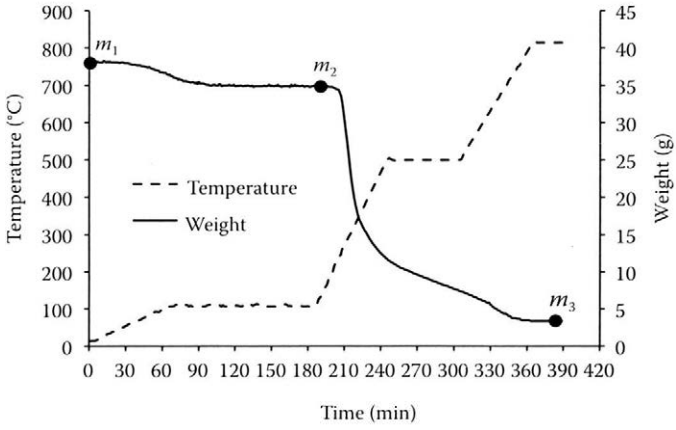


Fig. 2. Gravimetric record showing the used temperatures and periods of their application
$m_1$ – original weight of sample, $m_2$ – weight of dry mass, $m_3$ – weight of ash

heating value was determined on the basis of heating the water into which the pressure tank of the calorimeter with the fuel sample was immersed.

The calorimeter is characterised by its heat capacity, that is, the amount of heat that must be provided in order to increase the temperature of the system (pressure tank, calorimetric bucket, stirrer, thermometer, and water) by 1°C.

An isoperibolic calorimeter IKA C200 (IKA®-Werke GmbH & Co. KG, Staufen, Germany) (Fig. 3) was used to determine the higher heating value. The temperature of water in the casing must be adjusted to the temperature of the room (±0.5°C) before the measurements. After the preparation of the sample weighing 0.8–1.5 g, the temperature is recorded every 60 s until reaching the max. value and then for another five min. of the final stage.

The characteristic course of a temperature change is shown in Fig. 4. The course of temperature before ignition is called the initial stage, the course of temperature during combustion and temperature adjustment is called the main stage, and the course of temperature past max. is called the final stage.

The higher heating value $Q_s^a$ of a sample is calculated from the equation:

$$Q_s^a = \frac{C(D_t - K) - c}{m} \quad \text{(J/g)} \quad (8)$$

where:
$C$ – heat capacity of the system (J/°C)
$D_t$ – total increase of temperature during the main stage (°C)
$K$ – correction covering heat exchange with surroundings (°C)
$c$ – sum of corrections (J)
$m$ – weight of sample (g)

Correction $K$ is calculated from the equation:

$$K = 0.5\,(d_H + d_K) + (n - 1)\,d_K \quad (9)$$

where:
$d_H$ – average temperature change/min in the initial stage (°C/min)
$d_K$ – average temperature change/min in the final stage (°C/min)
$n$ – time of the main stage (min)

The sum of corrections is the sum of the types of heat that cause an increase in temperature in the calorimeter besides the heat released by the sample combustion. This includes the heat released by combustion of the iron wire, calorimetric paper or fastening stitch used, as well as the heat released by nitric acid and sulphuric acid generation. For this reason, all supplementary combustible materials must be accurately weighed before the measurements and their weights or weight losses (iron wire does not have to burn completely) is to be multiplied by their combustion heat in the corrections calculation.

## RESULTS AND DISCUSSION

### Measuring of moisture, percentage of combustible matter, and ash

The weights of the examined samples determined by the gravimetric analysis are presented in Table 2. The processed results of the gravimetric analysis of the samples are presented in Table 3.

The gravimetric analysis has shown that the moisture contents, of the materials examined were relatively low, with the highest one being 9.17%; these

Fig. 3. Calorimeter IKA C200

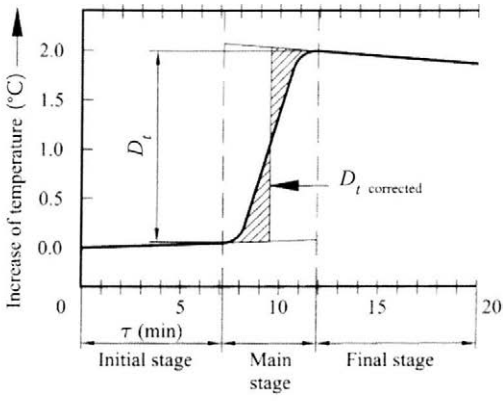


Fig. 4. Course of temperature in the calorimeter
$D_t$ – total increase of temperature during the main stage (°C); τ – time of the initial stage (min)

materials were not modified in any way before the analysis and were stored in regular atmospheric conditions. The results show that poppy screenings had the lowest combustible matter content (87.57%) while wheat grain had the highest one (97.76%).

In comparison with spruce chip pellets with 3.02% ash content (Malaťák, Vaculík 2008), a lower ash content was observed in wheat grain and Japanese knotweed. This topic was dealt with by other authors as well, for instance, Pepich (2009) states that Japanese knotweed contains 4.1% of ash and wheat grain contains 1.6% of ash. The same amount of ash in wheat grain was observed by Maga et al. (2008). These values are comparable to the results obtained in this research. The combustible matter content in all of the examined materials, except for poppy screenings, is comparable to that in beech chip, which contains 95.41% of combustible matter in its dry mass (Kažimírová et al. 2011).

### Estimation of higher heating value

The calculation of the higher heating value of the selected types of biomass was based on the observed values, gathered from the combustion of samples in the calorimeter. The calculated results are presented in Table 4.

Higher heating values of the examined fuel samples varied from 14,996 to 17,641 kJ/kg. The lowest higher heating value was observed in poppy screenings and the highest one in Japanese knotweed. Higher heating values of the analysed materials are comparable to those of other types of biomass which are used for energy production; for instance, the higher heating value of poplar is 17,556 kJ/kg (Brestovič 2006).

## CONCLUSION

The aim of the performed analyses resided in gathering the values of the selected attributes of several types of agricultural biomass, which can be obtained from the agricultural activity, agricultural produce processing, and pharmaceutical industry. According to the results of this research, the examined types of biomass are comparable in their attributes, to the biomass commonly used for energy production by means of direct combustion. The combustible matter content in the dry mass of the examined types of agri-

Table 2. Weight of samples determined by gravimetric analysis

| Weight (g) | Wheat grain | Wheat screenings | Hay | Cane | Japanese knotweed | Poppy screenings |
|---|---|---|---|---|---|---|
| Original sample | 28.021 | 25.444 | 38.194 | 30.729 | 13.050 | 12.962 |
| Dry mass | 26.802 | 23.111 | 34.794 | 28.329 | 12.150 | 11.762 |
| Ash | 0.600 | 1.333 | 3.094 | 1.329 | 0.350 | 1.462 |

Table 3. Gravimetric analysis of the samples

| Parameter | Wheat grain | Wheat screenings | Hay | Cane | Japanese knotweed | Poppy screenings |
|---|---|---|---|---|---|---|
| Moisture ratio in original sample | 0.0435 | 0.0917 | 0.0890 | 0.0781 | 0.0690 | 0.0898 |
| Ash content in original sample | 0.0214 | 0.0524 | 0.0810 | 0.0433 | 0.0268 | 0.1128 |
| Combustible matter content in original sample | 0.9351 | 0.8559 | 0.8300 | 0.8786 | 0.9042 | 0.7946 |
| Weight of combustible matter (g) | 26.202 | 21.778 | 31.700 | 27.000 | 11.800 | 10.300 |
| Ash content in dry mass | 0.0224 | 0.0577 | 0.0889 | 0.0469 | 0.0288 | 0.1243 |
| Combustible matter content in dry mass | 0.9776 | 0.9423 | 0.9111 | 0.9531 | 0.9712 | 0.8757 |

Table 4. Higher heating values of the samples

| Sample | (kJ/kg) |
|---|---|
| Wheat grain | 15,650 |
| Wheat screenings | 16,421 |
| Hay | 16,720 |
| Cane | 17,587 |
| Japanese knotweed | 17,641 |
| Poppy screenings | 14,996 |

cultural biomass varied from 87.57 to 97.76%, which also indicates a low amount of ash in the dry mass.

The ash contents in the examined materials approximate to the results obtained by other authors. The differences between the results can be explained by different varieties of the examined plants, different agricultural technologies used, and different macroclimatic conditions in which the plants were grown.

The results of the measurements of higher heating values of the samples vary from 14,996 to 17,641 kJ/kg and suggest that all of the examined types of agricultural biomass can be used in energy production by direct combustion.

The benefit of using agricultural biomass as a solid fuel resides in its energy value and a low amount of incombustible components.

## References

BRESTOVIČ T., 2006. Stanovenie tepelného obsahu niektorých zložiek biomasy. [Determination of heat capacity of some parts of biomass.] In: Proceedings Novus Scientia. Košice, Technical University: 65–70.

KAŽIMÍROVÁ V., OPÁTH R., BRESTOVIČ T., HORBAJ P., 2011. Gravimetric analysis of moisture and combustible and ash contents in selected biofuels. Acta Technologica Agriculturae, *14*: 8–10.

MAGA J., NOZDROVICKÝ L., PEPICH Š., MARHAVÝ Ľ., HAJDU Š., 2008. Komplexný model využitia biomasy na energetické účely. [A Complex Model of Biomass Use for Energy Purposes.] Nitra, Slovak University of Agriculture in Nitra: 183.

MALAŤÁK J., VACULÍK P., 2008. Biomasa pro výrobu energie. [Biomass for Energy Production.] Prague, Czech University of Life Sciences Prague: 206.

PEPICH Š., 2009. Využitie popola z biomasy ako hnojiva. [Use of biomass ash as fertiliser.] Agrobioenergia, *3*: 15–17.

STN ISO 1171, 2003. Tuhé palivá. Stanovenie obsahu popola. [Solid fuels. Determination of ash.] Bratislava, Slovak Office of Standards, Metrology and Testing.

STN ISO 1928, 2003. Tuhé palivá. Stanovenie spaľovacieho tepla kalorimetrickou metódou v tlakovej nádobe a výpočet výhrevnosti. [Solid fuels. Determination of higher heating value by the calorimetric method in a pressure tank and calculation of performance.] Bratislava, Slovak Office of Standards, Metrology and Testing.

STN 44 1377, 1978. Tuhé palivá. Stanovenie obsahu vody. [Solid fuels. Determination of water content.] Bratislava, Slovak Office of Standards, Metrology and Testing.

Received for publication July 10, 2012
Accepted after corrections December 12, 2012

*Corresponding author:*

Ing. VIERA KAŽIMÍROVÁ, Ph.D., Slovak University of Agriculture in Nitra, Faculty of Engineering, Department of Production Engineering, Tr. A. Hlinku 2, 949 76 Nitra, Slovak Republic
phone: + 421 376 414 403, e-mail: viera.kazimirova@uniag.sk

# Determining the guidance system accuracy with the support of a large GNSS dataset

V. Rataj, J. Galambošová, M. Vašek

*Department of Machines and Production Systems, Faculty of Engineering, Slovak University of Agriculture in Nitra, Nitra, Slovak Republic*

**Abstract**

Rataj V., Galambošová J., Vašek M., 2013. **Determining the guidance system accuracy with the support of a large GNSS dataset**. Res. Agr. Eng., *59* (Special Issue): S65–S70.

Several methods are used presently to assess the accuracy of machinery guidance systems. However, these offer a limited number of records and are time and cost consuming. As the machinery is often equipped with a monitoring system for the management purposes, these data can be used. The aim of this work was to develop and verify a method to determine the accuracy of the machinery guidance systems based on a large dataset obtained from the machinery monitoring system. The proposed method uses the transformation of global navigation satellite systems (GNSS) data into a rectangular coordinate system SJTSK (National projection system – Krovak projection). Based on the geometry principle, the ideal line can be determined, and afterwards, the off-track error of each actual position can be calculated. After the verification of this method, it can be concluded that it brings benefits in terms of further use of the data from the monitoring systems, the estimation of the error based on a robust dataset, elimination of subjective and measurement method errors, as well as spatial localisation of the off-track errors at the field.

**Keywords**: off-track error; geometry; rectangular coordinate system SJTSK

The machinery movement in the field is an important parameter of the machinery use efficiency. The research into this topic has been conducted for many years by many authors from many aspects. Among the first published results on the field traffic are those by Pavlov et al. (1973) and Ondřej et al. (1989). The problem of the machinery movement is connected with the technical level of tractors and implements. Because of the kinematics of modern tractors, it is necessary nowadays to study and model the machinery movement. Several authors deal with the aspects of machinery movement itself including the kinematics (Backman et al. 2012; Rovira-Más 2012). The issue of the machinery movement within a defined space, described by the shape and the area of a field, has been solved by Hameed et al. (2010). Besides the movement of machinery for the field operations, those of machinery for service operations such as e.g. field transport have been analysed (Bochtis et al. 2010a).

The analyses of the machinery movement, optimal direction of movement, algorithms and mathematical models of machinery field traffic were conducted by Bochtis et al. (2007, 2010a, b), Oksanen and Visala (2007), Bochtis and Vougioukas (2008), Yakusshev and Yakusshev (2008), Spekken and Bruin (2011) and others.

Supported by the European Union, research project under the title: ITEPAg – Application of information technologies to increase the environmental and economical efficiency of production agro-system. ITMS 26220220014.

The machinery guidance in the field is provided by guidance systems with sufficient accuracy. There are many of these. Optical or laser guidance systems can be used under specific conditions. The examples are the guidance based on the crop height, implement guidance during intra-row field operations (Slaughter et al. 1999). Nowadays, machinery guidance is based mostly on the signal from global navigation satellite systems (GNSS). This is efficient for wide implements during soil preparation, fertilisation, or crop protection (Nozdrovický et al. 2008; Trimble GPS 2012).

The use of these systems affects the work quality and overall economic efficiency of the machinery use (Grisso et al. 2004; Galambošová, Rataj 2010).

The economic effect and optimal return on investment are directly connected with the work quality. The criteria of the work quality when using the GNSS guidance systems are the accuracy of GNSS guidance and its transmission to the movement control. This issue is covered in world standards (ASABE 2007) as well as scientific papers (Gan-Mor et al. 2007; Gavric et al. 2011; Williams et al. 2012).

The data on machinery movement (traffic) in the field can be used for other analyses as well, e.g. the machinery management assessment (Taylor et al. 2002), soil compaction assessment (Kroulík et al. 2011) etc. The exact data, which are saved, can be used for traceability assurance as well (Cascone et al. 2010).

The aim of this work was to propose and verify a method for determining the accuracy of the machinery movement based on datasets obtained from the machinery monitoring system.

## MATERIAL AND METHODS

The proposed methodology enables to determine the accuracy of the machinery movement based on large datasets from the machinery monitoring system. The monitoring system is primarily used for the machinery management purposes. The monitoring system consists of a GNSS antenna (AgGPS; Trimble Navigation Ltd., Sunnyvale, USA) and a GPRS modem (RTKMD; FONS s.r.o., Františkovy Lázně, Czech Republic), which sends the data to the server. The data exported from the system (in its extended use) are gathered with a frequency of one record per six seconds. The data contain the information on GNSS coordinates with real time kinematics (RTK) precision as the system is connected to the machinery guidance system Trimble Autopilot (Trimble Navigation Ltd., Sunnyvale, USA) (Fig. 1). The calculation of the error is based on the geometry principle.

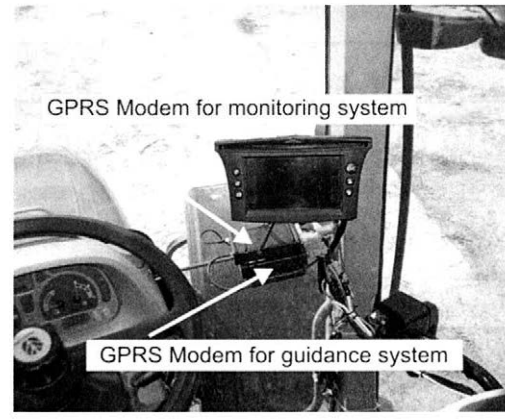


Fig. 1. Machinery monitoring system and machinery guidance system

The verification of the proposed method was conducted during field operations. The machinery guidance was provided by Trimble Autopilot with RTK accuracy (Trimble GPS 2012). The AB line mode of the guidance system was selected. The accuracy was calculated as the distance of the machinery real position from the AB line.

## RESULTS AND DISCUSSION

Based on the trajectory of the selected traffic line (AB line), the positions of the starting point $K(x_K; y_K)$ as well as the last point $L(x_L; y_L)$ can be obtained. The coordinates of this AB line give the "ideal line", which can be described by the linear dependence $y = A + Bx$ (Fig. 2). The measured error can be, based on the ASABE standard, defined as an "off-track error" and is equal to the perpendicular deviation from the actual travel course. The proposed method uses the transformation of GNSS data into a rectangular coordinate system SJTSK, which is a national coordinate system used mainly in the Czech and Slovak Republics as introduced by Krovak (Tuček 1998; Huml, Michal 2006).

The real implement working width can be determined as the following (Fig. 3):

$$Bp = Bk - \Delta B$$

where:

$Bk$ – construction width of the implement (m)

$\Delta B$ – overlaps – value set in the guidance system (m)

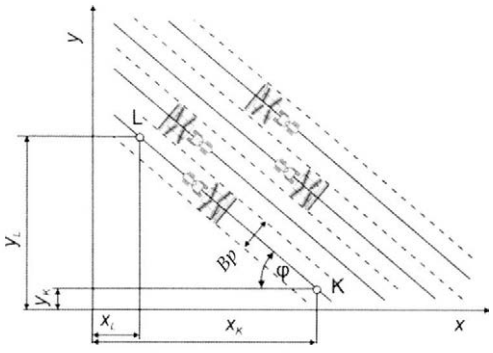


Fig. 2. Basic scheme of machinery movement
$K(x_K, y_K)$, $L(x_L, y_L)$ – position of the tractor and its coordinates; φ – angle of the traffic line; *Bp* – implement width

The efficiency of using the implement width during the field operation is commonly calculated as $\beta = Bp/Bk$, where β is the ratio of the effectively used implement (*Bp*) width to the implement width (*Bk*) (Pavlov et al. 1973; Ondřej et al. 1989).

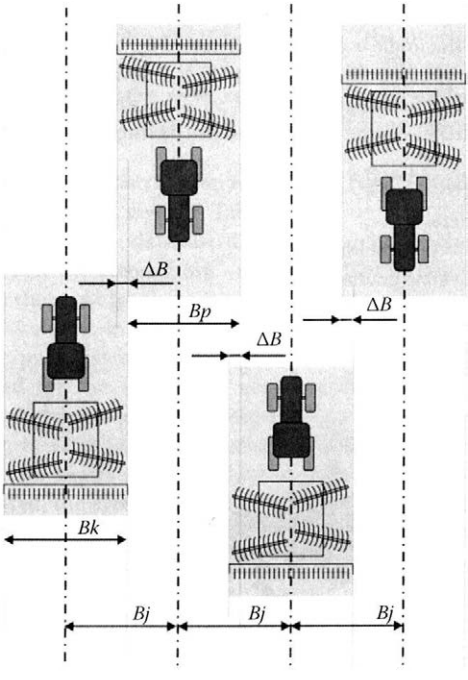


Fig. 3. The real working width of the machine during field operation
*Bk* – implement width; *Bp* – effectively used implement width; *Bj* – perpendicular distance of guidance lines; Δ*B* – overlaps

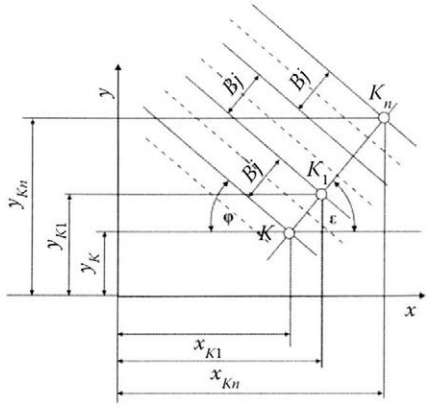


Fig. 4. Determining the starting and terminating points *Bj* – perpendicular distance of guidance lines; $K(x, y)$, $K_1(x_1, y_1)$, $K_n(x_n, y_n)$ – starting points of guidance lines and their coordinates; φ – angle of the traffic line, $\varepsilon = 180 - (90 + \varphi)$

The guidance system uses for the guidance of machinery "*n*" lines ($K_{1-n}$ $L_{1-n}$) of a perpendicular distance (*Bj*) from the ideal line. The distance (*Bj*) is equal to the implement working width (*Bk*). This line should be the trajectory of the machinery centre line during the field operation. However, due to the errors of GNSS as well as technical or terrain influences, off-track errors are present.

Several methods are used to determine the error: physical measurement with a measuring tape,

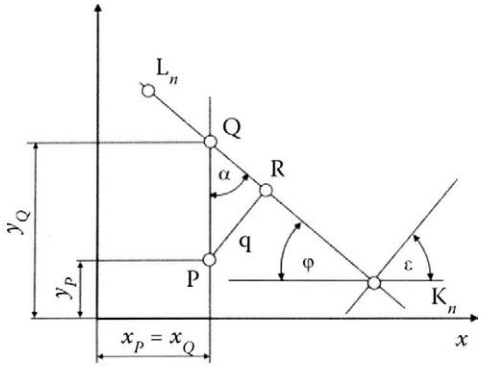


Fig. 5. Estimation of off-track error of a selected position
$K_n$ starting point of line"*n*"
$L_n$ – terminating point of line "*n*", $P(x_p, y_p)$ – selected position from a dataset with its coordinates, R – position of the point "P" on the ideal line, Q – vertex of the triangle PQR, q – off-track error

Fig. 6. Recorded data for the assessed field operation

measurement with a laser distance meter (MACÁK, ŽITŇÁK 2010), and measurement with a handheld GNSS receiver. Compared to that, the extended use of the machinery monitoring data provides the data in the structure: latitude, longitude, time, and date in large datasets. The transformation of these data into the rectangular coordinate system enables its geometric processing. The starting and ending points have to be determined (Fig. 4).

The coordinates of the points $K_1L_1$ to $K_nL_n$ can be estimated by angles φ and ε:

$$\tan\varphi = \frac{y_L - y_K}{x_K - x_L} \qquad \varepsilon = 180 - (90 + \varphi)$$

The coordinates of the ideal or previous lines are the base for the estimation.

Table 1. Basic statistics of off-track error

| | |
|---|---|
| Mean (m) | 0.002 |
| Standard deviation (m) | 0.058 |
| Minimum (m) | 0.216 |
| Maximum (m) | 0.184 |
| Number of records | 867 |

The coordinates of the first line points can be estimated as follows:

$$x_{K1} = x_K + B_j \times \cos\varepsilon$$

$$y_{K1} = y_K + B_j \times \sin\varepsilon$$

$$x_{L1} = x_L + B_j \times \cos\varepsilon$$

$$y_{L1} = y_L + B_j \times \sin\varepsilon$$

As mentioned above, when using the machinery monitoring systems in an extended mode, the actual position of the machine can be recorded. For example, the point $P(x_P, y_P)$ should lie on the line $K_nL_n$ (Fig. 5) The error is the perpendicular to the line $K_nL_n$. The solution proceeds from the triangle PRQ.

The angle α can be determined as: $\alpha = 90 - \varphi$; the error can be estimated as: $q = r \times \sin\alpha$.

The line segment $PQ = y_Q - y_P$ and the coordinate $y_Q$ can be determined as the linear function:

$$y_Q = A + B \times x_P$$

where:

A – vertical intercept

B – line gradient

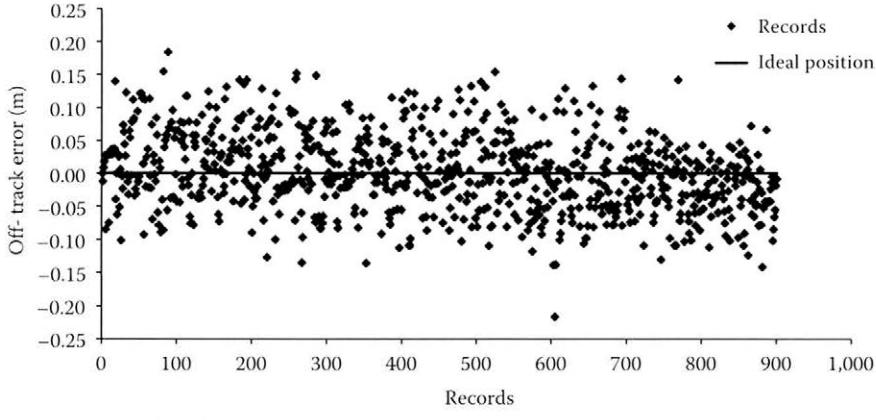


Fig. 7. Distribution of off-track errors

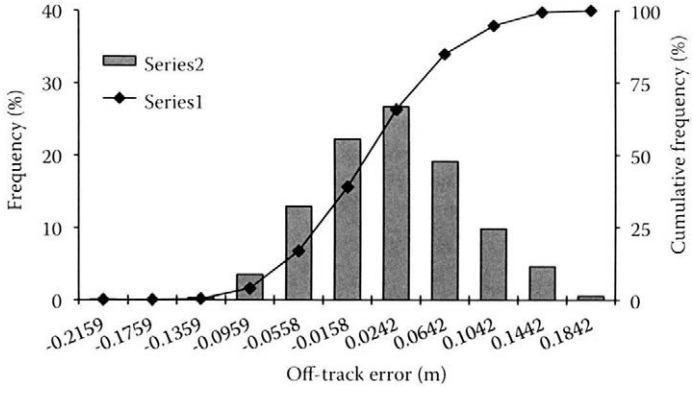


Fig. 8. Histogram of off-track errors

The methodology was evaluated for several field operations, which were monitored with the support of the on-line monitoring system. One example is described below. For the purposes of this paper, the data from a drilling field operation were used. The tractor NewHolland T6070 (New Holland Agriculture, New Holland, USA) with the guidance system Trimble Autopilot with RTK system together with the drilling machine Lemken Solitaire 9 (Lemken GmbH & Co. KG, Alpen, Germany) were assessed. The implement width (*Bk*) was 6 m. The overlapping width ($\Delta B$) was set up at 0.2 m. The tracks of the machinery were recorded. For the evaluation, 45 tracks were used (867 monitoring points) (Fig. 6).

The errors distribution is shown in Fig. 7. The basic statistics is given in Table 1.

Based on the data distribution, it can be concluded that the errors from –0.016 to 0.024 m (Fig. 8) are the most frequent.

As shown in the example, the data obtained for the purposes of machinery monitoring can to be used for the movement accuracy determination. Also, the errors which exceed the acceptable range can be later identified, localised, and their source can be analysed. In the case of the machinery assessed, the errors were present at headlands, while the machinery was turning.

## CONCLUSION

The proposed methodology is based on using large data sets obtained from the extended use of the machinery monitoring system. The evaluation of off-track errors with the proposed methodology provides reliable information on the accuracy compared to the traditional physical measurement methods. The method brings benefits in terms of:

- further use of the data coming from the monitoring systems,
- obtaining a robust dataset,
- elimination of subjective errors, errors of the measurement method,
- spatial localisation of off-track errors at the field.

## References

ASABE, 2007. X587 Dynamic Testing of Satellite-Based Positioning Devices used in Agriculture. St. Joseph, ASABE.

Backman J., Oksanen T., Visala A., 2012. Navigation system for agricultural machines: Nonlinear model predictive path tracking. Computers and Electronics in Agriculture, *82*: 32–43.

Bochtis D.D., Vougioukas S.G., 2008. Minimising the non-working distance travelled by machines operating in a headland field pattern. Biosystems Engineering, *101*: 1–12.

Bochtis D.D., Vougioukas S., Tsatsarelis C., Ampatzidis Y., 2007. Field operation planning for agricultural vehicles: A hierarchical modelling framework. Agricultural Engineering International. CIGR e-Journal.

Bochtis D.D., Sørensen C.G., Vougioukas S.G., 2010a. Path planning for in-field navigation-aiding of service units. Computers and Electronics in Agriculture, *74*: 80–90.

Bochtis D.D., Sørensen C.G., Green O., Moshou D., Olesen J., 2010b. Effect of controlled traffic on field efficiency. Biosystems Engineering, *106*: 14–25.

Cascone G., Arcidiacono C., Porto S., Anguzza U., 2010. Conceptual modelling for the design of computer based traceability system. Available at https://bioeng.ca/publications/meetings-papers?sobi2Task=sobi2Details&sobi2Id=669

Galambošová J., Rataj V., 2010. Determination of machinery performance for random and controlled traffic

farming. In: Stafford J.V. (ed.), Precision Agriculture. Prague, Czech Centre for Science and Society: 449–456.

Gan-Mor S., Clark Rex L., Upchurch B.L., 2007. Implement lateral position accuracy under RTK-GPS tractor guidance. Computers and Electronics in Agriculture, *59*: 31–38.

Gavric M., Martinov M., Bojic S., Djatkov Dj., Pavlovic M., 2011. Short- and long-term dynamic accuracies determination of satellite-based positioning devices using a specially designed testing facility. Computers and Electronics in Agriculture, *76*: 297–305.

Grisso R.D., Kocher M.F., Adamchuk V.I., Jasa P.J., Schroeder M.A., 2004. Field efficiency determination using traffic pattern Indices. Applied Engineering in Agriculture, *20*: 563–572.

Hameed I.A., Bochtis D.D., Sørensen C.G., Nøremark M., 2010. Automated generation of guidance lines for operational field planning. Biosystems Engineering, *107*: 294–306.

Huml M., Michal J., 2006. Mapování 10. [Maping 10.] Prague, ČVUT: 320.

Kroulík M., Kvíz Z., Kumhála F., Hula J., Loch T., 2011. Procedures of soil farming allowing reduction of compaction. Precision Agriculture, *12*: 317–333.

Macák M., Žitňák M., 2010. Efektívne využitie satelitnej navigácie v systéme presného poľnohospodárstva. [Efficient use of Satellite Guidance Systems in Precision Farming]. Nitra, Slovak University of Agriculture: 125.

Nozdrovický L., Rataj V., Galambošová J., Kollárová K., Macák M., Halva J., Tuček J., Koreň M., Smreček R., 2008. Presné poľnohospodárstvo. [Precision Agriculture.] Nitra, Slovak University of Agriculture: 168.

Oksanen T., Visala A., 2007. Path planning Algorithms for Agricultural Machines. Agricultural Engineering International. CIGR e-Journal.

Ondřej L., Kadlec V., Kavka M., Šařec O., 1989. Využitie mechanizačných prostriedkov v poľnohospodárstve. [Use of Mechanisation in Agriculture.] Bratislava, Príroda: 310.

Pavlov B.V., Puškareva P.V., Ščeglov P.S., 1973. Projektirovanie komplexnoj mechanizacii selsko-chozjajstvennych predprijatij. [Design of Complex Machinery for Agricultural Farms.] Moscow, Kolos: 288.

Rovira-Más F., 2012. Global-referenced navigation grids for off-road vehicles and environment. Robotics and Autonomous Systems, *60*: 212–287.

Slaughter D.C., Chen P., Curley R.G., 1999. Vision guided precision cultivation. Precision Agriculture, *1*: 199–216.

Spekken M., Bruin S., 2011. Optimizing routes on agricultural fields minimizing manoeuvring and servicing time. In: Stafford J.V. (ed.), Precision Agriculture. Prague, Czech centre for Science and Society: 411–426.

Taylor R.K., Schrock M.D., Staggengorg S.A., 2002. Extracting machinery management information from GPS Data. ASAE Paper 02-1008. St. Joseph, ASAE.

Trimble GPS, 2012. Available at www.leadingfarmers.cz/trimble (accessed April 4, 2012).

Tuček J., 1998. Geografické informační systémy. [Geographical Information Systems.] Prague, Computer Press: 424.

Williams T., Alves P., Lachapelle G., Basnayake C., 2012. Evaluation of GPS-based methods of relative positioning for automotive safety applications. Transportation Research Part C, *23*: 98–108.

Yakushev V.P., Yakushev V.V., 2008. Mathematical models and methods of realizing information technology procedures in precision agriculture. Russian Agricultural Sciences, *34*: 280–283.

Received for publication July 16, 2012
Accepted after corrections January 31, 2013

*Corresponding author*:

Ing. Jana Galambošová, Ph.D., Slovak University of Agriculture in Nitra, Faculty of Engineering, Department of Machines and Production Systems, Tr. A. Hlinku 2, 949 78 Nitra, Slovak Republic
phone: + 421 376 414 344, e-mail: jana.galambosova@uniag.sk

The journal publishes results of basic and applied research from all fields of agricultural engineering. Original scientific papers, short communications, review articles, and selectively book reviews from the disciplines concerned are published in the journal. Papers are published in English (British spelling). The author is fully responsible for the originality of the paper and formal correctness. The paper and its content must not be published previously elsewhere. The Board of Editors decides on the publication of papers, taking into account scientific importance, peer reviews and manuscript originality, quality and length. Standard size of paper (A4 format), type size 12 font, double-space lines, 2.5 cm margins on each edge of the page. **Scientific papers** and **review articles** shall not be longer than 15 standard pages, including tables and figures. **Short communications** should not be longer than 6 standard pages and book reviews should not be longer than 3 standard pages. Manuscripts must be submitted in MS Word text editor to the electronic editorial system (http://www.agriculturejournals.cz/web/rae.htm).

**Tables** should be placed at the end of the manuscript. Word editor should be used to create tables; each item should be placed into a separate cell. Tables are to be numbered with Arabic numerals in the order in which they are referred to in the text. **Figures.** Figure captions should be placed after the tables. Autotypes should be submitted in TIFF or JPG format in minimal resolution 300 dpi. Graphs should be provided in MS Excel and they should be stored with original data. All graphs and photos should be numbered, continually according to the order in which they are included in the text, using Arabic numerals. **Abbreviations and units.** If any abbreviations are used in a paper, they shall be explained appropriately when they are used in the text for the first time. It is not advisable to use any abbreviations in the paper title or in the abstract. The SI international system of measurement units should be used.

**Title page** must contain title of paper, complete name(s) of the author(s), the name(s) and address(es) of the institution(s) where the work was done.

**Abstract** is a short summary of the whole paper (as a single paragraph). It should describe all essential facts of a scientific paper. The abstract should not go to more than 170 words. The abstract is an important part of the paper because it is published and cited in world databases. No references are to be cited. **Keywords** (recommendation 5 words) should be different from words mentioned in the title.

**Introduction** should outline the main reasons why the research was conducted; describe a brief review of literature consisting of refereed periodicals, journals and books, and the goal of the authors.

**Material and Methods.** All preliminary material, experiments conducted, their extent, conditions and course should be described in detail in this section. All original procedures that were used for the processing of experimental material and all analytical methods used for evaluation should also be detailed. Data verifying the quality of acquired data should be indicated for the used methods. The whole methodology is only to be described if it is an original one; in other cases it is sufficient to cite the author of the method and to mention any particular differences. Methods of statistical processing including the software used should also be listed in this section.

**Results and Discussion.** More than one-year results should be published in the paper. The results obtained from the experiments including their statistical evaluation and any commentary should be presented graphically or in tables in this section. Each phenomenon should be commented and explained, using scientific arguments. The author should confront partial results with data published by other authors, whose names and year of publication are to be cited by including them in the text directly, e.g. ... as published by Lowe (1981), Novák and Šídlo (2002) found ..., or citing authors and years of publication in parenthesis (Lowe 1981; Novák, Šídlo 2002; Jakl et al. 2003).

**Conclusion.** In the conclusion it is necessary to mention briefly the most important results presented in article, the key points of next research and experimental work and recommendation for utilization in practice.

**References** should be preferably a list of refereed periodicals arranged in alphabetical order according to the surname of the first authors. The surnames and initials of all authors should be followed by the year of publication cited, the original title of the paper (if the cited source is not in English, it should be translated in brackets behind of the original title), the name of the periodical, the relevant volume and page number, in the case of a book or proceedings the title should be followed by the name of the publisher and the place of publication. Names of authors should be separated by commas, not by & or and. Examples:

**Journal article:** Litak G., Longwic R., 2009. Analysis of repeatability of diesel engine acceleration. Applied Thermal Engineering, 29: 3574–3578.

**Monographs:** Bouman A., 1995. Mechanical Damage in Potato Tubers – Enquiry of the EAPR Engineering Section. Wageningen, Institute of Agricultural and Environmental Engineering: 29.

**Papers published in collections and proceedings:** McClements D.J., 1994. Ultrasonic NDT of foods and drinks. In: McGonnagle W.J. (ed.), International Advances in Nondestructive Testing. Yverdon, Gordon and Breach Science, *17*: 63–95.

Toscano G., Riva G., Pedretti E.F., Corinaldesi F., 2008. Evaluation of solid biomass for energy use in relation to the ash qualitative and quantitative characteristics. In: International Conference on Agricultural Engineering, Agricultural and Biosystems Engineering for a Sustainable World, June 23–25, 2008. Hersonissos – Crete, Greece.

**Dissertation:** Vančurová P., 2008. Podmínky konkurenceschopnosti výroby bionafty v České republice. [Conditions of Competitiveness of Biodiesel Production in the Czech Republic.] [Ph.D. Thesis.] Prague, Czech University Life Sciences Prague: 1 – 159.

**Internet publications:** George G.C., 2001. Solids flowability. University of Akron. Available at www.ecgf.uakron.edu/chem/fclty/chase/solidsNote.PDF (accessed August 2, 2007).

**Contact address** should include the postal address, telephone and fax numbers, and e-mail of the corresponding author in English.

**Proof-sheets** will be sent to the corresponding author by e-mail. Your response, with or without corrections, should be sent within 48 hours.

**Offprints:** Corresponding author will receive a free "electronic reprint" in Portable Document Format (PDF).

**Compliance with these instructions is obligatory for all authors. If a manuscript does not comply with the above requirements, the editorial office will not accept it for a consideration and will return it to the authors without reviewing.**

# *Research in* AGRICULTURAL ENGINEERING

**Volume 59** **2013**

*Research in* AGRICULTURAL ENGINEERING • Published by the Czech Academy of Agricultural Sciences • Editorial Office: Slezská 7, 120 00 Prague 2, Czech Republic, phone: + 420 227 010 606, fax: + 420 227 010 116, e-mail: rae@cazv.cz • 
Distribution: Czech Academy of Agricultural Sciences, Slezská 7, 120 00 Prague 2, Czech Republic, phone: + 420 227 010 427, fax: + 420 227 010 116, e-mail: redakce@cazv.cz